Semi-analytical solutions for buckling and post-buckling of composite plates

Application to stiffened Panels

E. Cabot Talens

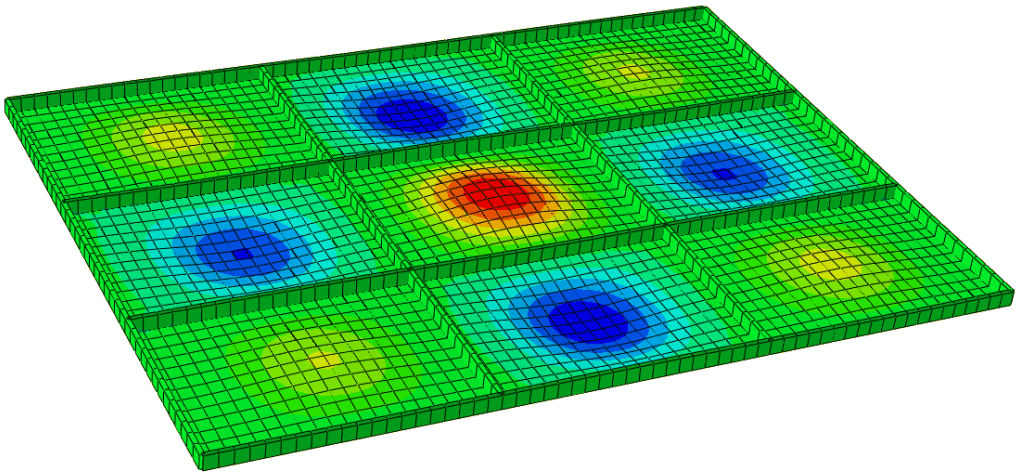

TU Delft

Fokker

GKN AEROSPACE

Semi-analytical solutions for buckling and post-buckling of composite plates

Application to stiffened panels

By

E. Cabot Talens

in partial fulfilment of the requirements for the degree of

Master of Science

in Aerospace Structures and Materials

at the Delft University of Technology,

to be defended publicly on Thursday August 25th, 2016 at 13:30

Supervisors:	Prof. Dr. Christos Kassapoglou	TU Delft
	Ing. B. Tijs	Fokker Aerostructures
Thesis committee:	Dr. Julien van Campen	TU Delft
	Dr. Derek Gransden	TU Delft

TU Delft

Acknowledgements

First of all I would like to thank both my supervisors, Christos Kassapoglou and Bas Tijs. It has been enriching having different supervisors from both TU Delft and Fokker Aerostructures. The fact that each of them have different backgrounds and points of view has helped me with my Thesis and I am grateful for their guidance.

Besides my supervisors, several professors have kindly given me advice when problems aroused. I would like to thank Mostafa Abdalla for his invaluable input on buckling and numerical methods, Sonell Shroff for his advice with Abaqus and finally Chiara Bisagni, whose papers on semi-analytical methods for buckling and post-buckling have been a true inspiration.

I would also like to thank Kemal Dahha, who was the first student to work in the stiffened panel project at Fokker, and has always been willing to give advice.

I would finally like to mention my parents, without their support and values this work would not have been possible.

Abstract

This MSc thesis addresses the study of buckling and post-buckling of composite plates with elastic restraints at the edges and under any combination of in-plane loading, aiming to solve the plate response in stiffened panel structures.

The implemented solutions are based on thin plate theory for mid-plane symmetric plates. The governing equations are solved using a semi-analytical formulation (not closed form) to combine advantages from analytical and numerical analysis. This approach allows to solve most of the typical laminates used in aerospace applications while allowing an improved performance when compared to FE models.

The developed formulation relies on eigenbeam functions to approximate the plate behaviour for any combination of arbitrary elastic restrains, with a minimum number of degrees of freedom. This approach has proved to be able to reproduce the buckling mode and load for buckling and the out-of-plane displacement for post-buckling. The results obtained have been verified against FE commercial software package Abaqus and good to excellent agreement has been achieved using a fraction of the computational power.

The relation between the ideal torsional springs and stiffeners' restrain is approximated in order to apply the developed formulations to more practical problems involving stiffened panels. Preliminary verifications show the validity of the proposed approaches and encourages the further development of the solution to achieve a more powerful stiffened panel formulation.

Moreover, the developed approaches can be extended to solve other relevant stability phenomena such as global buckling or stiffener crippling.

This work is part of a Fokker Aerostructures project to develop an analytical framework for analysis and design of composite stiffened panels with post-buckling capabilities. This framework will facilitate the preliminary design of composite stiffened structures and allow further optimization without requiring the prohibitive computational cost and complexity of finite element models.

Contents

List of Figures

List of Tables

1. Introduction

1.1. Background and Motivation

The use of fiber reinforced composites in structural design has become both an opportunity and a challenge. Such materials can provide improved performance with respect to metals because of their high specific strength and stiffness. Moreover, the capacity to distribute those properties in the different directions can be exploited to optimize the strength to specific load cases. However, this also means that the mathematic models necessary to describe the behaviour of such materials become more complex and challenging. This is the case when studying buckling and post-buckling of plates. The increasing mathematic complexity with the inclusion of new variables makes it difficult (or limits to very specific cases) obtaining analytic closed form solutions or semi-empiric fitted curves as in traditional structural design books for metallic structures [1, 2].

The use of finite element methods (FEM) has been successfully applied in many cases due to its flexibility in allowing very general configurations and the accurate results given. However, the use of FEM requires a significant computational effort and time. This fact limits the usefulness of this tool during preliminary design, when it is especially important to be able to test different configurations and understand the dependency of the results with the different design parameters.

The disadvantages or limitations that closed form solutions and FEM present has encouraged the development of alternative methods like semi-analytical procedures. Such methods have the advantages of less computational effort compared with FEM and the possibility to handle more general formulations as compared to closed-form solutions (specially in post-buckling, where closed-form solution are very limited). In conclusion, semi-analytical procedures can fill an intermediate gap between closed-form and FE solutions.

Therefore, the interest (especially in the industry) to implement faster and simpler design procedures to be used in preliminary design for composite structures can be fulfilled by developing analytic (when possible) and/or semi-analytic procedures.

This MSc thesis will address a thoughtful research on which is the state of the art in this field, finding out which are the most promising used methods, understanding their advantages and disadvantages and finally implementing or further developing the necessary formulations to solve buckling and post-buckling of thin composite plates.

This thesis has been done in collaboration with Fokker Aerostructures to further develop the tools that Fokker has available to design composite structures.

Current analytic procedures available at Fokker are limited to close form initial buckling for specially orthotropic materials. Post-buckling is mainly approached using complex FE models, limiting the possibility of performing design optimization.

This work forms part of a bigger project focused on obtaining approximate and fast solutions for all the failure modes of stiffened panels using an analytical approach. The resulting framework will allow design optimization during preliminary design.

1.2. Research Question and Objectives

The research questions and sub-questions proposed in this project are:

- Which are the most important methods developed to analytically and semi-analytically solve buckling of thin mid-plane symmetric plates under different boundary conditions and load combinations?
  - Which cases can be solved completely analytically (closed-form)?
  - Which degree of accuracy can be expected from semi-analytical methods in comparison with FEM?
  - How can stiffeners' rotation restriction, produced on the plate's edges, be translated into analytic and semi-analytic models?
  - Are the developed methods a good alternative to solve local buckling under different BC's, load combinations and materials properties (based on verifications with FEM)?
- Which are the most important methods currently used to semi-analytically solve post-buckling of thin orthotropic plates and which are their possibilities?
  - Which are the limitations of such methods estimating the displacement field of buckled plates?
  - Can further improvement be made in order to allow more flexibility in the treatment of post-buckling (allow different load combinations, elastically restrained boundary conditions, etc.)?
- How can the previous be used to model the more complex behaviour of a composite stiffened panel?

The objective of this project is the development and verification of a formulation able to solve buckling and post-buckling of thin mid-plane symmetric plates under uniaxial compression using BCs able to reproduce the behaviour imposed by stiffeners. In order to achieve this goal, the following sub-goals have been identified:

- Undergo research in the methods used for buckling of plates and develop a solution procedure.
- Verify the results obtained by such procedure with results obtained with FEM (and with test data if possible). With this verifications define and try to solve the possible limitations of the method.
- Undergo research in the methods used for post-buckling of plates comparing the results obtained by different researchers and choose the most promising in terms of highest possibility to accept different parameters (different boundary condition, material complexity) and achievable accuracy.
- Develop a procedure to calculate the out-of-plane displacement in the post-buckling range.

- Verify the results obtained with FEM and define the limitations of the developed procedure.
- Integrate the developed procedure in the analysis of stiffened panels.

After the research performed, it has been noticed that some additional goals that were not included in the Thesis proposal could be included as well. This has allowed to further extend the scope with the following points:

- Perform further calculations in the post-buckling range (such as in-plane load distribution, first ply failure, etc.) in order to assess plate strength.
- Extend the formulation and verifications to coupe with combined loading.

1.3. Theoretic Background

This following section presents a brief introduction of the theoretic background on plate stability. The objective of this section is putting the topic in context and give useful references for further reading.

1.3.1. Origins Plate Theory

The governing equations of plates have been studied for a long time. The article [3] from Love (in 1887) is considered the first to present a complete theory on elastic thin shells [4], though previous works already existed. Since then, there has been a huge amount of research on this area of mechanics.

One of the most important contributions to plate theory was done by Von Kármán [5]. Von Kármán's theory introduces moderately large plate displacements, making it suitable to solve buckling phenomena. This new theory constitute the foundation for most of the methods used to solve buckling and post-buckling of thin plates.

Both Love and Von Kármán theories share the Kirchhoff hypothesis [6]. Such assumptions allow a quick generalization of the 3 dimensions of the plate into a 2D body, helping in the simplification of the resulting governing equations.

Von Kármán theory was originally introduced for isotropic plates, but was further developed for anisotropic bodies by authors such as Lekhnitskii [7] and Ambartsumyan [8].

Further developments of the Von Kármán equations have allowed to account for additional cases. The most important for this thesis would be the so called Marguerre-Von Kármán equations [9]. These modified governing equations allow the introduction of imperfections in the undeformed plate, necessary to evaluate the post-buckling behaviour of the plate. Its derivation can be consulted from multiple literature, being section 2.10 of Chia's [10] a good source.

1.3.2. Classical Laminate Plate Theory

To cope with composite laminate plates it is necessary to model the material behaviour and introduce it in the formulation. The most extended model is the classical laminate plate theory or CLPT. This theory is based on the Kirchhoff hypothesis and the assumptions of perfect bonding between the layers to derivate the so called ABD matrix. This matrix determines all the relations between loads and moments with plate strains and curvatures.

$$\begin{pmatrix} N_x \\ N_y \\ N_{xy} \\ M_x \\ M_y \\ M_{xy} \end{pmatrix} = \begin{pmatrix} A_{11} & A_{12} & A_{16} & B_{11} & B_{12} & B_{16} \\ A_{12} & A_{22} & A_{26} & B_{12} & B_{22} & B_{26} \\ A_{16} & A_{26} & A_{66} & B_{16} & B_{26} & B_{66} \\ B_{11} & B_{12} & B_{16} & D_{11} & D_{12} & D_{16} \\ B_{12} & B_{22} & B_{26} & D_{12} & D_{22} & D_{26} \\ B_{16} & B_{26} & B_{66} & D_{16} & D_{26} & D_{66} \end{pmatrix} \begin{pmatrix} \epsilon_x^0 \\ \epsilon_y^0 \\ \epsilon_{xy}^0 \\ \kappa_x \\ \kappa_y \\ \kappa_{xy} \end{pmatrix} \quad (1)$$

The derivation of this relation is well known and can be consulted in several reference books. As an example, is remarked the chapter 3 of [11].

In the used formulation of CLPT is included the first non-linear strain terms, accordingly to Von Kármán's theory.

1.3.3. Introduction to Stability

In this section the topic of stability is briefly introduced. For a more detailed introduction see chapter 1 of Jones [12].

A system in equilibrium is defined as stable if a small perturbation produces only a small response, after which it return to its original state. A clear example of such system would be a ball placed in the bottom of a valley (see figure below).

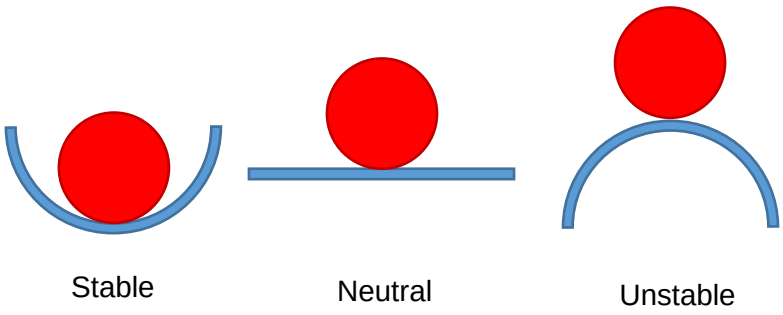

Figure 1: Stability examples

On the other hand, a system in unstable equilibrium would react with a non-small response to a small perturbation and would not return to its original equilibrium position.

In a structural element, the buckling load is the load (or load combination) for which the system changes from a stable to an unstable configuration. In plates, this instability means that the plate changes its original shape to another one which is also stable, known as buckled shape or mode. Due to the stable behaviour of plates under post-buckling, plate deformations are moderate and it is possible to achieve additional buckling modes if the load is kept increasing.

The stability is typically assessed by the study of the second variation of the total potential energy of the system, as followed in Jones [12]. The main point is that when the second variation of the energy is equal to zero there is a point of neutral stability which is typically followed by a change from stable to unstable behaviour.

An alternative procedure, the adjacent stable equilibrium path method can be used with the advantage that it works with the equilibrium equations (first variation of the energy) instead of the stability ones. Ashton and Whitney's [13] develop the approach for plates in

the section 2.7. For mid-plane symmetric plates without out-of-plane loads, the plate before buckling remains undeformed, so the solution of the adjacent method is practically equivalent to the equilibrium equation.

This conclusion is exposed in p.40 of Ashton [13]: " *Actually, the application of the theorem of stationary potential energy in the determination of buckling loads usually proceeds without explicitly considering the second variation of V and U. The criterion for the onset of instability is taken to be the existence of equilibrium solutions other than* $w = 0$ *for zero applied transverse loading. When such solutions are possible (which occurs just at the point of instability) then it is found that an infinity of such non-trivial bent equilibrium configurations exists*."

The equivalence of both approaches for the presented cases explains why many authors determine the stability from the equilibrium equations without further justification.

1.4. Document Structure

This Thesis is divided in 6 chapters. After the introduction, the second chapter introduces a Literature review on analytic and semi-analytic methods for buckling and post-buckling. Chapters 3 and 4 incorporate the main topics of the Thesis, presenting the development of the formulations for buckling and post-buckling, the final solutions obtained and the undergone verifications. The next chapter extends the analysis developed for plates to stiffened panels. Finally, chapter 6 gathers the final conclusions and recommendations.

2. Literature review

This literature review covers different theories used in the study of plate stability, focusing on the objectives developed for this Thesis. First, brief introduction on the topic is presented. Then the state of the art procedures used to solve buckling and post-buckling of composite laminated plates are reviewed. Additional topics have been also been briefly developed at the end of this chapter.

The purpose of this thesis is to study and develop analytical and semi-analytical solutions, so the further review will be limited to such cases when necessary.

2.1. Introduction

The determination of stability phenomena is of crucial importance in structural design due to multiple reasons. Some structural elements behave badly after their critical buckling load (first load for which the element equilibrium becomes unstable). For example, in beams, loads above buckling typically result in very large deformations which cause the immediate failure of the element. The reason of this phenomenon is that beams usually[1] have stable but close to neutral post-buckling behaviour. In such cases the stability analysis can typically be limited to the study of their critical buckling load as this value can be taken as the ultimate load of the element.

However, the post-buckling behaviour in plates is more stable, resulting then in more moderate deformations and typically allowing important post-buckling capabilities after a load redistribution. In this case, the proper study of the stability will require a more advanced analysis including the non-linear behaviour after the critical buckling load. All the same, it is always a good idea to start solving first the buckling loads and modes and then progress to analyse the post-buckling behaviour.

Most of the studied articles in buckling and also post-buckling are based on the Von Kármán governing equations for plates presented in [5]. As it has been already mentioned, those equations are built over the Kirchhoff hypothesis which assume that the mid-section of the plate can be used to describe the 3D state of the plate [6]. This provides a good approximation for thin plates and is a generalization of the work done by Euler and Bernoulli in beam theory (as shown in Timoshenko's [14][2]).The use of the Von Kármán equations simplify significantly the problem and allow an easier analytical approach.

[1] In their most simple configurations such as hinged-hinged ends.
[2] Euler and Bernoulli developed their theory around 1750. Timoshenko in his book explains this theory among others and further develops it.

2.1.1. Isotropic and anisotropic materials

Before starting with the different procedures and solutions available in the literature, it is important to review the different models used to define the material behaviour.

The fact that the resolution of Von Kármán equations is easier for isotropic materials (together with the fact that were originally derived for such materials) resulted in the first procedures and solutions being obtained for this more limited cases. Later, formulations were typically further developed to account for more complex material behaviour.

The introduction of the fiber reinforced laminated composites are the most important example of materials with a more complex behaviour. However, solutions were also sought before to solve wood or wood laminated structures, as shown in Lekhnitskii [7]. It has already been commented in section 1.3.2 that composite laminates can be successfully modelled through the use of CLPT.

It is useful to distinguish between different types of laminates depending on their degree of anisotropy and the resulting ABD matrix obtained from CLPT. This practice allows different degrees of complexity in the formulations. Apart from isotropic materials three different categories are distinguished in this Thesis (similarly to reference [15]).

- **Specially Orthotropic laminates**: These laminates are characterized for their mid-plane symmetry altogether with no coupling between bending and twisting moments. In such cases all the terms in the B matrix are always 0, as well as components D_{16} and D_{26}. These laminates present orthotropic behavior in the principal directions, which simplifies the required formulation. However, only very specific layups present this behaviour.
- **Mid-plane symmetric laminates**: This category includes all the laminates with a symmetric layup with resect to their mid-plane, therefore presenting $B_{ij} = 0$. Symmetric laminates are widely used because of the uncoupling between in-plane and out of plane forces and deformations.
- **General laminates**: This category includes any possible laminate following the assumptions of CLPT. The different coupling existent make them very difficult to analyze and even to manufacture. Due to their most limited use and complexity, its formulation will not be included in the solution procedures presented in this Thesis.

Chapters 2 and 3 of Whitney [15] give an idea of the degree of complexity reduced by limiting the formulation to mid-plane symmetric plates. In the Von Kármán equilibrium equation the in-plane and bending problems become uncoupled. Otherwise, with ($B_{ij} \neq 0$) the equilibrium equation is:

$$
\begin{aligned}
D_{11}\frac{\partial^4 w}{\partial x^4} + 4D_{16}\frac{\partial^4 w}{\partial x^3 \partial y} + 2(D_{12}+2D_{66})\frac{\partial^4 w}{\partial x^2 \partial y^2} + 4D_{26}\frac{\partial^4 w}{\partial x \partial y^3} + D_{22}\frac{\partial^4 w}{\partial y^4} \\
- B_{11}\frac{\partial^3 u_o}{\partial x^3} - 3B_{16}\frac{\partial^3 u_o}{\partial x^2 \partial y} - (B_{12}+2B_{66})\frac{\partial^3 u_o}{\partial x \partial y^2} - B_{26}\frac{\partial^3 u_o}{\partial y^3} \\
- B_{16}\frac{\partial^3 v_o}{\partial x^3} - (B_{12}+2B_{66})\frac{\partial^3 v_o}{\partial x^2 \partial y} - 3B_{26}\frac{\partial^3 v_o}{\partial x \partial y^2} - B_{22}\frac{\partial^3 v_o}{\partial y^3} \\
= q + N_x\frac{\partial^2 w}{\partial x^2} + 2N_{xy}\frac{\partial^2 w}{\partial x \partial y} + N_y\frac{\partial^2 w}{\partial y}
\end{aligned}
\tag{2}
$$

The main difficulties imposed by the formulation for general laminates are:

- It is necessary to deal with more unknowns, u and v must be solved as well, so it is necessary to introduce functions to reproduce their behaviour and the extra degrees of freedom will have to be solved when the Galerkin or Ritz methods are applied.
- Formulation becomes more extended. Transform the differential equations into ordinary equations does not only require a bigger system of equation (to cope with the new degrees of freedom) but also every equation has more terms with more integrations to be carried, resulting in significantly increased computation time
- The approximation of the out-of-plane function for the different boundary conditions becomes more challenging due the coupling between in-plane and bending behaviour.

2.2. Buckling

This section reviews the State of the Art on buckling of plates. The solutions achieved by different authors have been classified depending on their form. In the first category, closed form solutions are considered. Those include the expressions which can be evaluated in a finite number of operations. In such solutions the dependency between the result and the variables is immediately clear. In the second category are included the semi-analytical solutions. Those solutions are developed from the analytical formulation of the problem, but their complexity makes it necessary to numerically evaluate some steps. The intermediate steps make it more difficult seeing the exact relation between the variables and the result.

2.2.1. Closed form solutions

Analytical approaches for buckling of thin plates have been widely studied by many different authors. Starting from Von Kármán equations, it has been possible to find closed form solutions for buckling under different conditions. However, not all closed form solutions have been obtained using the same method or have the same accuracy.

2.2.1.1. Exact closed form solutions

Those solutions are based on the use of expressions that exactly solve the governing equation of the problem, as well as the boundary conditions. Such solutions are difficult to find by, due to the relative complexity of the Von Kármán equations. The most important examples are the solutions for simply supported plates under uniaxial or biaxial loading for isotropic plates, as presented in Timoshenko's [14], or specially orthotropic in Lekhnitskii

[7]. Those solutions are well known and have been presented in most of the literature that reviews the topic, for example [11, 12, 15].

It must be acknowledged that the exact solution of the governing equations does not mean the solution is perfect. Several assumptions have been done to develop such formulation (for example Kirchhoff hypothesis) so the Von Kármán equations are still an approximate model of the reality.

2.2.1.2. Approximated closed form solutions

Sometimes it is possible to find expressions that do not solve exactly the governing equation and the boundary conditions, but which are able to approximately solve them under different conditions. A great amount of literature can be found treating such solutions due to their usefulness in giving quick approximate solutions. Once again [7, 12, 14] gather several approximate solutions, including different boundary conditions (specially simply supported or clamped) and also shear loading. Whitney also gathers several approximate closed form solutions [15]. Among those it can be highlighted the solution for simply supported in two edges and elastically restrained in the other two, as it is a good approximation to solve buckling in stiffened panels. Kassapoglou also gathers several approximate solutions for different BCs combinations and different load combinations [11].

There has also been extensive research on using semi-analytical approaches to find solutions for more general cases, but using one term approximation to achieve closed form solutions. This approach is followed by Kollar [16] using Ritz method.

Bisagni and Vescovini also arrive to closed form solutions for buckling under uni-axial compressed plates with elastically restrained unloaded edges by different procedures such as Kantorovich, Ritz and Galerkin [17, 18].

It is interesting to point out the range of accuracy obtained by the approximated close form solutions in comparison with FEM results. Kollar [16] claims that the maximum error obtained is below 8%. Bisagni and Vescovini find different accuracies depending on the methods and the formulations used. Using Galerkin in [18] the maximum error obtained ranges between 2 and 4 % depending on the BCs, while in [17] the error is higher, mainly because the verification is performed with a stiffened panel instead of an individual plate (below 8% for Kantorovich and 13% for Ritz).

2.2.1.3. Fitted closed form solutions

A third group of closed form solutions is based on the numerical fitting of a known set of solutions. This has been a typical approach in metals, where the isotropy of the material makes it easy to distinguish between different materials with a minimum set of variables (typically the Young modulus and Poisson). Books like Bruhn [19] and Niu [2, 20] use such approach and organize the solutions in design curves. Those curves are usually based on empirical data, however Paik [21] uses numerically obtained solutions to extend design curves to isotropic plates with elastically restrained edges. Such approach is an example of the suitability of closed form solutions even when some accuracy is lost during fitting. The higher number of variables in composite laminated plates limits the usefulness of such approach.

Unfortunately, closed form solutions are typically limited to isotropic or specially orthotropic plates, being difficult to find closed form solutions in the literature for mid-plane symmetric plates. Moreover, short plates under shear (or combined loading) are also difficult to come by. These are the main reasons that has motivated the further study of semi-analytical solutions.

2.2.2. Semi-analytical solutions

In this group have been included the solutions based on the analytical resolution of the Von Kármán governing equations, but where the use of series and their numerical evaluation have resulted in non-closed forms (such solutions are usually implemented in computer programs).

Further works have been done in the study of local instability of beam's flanges (or crippling). In those cases the flanges are modelled as plates with an elastically restrained edge at their connection with the rest of the beam. This approach is basically analogous to the one used in elastically restrained plates. An example of such approach is Bank's [22] using Kantorovich method. This method is based on the Newton-Kantorovich theorem [23], an iterative convergent procedure to reach the desired solution. Additionally Qiao in [24] also studies similar cases but using the Ritz method instead. It is interesting how the torsional stiffness is calculated for different beam sections. However, despite the interesting points shown, a drawback of the given formulations by these articles is that they only contemplate uniaxial compression as it's the typical load case in beams.

Whitney in [15] develops the formulation for mid-plane symmetric plates under any constant in-plane load combinations for both Galerkin and Ritz methods. Such formulations allow the resolution of the problem for simply supported and clamped BCs, but can be extended to the intermediate cases (elastically restrained edges), as seen in Chen and Qiao [25] only for shear loads. The verification performed in this last work shows the potential of such methods. Using a maximum of 36 terms to approximate the out-of-plane displacement, a maximum error below 2% is achieved (taking into account that laminates are not limited to specially orthotropic).

The impossibility to find a completely developed formulation suitable for the requirements of this Thesis has motivated the development of a new one, mainly based on the work presented by the last two references. In chapter 3 the solution for Buckling is presented in detail. The different approaches used are developed together with an extended study of the validity of the obtained solutions.

2.3. Post-buckling

Post-buckling of plates has been studied extensively in the literature as it allows the design of structures with higher specific strength. An example of such a case are the so called Wagner beams. The flange of the Wagner beams consists of thin shear plates capable of holding integrity after buckling thanks to the vertical chords (a detailed explanation of Wagner beams is presented in chapter C.11 of Bruhn [19]).

During post-buckling plates ideally show a linear behaviour until they reach the critical buckling load over which out-of-plane displacements appear and take important values, as presented in figure 2.

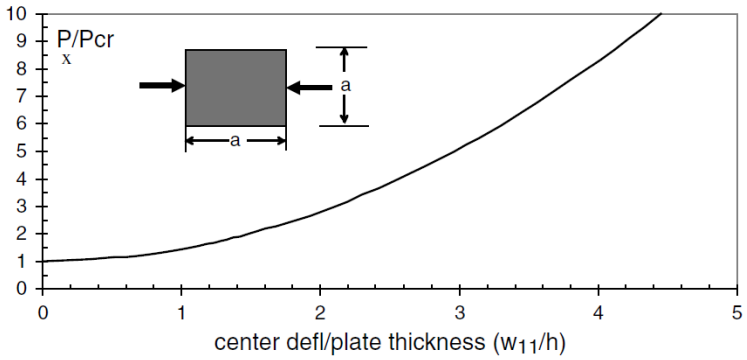

Figure 2: Typical out-of-plane displacement trend of a plate during post-buckling, figure 7.7 from [11]

The literature studied focuses in the solutions developed for stiffened panels as the implementation of design tools for such panels is the main motivation of this Thesis. Once again the studied literature has been divided into closed form and semi analytical solutions.

It should be kept in mind that buckling analysis is linear whereas post-buckling is fundamentally nonlinear. The load redistribution due to the new shape makes it necessary to solve also the compatibility equation (also called second Von Kármán equation) and introduce the Airy stress function. This second equation couples in-plane and out-of-plane behaviour.

This coupling was avoided during linear buckling with the limitation to mid-plane symmetric plates, however, during post-buckling coupling is impossible to avoid due to the existence of the load redistribution. However, the required formulation is still way simpler than for arbitrarily laminated plates.

The reason of the load redistribution during post-buckling is straightforward. The out-of-plane displacement alters the local stiffness of the plate. The curvature in the plate reduces the capacity to transfer loads through the axial stiffness, therefore, part of the load starts to be transferred through the bending stiffness (which for thin plates takes lower values). For a square, simply supported plate, the deflection and curvature are more important at the center, while the edges remain straight. Therefore, the local stiffness at the edges is higher and the load is attracted to them. In the following figure, we have an example from Chapter 7 of Kassapoglou [11] with an analytical solution of how this redistribution evolves with the PB ratio.

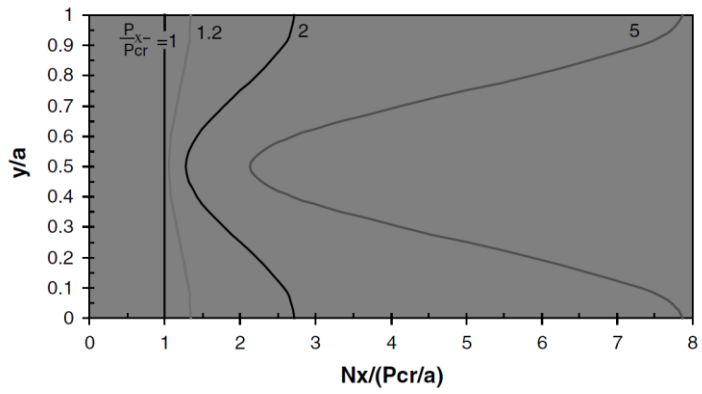

Figure 3: Edge force redistribution during post-buckling, figure 7.8 from [11]

2.3.1. Closed form solutions

The increasing complexity of post-buckling in comparison with buckling reduces the amount of closed form solutions available in the literature. Moreover, those (at the best knowledge of the author) are limited to approximate expressions, as exact solutions are not possible to come by.

The studied available solutions are mainly based on one term approximations, which in some simplified cases has shown their ability to reproduce meaningful solutions.

Kassapoglou in [11] (chapter 7) introduces a one term approximation for both the out of plane and the airy stress function to solve simply supported, square, specially orthotropic plates; achieving a closed form expression (see eq. 3) that has proved to work well under such conditions.

$$w_{11} = \sqrt{\frac{16A_{11}A_{22}(D_{11} + 2(D_{12} + 2D_{66}) + D_{22})}{(A_{11}A_{22} - A_{12}^2)(A_{11} + 3A_{22})} \left[\frac{P_x}{\frac{\pi^2}{a}(D_{11} + 2(D_{12} + 2D_{66}) + D_{22}) \left(1 + \frac{A_{12}}{A_{11}}\right)} - 1 \right]} \quad (3)$$

Kassapoglou's equation has been further developed in chapter 4 to account for any bi-axial load combination and number of half-waves, and has been used to compare against FE and semi-analytical solutions. Therefore, more conclusions on its accuracy will be drawn in the chapter. However, it has not been possible to generalize such solution to different BCs.

More complex post-buckling cases are approximately solved by Bisagni and Vescovini for uniaxial compression in [18] using the most relevant out of plane displacement term (obtained previously from the linear buckling analysis). Marguerre-Von Kármán equations [9] are used in order to allow initial imperfections and avoid numerical problems at the neighbourhood of the bifurcation point. The developed formulation made possible to solve plates with two elastically restrained edges to simulate the effect of stiffeners. The verification performed in this article shows the higher amount of variables to be considered. Out of plane displacement, axial stiffness and stress distribution are highlighted. Very good values are obtained in general (especially taking into account it is an approximate closed form solution), only surpassing 10% maximum error in the determination of the stresses.

It must be remarked the fundamental difference between the two methods. Kassapoglou's is based on the direct approximate resolution of the governing equations while Bisagni and Vescovini relay on the Galerkin method to numerically approximate the result.

Closed form solutions also exist for post-buckling under shear for specially orthotropic plates with high aspect ratio, Mittelsted [26]. Due to the approximations made to obtain a closed form expression, the solutions obtained are only accurate for relatively low PB ratios.

2.3.2. Semi-analytical solutions

Post-buckling has been mainly studied through semi-analytical solutions, since closed form ones exist for very limited cases. The presented works use the Marguerre-Von Kármán equation due to the aforementioned reasons.

Chia [10] presented in his book multiple semi-analytical solutions for isotropic and anisotropic plates (not limited to mid-plane symmetric laminates) in uniaxial and biaxial compression under different boundary conditions. The important amount of cases covered and methods used (Galerkin, Ritz, etc.) have influenced a great deal of further work, becoming a common reference on post-buckling of plates.

For isotropic materials Byklum [27] developed a model for stiffened panels using Ritz and allowing combined loading. It is very interesting how the Airy stress function (ϕ) is approximated with a group of terms accounting for the constant in plane loads and a double cosine series that introduces the effect of the load redistributions.

$$\phi(x,y) = -\frac{N_x y^2}{2} - \frac{N_y x^2}{2} - N_{xy} xy + \sum_{0}^{2M}\sum_{0}^{2N} f_{mn} \cos\left(\frac{m\pi x}{a}\right)\cos\left(\frac{n\pi y}{b}\right) \tag{4}$$

Where $f_{00} = 0$.

This Airy stress function presented is able to reproduce the stress distribution produced by loads applied with constant displacement (the edges are kept straight). Analogous Airy stress function has been used for laminated materials, in fact, the exposed Kassapoglou's closed form solution for post-buckling (eq. 3) is based on the same Airy stress function but only taking the first two non-zero terms.

This analysis was extended to mid-plane symmetric plates by Romeo and Frulla using the Galerkin method [28]. Similarly to Chia´s work, the Airy stress function is based on keeping the forces applied along the edges constant. The in-plane forces can be obtained deriving the Airy Stress function:

$$N_x(x,y) = \frac{\partial^2 \phi(x,y)}{\partial y^2}, \qquad N_y(x,y) = \frac{\partial^2 \phi(x,y)}{\partial x^2}, \qquad N_{xy}(x,y) = -\frac{\partial^2 \phi(x,y)}{\partial x \partial y} \tag{5}$$

The Airy stress function has then the following form:

$$\phi(x,y) = -\frac{N_x y^2}{2} - \frac{N_y x^2}{2} - N_{xy} xy + \sum_{1}^{M}\sum_{1}^{N} f_{mn} X_m Y_n \tag{6}$$

To vanish the terms for load redistribution at the edges the chosen functions must verify:

$$X_m(0) = X_m(a) = Y_n(0) = Y_n(b) = 0 \;\forall\; m \; and \; n$$
$$X'_m(0) = X'_m(a) = Y'_n(0) = Y'_n(b) = 0 \;\forall\; m \; and \; n \tag{7}$$

The main problem of this approach is that if N_x, N_y and N_{xy} are taken as constant values (which simplifies greatly the formulation and is typically the case) then the stress distribution is analogous to constant load application. However, in a stiffened panel the beam members keep approximately straight and distribute the load on the panels keeping constant displacement.

Therefore, after realizing so, Romeo and Frulla modified their formulation in [29] and used the same approach as Byklum [27] for the Airy stress function (however, dropping the possibility of shear loading). The main difference with Byklum's approach consists on the way the compatibility equation is solved. For isotropic or specially orthotropic laminates it is possible to explicitly solve the f_{mn} terms after substituting the out of plane displacement in the compatibility equation. However, Romeo and Frulla, by using Galerkin on the compatibility equation as well, are able to work with more complex out of plane displacement equations and introduce the possibility to work with any mid-plane symmetric laminate.

Romeo and Frulla, due to the limited experimental results available, build a test set-up to verify their solution. Results are very interesting as they highlight the main problems and point out the possible source of errors. In article [28] they claim the results obtained are only accurate for small post-buckling ratios (up to 1.5) and suggest that mode changing and the fact that the machine uses displacement controlled loading (while the formulation used is based in constant applied load), are the main sources of error. In [29], the new formulation is compared with the old one (load controlled) and the experimental results, yielding better results. The main source of error is claimed to be the load redistribution caused by the stiffeners in the test.

Shin [30] worked with simpler post-buckling cases (uniaxial compression and hinged BCs) for displacement applied load. However, it is interesting the use of truncated series to improve the computational efficiency of the method. Moreover, the problematic of mode changing is discussed.

Bisagni and Vescovini also presented different works using semi-analytical solutions for elastically restrained plates on two edges using the Ritz method [31]. By not limiting the formulation to closed form solutions, they were able to extend the possibilities to combined loading and mid-plane symmetric laminates. Similarly to Byklum [27], the formulation is developed for stiffened panels and accounts for the compatibility of displacements between the different members of it. Moreover, an arc length solver is used for the nonlinear system of equations to be able to capture mode jumping. Verifications are performed with FEM and experimental results showing good agreement in the mode prediction and focusing in the remaining stiffness of the plates in a stiffened panel after buckling.

A solution for plates under similar conditions is developed by Beerhorst in [32] when they can be considered infinitely long. Verifications shows good results but is pointed out the limitation of Von Kármán equation with thick laminates (when transverse shear cannot be neglected).

The modelling of the elastically restrained edges is usually done by approximating the stiffeners to a constant torsional stiffness introduced along the edge of the plate. For the idealized cases (torsional stiffness 0 or infinite) this becomes the well-known simply supported and clamped situations. However, the stiffener does not constantly restrain the torsion along the plate's edge, and it also provides transverse stiffness. Therefore, Stamatelos in [33] introduces a more complex formulation to account for those extra effects (see figure 4). The differences introduced by using different models will be studied in Chapter 6.

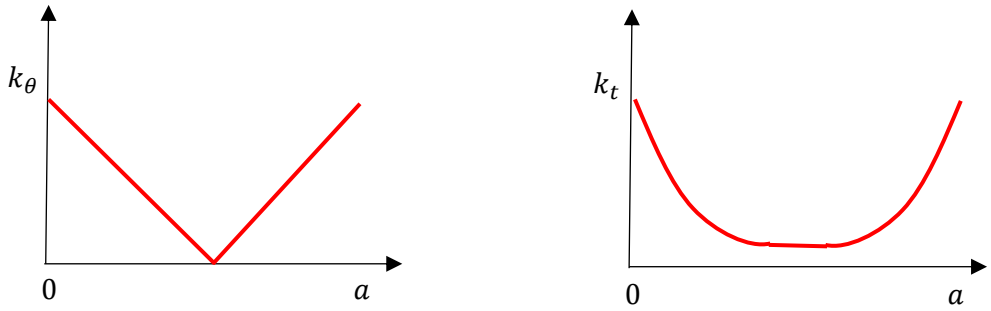

Figure 4: Torsional and transverse stiffness as introduced in Stamatelos [33]

It is difficult to compare the accuracy gained by this approach as solutions are given for whole stiffened panels.

Further improvement in the possibilities of the boundary conditions of elastically restrained plates is presented by Qiao in [34]. The developed formulation is based on the same approach as Romeo and Frulla's [28]. However, by using a linear interpolation between the beam eigenfunctions for simply suported and clamped BCs, Qiao is able to solve the problem for the intermediate cases (torsional springs). The procedure is similar to the ones presented by Vescovini and Bisagni but allowing elastic restrains in all edges. Achieved solutions show almost perfect agreement with FEM using a fraction of computational power.

The main limitation of the work presented is that, by using also the same approach for the Airy stress function as [28], the method is not able to account for the load redistribution introduced by the stiffeners when keeping the edges of the plate straight (load applied as constant displacement). It has been seen in the development of a post-buckling formulation (chapter 4) and verification presented in [29] that the approaches (using Airy stress function from eq. 4 or 6) give completely different results.

A modified formulation is proposed in chapter 4, accounting for different loading possibilities (load and displacement controlled) aiming to cover all the possible cases covered by the developed buckling formulation (chapter 3).

2.4. Plate Strength

The possibilities of developing a plate strength analysis from the post-buckling results is of great interest. The resolution of the Airy stress function and the deformed shape can be used to obtain the stress and strain distribution for every ply of the laminate. First ply failure

analysis can be then developed in a straight forward way as presented, for example, in chapter 4 of [11].

Plate strength has been applied in semi-analytical post-buckling analysis before, such as Yang and Hayman [35]. In this publication progressive damage propagation is also studied (in addition to first ply failure), modifying either the stiffness of the whole damaged ply or only the region of the failure. Such approach is out of the scope of this Thesis but shows the possibilities of coupling plate stability with strength analysis.

2.5. Stiffened Panel Integration

Many of the reviewed solutions aim at solving stiffened panels also. It has been pointed out that the inclusion of more complex BCs, like torsion springs, appeared as a simple way to model stiffeners. Several of the articles reviewed [17, 27, 29, 31, 33] presented verifications against stiffened panels instead of only individual plates.

Vescovini and Bisagni put special attention in the calculation of the remaining stiffness of the buckled plate in all the articles reviewed [17, 18, 31]. This variable is very important to recalculate the load distribution between the plates and the stiffeners once the plates have buckled. It has been seen that successive buckling modes reduce even more the stiffness of the plates.

Most of the literature found describes the torsional restrain provided by the stiffeners as a function of their torsion stiffness *GJ*, therefore it has been necessary to research a convenient method to find this value for composite laminated beams.

Vlasov [36] developed a theory for isotropic thin-walled beams, including open and closed sections. The theory was further extended to account for orthotropic beams by Ever [37]. Laminated composite beams with arbitrary lay-up where included by Kollar in [38]. This last work provides the additional level of generality required. Shear deformation and warping are neglected which can result in inaccurate results in some cases, as analysed by Pluzsik in [39]. Salim [40] included this phenomenon in his formulation, but the increasing complexity of the solution might not be attractive for the required application (no longer closed form).

Stamatelos [33] accurately described the way to calculate the elastic restrain the stiffeners provide. He defined the elastic restrain against rotation as a function of torsional stiffness *GJ* of the adjacent stiffeners, and the transverse stiffness (out-of-plane) as a function of their bending stiffness *EI* with the following equations:

$$k_{i1}(x) = \begin{cases} \dfrac{48EI_z}{x^3}, & x \le \dfrac{a}{2} \\ \dfrac{48EI_z}{(a-x)^3}, & x > \dfrac{a}{2} \end{cases} \quad k_{i2}(x) = \begin{cases} -\dfrac{2GI_p x}{a} + GI_p, & x \le \dfrac{a}{2} \\ \dfrac{2GI_p x}{a} - GI_p \quad , & x > \dfrac{a}{2} \end{cases} \tag{8}$$

Similar approaches were used in [21, 27].

Vescovini and Bisagni in [17] defined the restrain as De Saint Venant torsional bars using half the torsional stiffness *GJ* of the surrounding stiffener (half for every plate at each side). Paik [21] used also half *GJ* of the stiffener to represent that both plates at each side had to be restrained. Other alternatives to see how the torsional stiffness of the stiffener is distributed among the plates are based on more complex approaches where the stiffeners

are included (as beams instead of as boundary conditions). Then the elastic restrain is solved imposing the compatibility of displacements between the different members.

The method developed in this report works with any arbitrary constant elastic torsional restrain along every edge of the plate, using a model developed for 1D beams. As in most of the literature found, the transverse stiffness is not taken into account assuming that the out-of-plane displacement is zero (corresponding to an infinite bending stiffness). Most of the authors take this assumption as valid without further considerations (as far as there is no instability of the stiffener), however it is evident that for stiffeners with bending stiffness tending to zero, this displacement cannot be neglected. Mittelstedt in [41] works with no out-of-place displacement at the edges, but defines a minimum bending stiffness EI for which this assumption is a good approximation.

Most of the articles use constant torsional elastic restrains along the edge. De Saint Venant model has the important inconvenience of adding significant complexity on the boundary conditions. The moment generated by such restrain depends on a cross derivative of the out-of-plane function with the two in-plane directions, therefore coupling them. The solutions studied using this method [17] have coped with this problem by applying the restrain in only two edges, so the buckled shape in the perpendicular direction to the restrains is already known (more precisely, it has been already approximated with the coupling introduced by Saint Venant model neglected). The necessity of making approximations at some point and having elastic restrains in all 4 edges has motivated the generalized use of constant torsional springs along the edge.

Despite being a commonly used model, authors have had difficulties to establish a good relation between the torsional stiffness of the stiffener and the boundary conditions modelled as constant torsional springs. Tarján in [42] works with both De Saint Venant beams and torsional springs using a semi-empirical formulation for the restrain. Linking both approaches is possible to get a relation between *GJ* and the torsional spring stiffness *k*. However, this approach has been shown to provide very limited accuracy.

$$\frac{1}{1+\frac{10D_{22}}{k_x b}} = \frac{1}{1+0.61\left(\frac{D_{22}b}{GI_x}\right)^{1.2}} \tag{9}$$

Vescovini and Bisagni in [18] used the work developed by Mittelstedt [43] to establish the relation between *GJ* and *k* is defined for closed hat stiffeners. The usefulness of the method is limited since it was developed for a specific type of stiffener. Moreover, during the verifications performed by Mittelstedt, the method seems to over constrain the plate, resulting in not too accurate results.

Shan [24] also indicated how the elastic restrains could be calculated, however, the article intends to describe the elastic restrains between the flanges of composite beams. He found that the restrain depends on the ratio between the buckling load of the restrained flange and the buckling load of the restraining flange. Is not really clear that the approach can be extrapolated to stiffened panels.

Vescovini and Bisagni in [31] introduced a more complex method to link *GJ* and *k* for post-buckling of plates. The proposed solution solves the linear buckling of a section of the

stiffened panel, including the stiffeners in the derivation of the total potential energy (modelling the stiffeners flanges with plates). The restrain between the different elements is imposed with the use of a penalty term that ensures the compatibility of displacements between the different elements. Finally, the post-buckling behaviour is solved for a model with constant torsional springs, where their value is obtained with an iterative calculation to match the buckling load of the first models.

Since a solution with the desired accuracy has not been found in the literature, a new method will be developed based on matching the energy stored by the restrain provided by De Saint Venant bars and constant torsional springs. This method intends to be a simpler approach than the one shown in [31], however it uses the same assumption that the post-buckling solution given by De Saint Venant torsional bars and torsional springs are equivalent if both models have the same critical buckling load.

2.6. Research conclusions

During the literature research, different analytical solutions for buckling and post-buckling have been studied and their capabilities and limitations analyzed. It has been concluded that current closed form solutions are not able to cope with all the cases required due to the complexities introduced by including mid-plane symmetric laminates, elastic restrains and shear loading.

Under such conditions, it has been seen that semi-analytical formulations present several advantages and that the work done by several authors can be used to build a new formulation that can adapt to the necessities expressed by Fokker for this project.

The solution of plates have been typically linked to the solution of stiffened panels. However, there is no consensus on how the elasic restrain provided by stiffeners and frames should be imposed in the boundary conditions of the individual plates.

3. Buckling of plates

This chapter presents the solution developed to solve buckling of thin rectangular mid-plane symmetric plates. As it has been presented during the literature review, multiple closed-form solutions exist for linear buckling, especially when the plate is either isotropic or specially orthotropic. However, the objective of this thesis is to deal with more general configurations that are of interest in industry applications, including combined loading and elastically restrained boundary conditions.

First, the semi-analytical model developed is described. Afterwards, a brief description of the FE model used to compare results is also presented. Finally, the agreement between both methods is studied in order to verify the accuracy of the semi-analytical solution. The limitations and conclusions reached are summarized in the last section.

3.1. Semi-analytical model

3.1.1. Introduction

The objective of this thesis is to develop a proper general solution for buckling and post-buckling of plates. It has already been mentioned, that it is intended to overcome the present limitations of existent closed form solutions in order to solve more complex problems. The main features of the proposed formulation are the possibility to work with multiple loading, the proper modelling of bending-twisting terms (mid-plane symmetric model) and the use of elastic torsional restrains along all the edge as boundary conditions. These last, ought to be able to reproduce any restrain between simply supported and clamped in order to model plates constrained by stiffeners, since plates usually appear as part of stiffened panels in common aerospace applications.

The semi-analytical model section has been divided in three sub-sections. After the introduction, the energy formulation required to derive the stability equations is presented. Finally, the stability analysis and the proposed solutions are developed.

3.1.1.1. Assumptions

First the assumptions for thin laminated anisotropic plates are introduced[3]:

- The plate is built from arbitrary number of orthotropic layers perfectly bonded.
- The thickness of the plate t is much smaller than the other two dimensions.
- Displacement are moderate.
- In-plane strains are small.
- The first order non-linear terms involving products of stresses and plate slopes are reatained in the equations of motion.

[3] The assumptions are based on the section 2.1 of Whitney [15]. However, such assumptions are analogous to thin plate theory for laminated anisotropic plates.

- Plate follows Kirchhoff classical assumptions:
  - Transverse shear strains are negligible.
  - In-plane displacements u and v are linear functions of the out-of-plane coordinate z.
- Transverse normal strain is negligible.
- Transverse shear stresses vanish on the surfaces.
- Plate has constant thickness.
- Every layer follows Hooke's Law and is orthotropic.
- There are no body forces acting on the plate.
- Rotatory inertia is negligible.

Additional assumptions:

- Only constant in-plane loads are considered. The formulation could be adapted to include non-constant in-plane loads, however, the integration of the terms in the Galerkin and Ritz methods would become more complex.
- Plates are mid-plane symmetric. The lay-up of the plate is symmetric so all the terms of the B matrix are equal to zero.
- Quasi-static loading. No dynamic effects are considered.
- The plate has no imperfections (this assumption is discarded for post-buckling analysis).
- Edges keep straight (this assumption is discarded for post-buckling analysis under constant applied loading).
- The boundary conditions of the plate are idealized as a set of linear torsional springs along the edges. The torsion coefficient at every edge can vary from zero (simply support) to infinite (clamped).

3.1.1.2. Sketch of the proposed model

The following figure shows the proposed plate sketch for buckling and post-buckling.

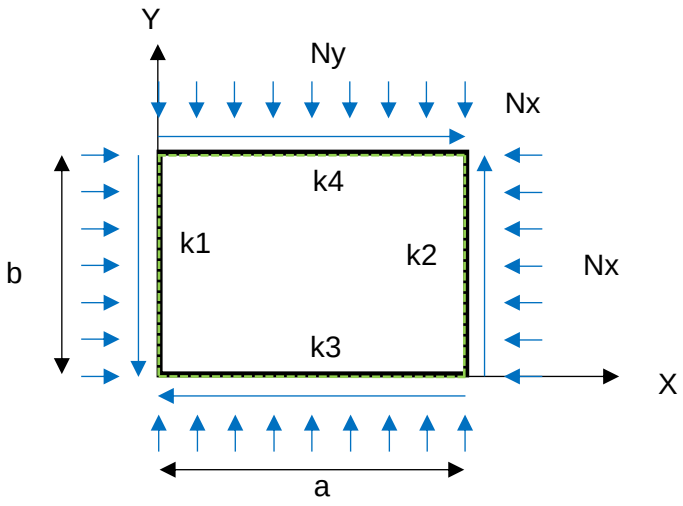

Figure 5: Sketch of the plate geometry, boundary conditions and loads

The plate has a rectangular shape of dimensions a, b. The applied in-plane loads on the edges are constant. N_x and N_y are the axial loading (positive in compression) and N_{xy} is the shear loading. The boundary conditions consist on torsional springs of constant value k_i along the edge. Although, values are independent between edges, making it possible to reproduce fairly complex boundary conditions. Additionally, the out-of-plane displacement of the edges is restricted while leaving the in-plane free.

3.1.2. Energy formulation

Classical stability theory is based on the energy state of the system, therefore the more rigorous way to approach buckling is by determining the different terms that contribute to the energy of the plate and what their variations are.

The required terms for buckling are the strain energy and the potential energy of the external loads, which give the total potential energy of the plate.

The strain energy is calculated from the volume integral of the scalar product between stress and strain matrices. In laminated plates in plane stress it is taken advantage of the ABD matrix to simplify the expression to:

$$\begin{aligned} U = \frac{1}{2}\iint \Bigg\{ & A_{11}\left(\frac{\partial u_o}{\partial x}\right)^2 + 2A_{12}\frac{\partial u_o}{\partial x}\frac{\partial v_o}{\partial y} + A_{22}\left(\frac{\partial v_o}{\partial y}\right)^2 \\ & + 2\left(A_{16}\frac{\partial u_o}{\partial x} + A_{26}\frac{\partial v_o}{\partial y}\right)\left(\frac{\partial u_o}{\partial y} + \frac{\partial v_o}{\partial x}\right) + A_{66}\left(\frac{\partial u_o}{\partial y} + \frac{\partial v_o}{\partial x}\right)^2 \\ & - B_{11}\frac{\partial u_o}{\partial x}\frac{\partial^2 w}{\partial x^2} - 2B_{12}\left(\frac{\partial v_o}{\partial y}\frac{\partial^2 w}{\partial x^2} + \frac{\partial u_o}{\partial x}\frac{\partial^2 w}{\partial y^2}\right) - B_{22}\frac{\partial v_o}{\partial y}\frac{\partial^2 w}{\partial y^2} \\ & - 2B_{16}\left[\frac{\partial^2 w}{\partial x^2}\left(\frac{\partial u_o}{\partial y} + \frac{\partial v_o}{\partial x}\right) + 2\frac{\partial u_o}{\partial x}\frac{\partial^2 w}{\partial x \partial y}\right] \\ & - 2B_{26}\left[\frac{\partial^2 w}{\partial y^2}\left(\frac{\partial u_o}{\partial y} + \frac{\partial v_o}{\partial x}\right) + 2\frac{\partial v_o}{\partial y}\frac{\partial^2 w}{\partial x \partial y}\right] \\ & - 4B_{66}\frac{\partial^2 w}{\partial x \partial y}\left(\frac{\partial u_o}{\partial y} + \frac{\partial v_o}{\partial x}\right) + D_{11}\left(\frac{\partial^2 w}{\partial x^2}\right)^2 + 2D_{12}\frac{\partial^2 w}{\partial x^2}\frac{\partial^2 w}{\partial y^2} \\ & + D_{22}\left(\frac{\partial^2 w}{\partial y^2}\right)^2 + 4\left(D_{16}\frac{\partial^2 w}{\partial x^2} + D_{26}\frac{\partial^2 w}{\partial y^2}\right)\frac{\partial w^2}{\partial x \partial y} \\ & + 4D_{66}\left(\frac{\partial w^2}{\partial x \partial y}\right)^2 \Bigg\} dx\, dy \end{aligned} \tag{8}$$

For mid-plane symmetric plates $B_{ij} = 0$, therefore in-plane and out-of-plane variables become uncoupled. The separated terms are identified as membrane and bending energy respectively. For pure bending problems, the membrane energy can be considered as an arbitrary constant that will cancel out when its variation is considered.

$$U_b = \frac{1}{2}\iint \left\{ D_{11}\left(\frac{\partial^2 w}{\partial x^2}\right)^2 + 2D_{12}\frac{\partial^2 w}{\partial x^2}\frac{\partial^2 w}{\partial y^2} + D_{22}\left(\frac{\partial^2 w}{\partial y^2}\right)^2 + 4\left(D_{16}\frac{\partial^2 w}{\partial x^2} + D_{26}\frac{\partial^2 w}{\partial y^2}\right)\frac{\partial w^2}{\partial x \partial y} + 4D_{66}\left(\frac{\partial w^2}{\partial x \partial y}\right)^2 \right\} dx\, dy \tag{9}$$

Under elastically restrained boundary conditions an additional term might need to be considered if the springs in the boundary conditions are considered as part of the system.

$$U_k = \frac{1}{2}\int \left\{ k_1 \left(\frac{\partial w}{\partial x}\right)^2 \Big|_{x=0} + k_2 \left(\frac{\partial w}{\partial x}\right)^2 \Big|_{x=a} \right\} dy + \frac{1}{2}\int \left\{ k_3 \left(\frac{\partial w}{\partial y}\right)^2 \Big|_{y=0} + k_4 \left(\frac{\partial w}{\partial y}\right)^2 \Big|_{y=b} \right\} dx \tag{10}$$

Where k_i is the linear torsion spring constant for the i-th edge. The different terms represent the elastic restrains introduced at every edge.

Analogously, the potential energy of the elastic restrain can also be accounted as the energy introduced by applied bending moments at the edges. The sign change is due to the criteria for positive applied bending moment.

$$U_k = \frac{1}{2}\int \left\{ \bar{M}_x \frac{\partial w}{\partial x}\Big|_{x=0} - \bar{M}_x \frac{\partial w}{\partial x}\Big|_{x=a} \right\} dy + \frac{1}{2}\int \left\{ \bar{M}_y \frac{\partial w}{\partial y}\Big|_{y=0} - \bar{M}_y \frac{\partial w}{\partial y}\Big|_{y=b} \right\} dx \tag{11}$$

The resulting strain energy and its variation are given by:

$$U = U_m + U_b + U_k = C + U_b + U_k \rightarrow \delta U = \delta U_b + \delta U_k \tag{12}$$

The potential energy of the external forces can by subdivided in two main terms, the energy of the transverse loads *W* and the energy of the in-plane loads *V*. Only the last term is relevant as only in-plane loads are considered in this thesis (additionally, the second variation of W for plates is always 0, as stated in p.39 of Ashton [13], so the transverse load does not affect the linear buckling solution).

$$V = \frac{1}{2}\iint \left\{ -N_x \left(\frac{\partial w}{\partial x}\right)^2 - N_y \left(\frac{\partial w}{\partial y}\right)^2 + 2N_{xy}\frac{\partial w}{\partial x}\frac{\partial w}{\partial y} \right\} dx\, dy \tag{13}$$

It should be pointed out that the axial loads are taken positive for compression.

3.1.3. Stability of plates

It has been seen in the introduction that stability is typically studied via the second variation of the total potential energy. However, the adjacent equilibrium method proposed an equivalent solution from the study of the equilibrium paths, determining that the existence of additional stable equilibrium paths is caused by the change of the stability behaviour. This method is outlined by Whitney in the section 2.7 of [15].

Two different solution methods are proposed to solve the differential equations:

- The Galerkin method is more general than Ritz and does not require the formulation of an energy principle. The method is based on minimizing the error of an approximate solution by orthogonalizing the residual with respect to a set of given functions. The method is intended to solve boundary value problems, but since the formulation used is equivalent to the equilibrium equations, the Galerkin approach is able to give proper solutions.
- The Ritz method is a procedure to apply the principle of minimum potential energy, assuming that the desired extremal of a problem can be approximated by a linear combination of suitable functions. The solution obtained, returns the best combination of coefficients that approximate the exact solution, being therefore essential to have proper functions to represent the solution.

Both Galerkin and Ritz methods allow for approximate solutions if the essential[4] boundary conditions are satisfied. The accuracy and convergence of the solutions depends greatly on the choice of the set of functions.

3.1.3.1. Adjacent equilibrium method

In the adjacent equilibrium method it is sought a critical load which produces an infinitesimally small shift in the equilibrium position. Therefore the variables are rewritten as an initial pre-buckling displacement or load plus an increment.

$$\begin{cases} u_o = u_o^i + \epsilon u_o \\ v_o = v_o^i + \epsilon v_o \\ w = w^i + \epsilon w \\ \boldsymbol{N} = \boldsymbol{N}^i + \epsilon N \end{cases} \tag{14}$$

For flat symmetric plates (B_{ij}=0) the in-plane and bending behaviour uncouple, therefore:

$$u_o = v_o = N_x = N_y = N_{xy} = 0 \tag{15}$$

And there is no initial out-of-plane displacement prior to buckling:

$$w^i = 0 \tag{16}$$

These results make it unnecessary to distinguish between pre-buckling and equilibrium positions as given in p.38 of Whitney [15].

[4] The boundary conditions (named also geometric boundary conditions) might be divided in two groups. The first one is the essential boundary conditions, where the solution of a differential equation is specified along the boundary of the domain (Dirichlet boundary condition). In the concerning case, these are the values of the out-of-plane displacement along the edges. The second group are the natural boundary conditions, which specify the value of some derivative along the boundary (Neumann boundary condition). In the concerning case, these make reference to the value of the bending moments along the edges.

$$D_{11}\frac{\partial^4 w^i}{\partial x^4} + 4D_{16}\frac{\partial^4 w^i}{\partial x^3 \partial y} + 2(D_{12} + 2D_{66})\frac{\partial^4 w^i}{\partial x^2 \partial y^2} + 4D_{26}\frac{\partial^4 w^i}{\partial x \partial y^3} + D_{22}\frac{\partial^4 w^i}{\partial y^4} = N_x^i \frac{\partial^2 w}{\partial x^2} + 2N_{xy}^i \frac{\partial^2 w}{\partial x \partial y} + N_y^i \frac{\partial^2 w}{\partial y^2} \quad (17)$$

For the sake of notation's simplicity the super index 'i' is not used in further developments of equation 17. Notice also that Whitney's equation uses positive values for tensile axial stresses.

3.1.3.2. The Galerkin method

To apply the Galerkin method the equilibrium equations are calculated applying Hamilton's principle for statics.

$$\delta U + \delta V = 0 \quad (18)$$

The first variation of the energy has been fully developed for isotropic materials in the sections 3.2.2. and 3.2.3. of Jones [12]. A similar approach is used to develop the stability equations in this thesis, however, it involves less detail and has been adapted for mid-plane symmetric plates.

$$\begin{aligned}
\delta U &= \delta U_b + \delta U_k \\
&= \frac{1}{2}\int\int\left\{D_{11}\left(2\frac{\partial^2 w}{\partial x^2}\frac{\partial^2 \varphi}{\partial x^2}\right) + 2D_{12}\left(\frac{\partial^2 w}{\partial x^2}\frac{\partial^2 \varphi}{\partial y^2} + \frac{\partial^2 w}{\partial y^2}\frac{\partial^2 \varphi}{\partial x^2}\right)\right. \\
&+ D_{22}\left(2\frac{\partial^2 w}{\partial y^2}\frac{\partial^2 \varphi}{\partial y^2}\right) \\
&+ 4\left(D_{16}\left(\frac{\partial^2 w}{\partial x^2}\frac{\partial^2 \varphi}{\partial x \partial y} + \frac{\partial^2 w}{\partial x \partial y}\frac{\partial^2 \varphi}{\partial x^2}\right)\right. \\
&+ D_{26}\left(\frac{\partial^2 w}{\partial y^2}\frac{\partial^2 \varphi}{\partial x \partial y} + \frac{\partial^2 w}{\partial x \partial y}\frac{\partial^2 \varphi}{\partial y^2}\right) \\
&\left.\left.+ 4\,D_{66}\left(2\frac{\partial^2 w}{\partial x \partial y}\frac{\partial^2 \varphi}{\partial x \partial y}\right)\right)\right\} dxdy \quad (19) \\
&+ \frac{1}{2}\int\left\{[\bar{M}_x|_{x=0} - \bar{M}_x|_{x=a}]\frac{\partial \varphi}{\partial x}\right\} dy \\
&+ \frac{1}{2}\int\left\{\left[\bar{M}_y\big|_{y=0} - \bar{M}_y\big|_{y=b}\right]\frac{\partial \varphi}{\partial y}\right\} dx \\
&= \int\int\left\{\left[D_{11}\frac{\partial^2 w}{\partial x^2} + D_{12}\frac{\partial^2 w}{\partial y^2} + 2D_{16}\frac{\partial^2 w}{\partial x \partial y}\right]\frac{\partial^2 \varphi}{\partial x^2}\right. \\
&+ \left[D_{12}\frac{\partial^2 w}{\partial x^2} + D_{22}\frac{\partial^2 w}{\partial y^2} + 2D_{26}\frac{\partial^2 w}{\partial x \partial y}\right]\frac{\partial^2 \varphi}{\partial y^2} \\
&\left.+ \left[2D_{16}\frac{\partial^2 w}{\partial x^2} + 2D_{26}\frac{\partial^2 w}{\partial y^2} + 4D_{66}\frac{\partial^2 w}{\partial x \partial y}\right]\frac{\partial^2 \varphi}{\partial x \partial y}\right\} dxdy
\end{aligned}$$

The first variation is defined as $= \frac{\partial(U(w+\alpha\varphi)}{\partial\alpha}\Big]_{\alpha=0}$, where φ might be any function with C^2 continutiy vanishing at the ends.

In order to take out the derivatives of φ it is necessary to use Green's theorem to perform an integration by parts.

$$\int\int \phi \frac{\partial \psi}{\partial x}\, dx\, dy = -\int\int \psi \frac{\partial \phi}{\partial x}\, dx\, dy + \oint \phi\psi dy \tag{20}$$

Apart from Green's theorem, it is also convenient to make the following substitution on the linear boundary integrals to simplify the boundary conditions to be derived.

$$\begin{cases} M_x = -D_{11}\dfrac{\partial^2 w}{\partial x^2} - 2D_{16}\dfrac{\partial^2 w}{\partial x \partial y} - D_{12}\dfrac{\partial^2 w}{\partial y^2} \\ M_y = -D_{12}\dfrac{\partial^2 w}{\partial x^2} - 2D_{26}\dfrac{\partial^2 w}{\partial x \partial y} - D_{22}\dfrac{\partial^2 w}{\partial y^2} \\ M_{xy} = -D_{16}\dfrac{\partial^2 w}{\partial x^2} - 2D_{66}\dfrac{\partial^2 w}{\partial x \partial y} - D_{26}\dfrac{\partial^2 w}{\partial y^2} \end{cases} \tag{21}$$

The result after applying Green's theorem and substituting the boundary terms is:

$$\begin{aligned} \delta U = \int\int \Bigg\{ \Bigg[& D_{11}\frac{\partial^4 w}{\partial x^4} + 4D_{16}\frac{\partial^4 w}{\partial x^3 \partial y} + 2(D_{12}+2D_{66})\frac{\partial^4 w}{\partial x^2 \partial y^2} + 4D_{26}\frac{\partial^4 w}{\partial x \partial y^3} \\ & + D_{22}\frac{\partial^4 w}{\partial y^4}\Bigg]\varphi\Bigg\} dx\, dy \\ & - \int \left\{ \left[\left[\frac{\partial M_x}{\partial x} + 2\frac{\partial M_{xy}}{\partial y}\right]\varphi \right|_{x=0} \right\} dy \\ & + \int \left\{ \left[\left[\frac{\partial M_x}{\partial x} + 2\frac{\partial M_{xy}}{\partial y}\right]\varphi \right|_{x=a} \right\} dy \\ & - \int \left\{ \left[\left[\frac{\partial M_y}{\partial y} + 2\frac{\partial M_{xy}}{\partial x}\right]\varphi \right|_{y=0} \right\} dx \\ & + \int \left\{ \left[\left[\frac{\partial M_y}{\partial y} + 2\frac{\partial M_{xy}}{\partial x}\right]\varphi \right|_{y=b} \right\} dx + \int \left| [M_x - \bar{M}_x]\, \frac{\partial \varphi}{\partial x} \right|_{x=0} dy \\ & - \int \left| [M_x - \bar{M}_x] \frac{\partial \varphi}{\partial x} \right|_{x=a} dy - \int \left| [M_y - \bar{M}_y] \frac{\partial \varphi}{\partial y} \right|_{y=0} dx \\ & + \int \left| [M_y - \bar{M}_y] \frac{\partial \varphi}{\partial y} \right|_{y=b} dx - 2\left| M_{xy}\varphi \right|_{\substack{x=0 \\ y=0}} + 2\left| M_{xy}\varphi \right|_{\substack{x=a \\ y=0}} \\ & - 2\left| M_{xy}\varphi \right|_{\substack{x=a \\ y=b}} + 2\left| M_{xy}\varphi \right|_{\substack{x=0 \\ y=b}} \end{aligned} \tag{22}$$

$$\begin{aligned}\delta V = \int\int \left\{ -\left[-N_x \frac{\partial^2 w}{\partial x^2} + 2N_{xy} \frac{\partial^2 w}{\partial x \partial y} - N_y \frac{\partial^2 w}{\partial y^2} \right] \varphi \right\} dx\, dy \\ - \int \left\{ \left| \left[-N_x \frac{\partial w}{\partial x} + 2N_{xy} \frac{\partial w}{\partial y} \right] \varphi \right|_{x=0} \right\} dy \\ + \int \left\{ \left| \left[-N_x \frac{\partial w}{\partial x} + 2N_{xy} \frac{\partial w}{\partial y} \right] \varphi \right|_{x=a} \right\} dy \\ - \int \left\{ \left| \left[-N_y \frac{\partial w}{\partial y} + 2N_{xy} \frac{\partial w}{\partial x} \right] \varphi \right|_{y=0} \right\} dx \\ + \int \left\{ \left| \left[-N_y \frac{\partial w}{\partial y} + 2N_{xy} \frac{\partial w}{\partial x} \right] \varphi \right|_{y=b} \right\} dx \end{aligned} \tag{23}$$

The variation of the total potential energy is obtained adding both last terms

$$\begin{aligned}\delta\Pi = \delta U + \delta V = \int\int \left\{ \left[D_{11} \frac{\partial^4 w}{\partial x^4} + 4D_{16} \frac{\partial^4 w}{\partial x^3 \partial y} + 2(D_{12} + 2D_{66}) \frac{\partial^4 w}{\partial x^2 \partial y^2} \right.\right. \\ \left. + 4D_{26} \frac{\partial^4 w}{\partial x \partial y^3} + D_{22} \frac{\partial^4 w}{\partial y^4} \right. \\ \left.\left. - \left[-N_x \frac{\partial^2 w}{\partial x^2} + 2N_{xy} \frac{\partial^2 w}{\partial x \partial y} - N_y \frac{\partial^2 w}{\partial y^2} \right] \right] \varphi \right\} dx\, dy \\ - \int \left\{ \left| \left[\frac{\partial M_x}{\partial x} + 2\frac{\partial M_{xy}}{\partial y} - N_x \frac{\partial w}{\partial x} + 2N_{xy} \frac{\partial w}{\partial y} \right] \varphi \right|_{x=0} \right\} dy \\ + \int \left\{ \left| \left[\frac{\partial M_x}{\partial x} + 2\frac{\partial M_{xy}}{\partial y} - N_x \frac{\partial w}{\partial x} + 2N_{xy} \frac{\partial w}{\partial y} \right] \varphi \right|_{x=a} \right\} dy \\ - \int \left\{ \left| \left[\frac{\partial M_y}{\partial y} + 2\frac{\partial M_{xy}}{\partial x} - N_y \frac{\partial w}{\partial y} + 2N_{xy} \frac{\partial w}{\partial x} \right] \varphi \right|_{y=0} \right\} dx \\ + \int \left\{ \left| \left[\frac{\partial M_y}{\partial y} + 2\frac{\partial M_{xy}}{\partial x} - N_y \frac{\partial w}{\partial y} + 2N_{xy} \frac{\partial w}{\partial x} \right] \varphi \right|_{y=b} \right\} dx \\ + \int \left| [M_x - \bar{M}_x] \frac{\partial \varphi}{\partial x} \right|_{x=0} dy \\ - \int \left| [M_x - \bar{M}_x] \frac{\partial \varphi}{\partial x} \right|_{x=a} dy - \int \left| [M_y - \bar{M}_y] \frac{\partial \varphi}{\partial y} \right|_{y=0} dx \\ + \int \left| [M_y - \bar{M}_y] \frac{\partial \varphi}{\partial y} \right|_{y=b} dx - 2\left| M_{xy} \varphi \right|_{\substack{x=0 \\ y=0}} + 2\left| M_{xy} \varphi \right|_{\substack{x=a \\ y=0}} \\ - 2\left| M_{xy} \varphi \right|_{\substack{x=a \\ y=b}} + 2\left| M_{xy} \varphi \right|_{\substack{x=0 \\ y=b}} \end{aligned} \tag{24}$$

The equilibrium equation is then given by the term inside the double integral (Euler equation) with all the surface and corner terms reflecting the required boundary conditions. Each term of the first variation ought to be zero to satisfy equilibrium and its boundary conditions.

However, the material complexity of mid-plane symmetric laminates (remember the presence of D_{16} and D_{26} terms for example) can make it impossible to exactly satisfy natural[4] boundary conditions using the typical approach for shape functions (see eq. 28).

In those cases, the moment applied (or given by the elastic restrain) is not the same as the moment corresponding due to plate deflection. The error between these two makes the following surface terms different to zero and therefore ought to be accounted for when applying the Galerkin method.

$$\begin{aligned}
\int \left|[M_x - \bar{M}_x]\frac{\partial\varphi}{\partial x}\right|_{x=0} dy &= \int \left|[E_1]\frac{\partial\varphi}{\partial x}\right|_{x=0} dy \\
\int \left|[M_x - \bar{M}_x]\frac{\partial\varphi}{\partial x}\right|_{x=a} dy &= \int \left|[E_2]\frac{\partial\varphi}{\partial x}\right|_{x=1} dy \\
\int \left|[M_y - \bar{M}_y]\frac{\partial\varphi}{\partial y}\right|_{y=0} dx &= \int \left|[E_3]\frac{\partial\varphi}{\partial y}\right|_{y=0} dx \\
\int \left|[M_y - \bar{M}_y]\frac{\partial\varphi}{\partial y}\right|_{y=b} dx &= \int \left|[E_4]\frac{\partial\varphi}{\partial y}\right|_{y=b} dx
\end{aligned} \tag{25}$$

Note that the error between bending moments will depend on how the selected out-of-plane functions can approximate the real result. For simplicity the E_i coefficients will be used in the following equations to refer to this error. After removing all the boundary terms that ought to be 0, the resulting first variation is:

$$\begin{aligned}
\delta\Pi = \delta U + \delta V = \int\int \Bigg\{\Bigg[& D_{11}\frac{\partial^4 w}{\partial x^4} + 4D_{16}\frac{\partial^4 w}{\partial x^3\partial y} + 2(D_{12}+2D_{66})\frac{\partial^4 w}{\partial x^2\partial y^2} \\
& + 4D_{26}\frac{\partial^4 w}{\partial x\partial y^3} + D_{22}\frac{\partial^4 w}{\partial y^4} + N_x\frac{\partial^2 w}{\partial x^2} - 2N_{xy}\frac{\partial^2 w}{\partial x\partial y} \\
& + N_y\frac{\partial^2 w}{\partial y^2}\Bigg]\varphi\Bigg\} dx\, dy + \int \left|[E_1]\frac{\partial\varphi}{\partial x}\right|_{x=0} dy \\
& - \int \left|[E_2]\frac{\partial\varphi}{\partial x}\right|_{x=a} dy - \int \left|[E_3]\frac{\partial\varphi}{\partial y}\right|_{y=0} dx \\
& + \int \left|[E_4]\frac{\partial\varphi}{\partial y}\right|_{y=b} dx = 0
\end{aligned} \tag{26}$$

On the other hand, if the natural boundary conditions are exactly satisfied, the governing equation for stability reduces to the differential Euler equation.

$$\begin{aligned}
D_{11}\frac{\partial^4 w}{\partial x^4} + 4D_{16}\frac{\partial^4 w}{\partial x^3\partial y} + 2(D_{12}+2D_{66})\frac{\partial^4 w}{\partial x^2\partial y^2} + 4D_{26}\frac{\partial^4 w}{\partial x\partial y^3} + D_{22}\frac{\partial^4 w}{\partial y^4} \\
+ N_x\frac{\partial^2 w}{\partial x^2} - 2N_{xy}\frac{\partial^2 w}{\partial x\partial y} + N_y\frac{\partial^2 w}{\partial y^2} = 0
\end{aligned} \tag{27}$$

To apply the Galerkin method, the out-of-plane displacement must be represented by a linear combination of suitable functions.

$$w = \sum_{m=1}^{M}\sum_{n=1}^{N} w_{mn} X_m(x) Y_n(y) \tag{28}$$

The used linear combination is based on splitting the out-of-plane displacement in an amplitude term (w_{mn}), an x dependent term (X_m) and a y dependent term (Y_n). The functions X_m and Y_n represent ideally the buckled shape when the number of half-waves in x and y directions are m and n. However, except for ideal cases, it is required to use several terms to properly approximate the solution.

Then, the equilibrium equation is multiplied by (preferably) orthogonal functions, in our case, φ. φ is usually referred to as the characteristic or the virtual displacement function. Typical solutions relay on using the same form for both the out-of-plane and characteristic functions (but obviously without amplitude in this last one). This option is followed in this solution.

$$\varphi = \sum_{m=1}^{M}\sum_{n=1}^{N} X_m(x) Y_n(y) \tag{29}$$

Substituting the last two equations and replacing again the moments in 26, a system of equation is build:

$$\begin{aligned}
\int\int \Bigg\{ \sum_{i=1}^{M}\sum_{j=1}^{N} w_{ij} \Bigg[& D_{11}\frac{\partial^4 X_i}{\partial x^4} Y_j + 4D_{16}\frac{\partial^3 X_i}{\partial x^3}\frac{\partial Y_j}{\partial y} + 2(D_{12}+2D_{66})\frac{\partial^2 X_i}{\partial x^2}\frac{\partial^2 Y_j}{\partial y^2} \\
& + 4D_{26}\frac{\partial X_i}{\partial x}\frac{\partial^3 Y_j}{\partial y^3} + D_{22} X_i \frac{\partial^4 Y_j}{\partial y^4} + N_x \frac{\partial^2 X_i}{\partial x^2} Y_j - 2N_{xy}\frac{\partial X_i}{\partial x}\frac{\partial Y_j}{\partial y} \\
& + N_y X_i \frac{\partial^2 Y_j}{\partial y^2} \Bigg] \sum_{i=1}^{M}\sum_{j=1}^{N} X_m Y_n \Bigg\} dx\, dy \\
& - \int \left\{ \sum_{i=1}^{M}\sum_{j=1}^{N} w_{ij} \left|[E_1]\right|_{x=0} \sum_{m=1}^{M}\sum_{n=1}^{N} \left| \frac{\partial X_m}{\partial x} Y_n \right|_{x=0} \right\} dy \\
& + \int \left\{ \sum_{i=1}^{M}\sum_{j=1}^{N} w_{ij} \left|[E_2]\right|_{x=a} \sum_{m=1}^{M}\sum_{n=1}^{N} \left| \frac{\partial X_m}{\partial x} Y_n \right|_{x=a} \right\} dy \\
& - \int \left\{ \sum_{i=1}^{M}\sum_{j=1}^{N} w_{ij} \left|[E_3]\right|_{y=0} \sum_{m=1}^{M}\sum_{n=1}^{N} \left| X_m \frac{\partial Y_n}{\partial y} \right|_{y=0} \right\} dx \\
& + \int \left\{ \sum_{i=1}^{M}\sum_{j=1}^{N} w_{ij} \left|E_4\right|_{y=b} \sum_{m=1}^{M}\sum_{n=1}^{N} \left| X_m \frac{\partial Y_n}{\partial y} \right|_{y=b} \right\} dx \; = 0
\end{aligned} \tag{30}$$

At this point is convenient to convert the equation to dimensionless variables:

$$W = \frac{w}{h}, \qquad \xi = \frac{x}{a}, \qquad \eta = \frac{y}{b}, \qquad \lambda = \frac{a}{b}, \qquad \boldsymbol{D}^* = \frac{\boldsymbol{D}}{A_{22}h^2} \tag{31}$$

The loads are also transformed to dimensionless units, but before a common factor is taken. In this approach, this factor (N_o) is given the value of the maximum load applied and will account for the results of the eigenvalue problem.

$$N_o = \max(\boldsymbol{N}), \qquad \boldsymbol{N_f} = \frac{1}{N_o}\boldsymbol{N}, \qquad \boldsymbol{N}^* = \frac{b^2}{A_{22}h^2}\boldsymbol{N_f} \tag{32}$$

For a further simplification the following coefficients are introduced:

$$a_1 = \frac{4D_{16}^*}{D_{11}^*}\lambda, \qquad a_{2a} = \frac{2D_{12}^*}{D_{11}^*}\lambda^2, \qquad a_{2b} = \frac{4D_{66}^*}{D_{11}^*}\lambda^2, \qquad a_2 = a_{2a} + a_{2b}\,,$$
$$a_3 = \frac{4D_{26}^*}{D_{11}^*}\lambda^3, \qquad a_4 = \frac{D_{22}^*}{D_{11}^*}\lambda^4 \tag{33}$$

$$c_1 = \frac{N_1^*}{D_{11}^*}\lambda^2, \qquad c_2 = -\frac{2N_{12}^*}{D_{11}^*}\lambda^3, \qquad c_3 = \frac{N_2^*}{D_{11}^*}\lambda^4 \tag{34}$$

To avoid confusion, the shear load is non-dimensionalized in negative form to have the same sign as the other non-dimensionalized loads (remember that axial loads were flipped to have compression as positive).

The resulting dimensionless equation is:

$$\begin{aligned}
&\sum_{i=1}^{M}\sum_{j=1}^{N} W_{ij} \sum_{m=1}^{M}\sum_{n=1}^{N} \int\int \left\{ \left[\frac{\partial^4 X_i}{\partial\xi^4} Y_j + a_1 \frac{\partial^3 X_i}{\partial\xi^3}\frac{\partial Y_j}{\partial\eta} + a_2 \frac{\partial^2 X_i}{\partial\xi^2}\frac{\partial^2 Y_j}{\partial\eta^2} + a_3 \frac{\partial X_i}{\partial\xi}\frac{\partial^3 Y_j}{\partial\eta^3} \right.\right. \\
&\qquad + a_4 X_i \frac{\partial^4 Y_j}{\partial\eta^4} \\
&\qquad \left.\left. + N_o \left(c_1 \frac{\partial^2 X_i}{\partial\xi^2} Y_j + c_2 \frac{\partial X_i}{\partial\xi}\frac{\partial Y_j}{\partial\eta} + c_3 X_i \frac{\partial^2 Y_j}{\partial\eta^2} \right) \right] X_m Y_n \right\} d\xi\, d\eta \\
&\qquad + \sum_{i=1}^{M}\sum_{j=1}^{N} W_{ij} \sum_{m=1}^{M}\sum_{n=1}^{N} \int \left\{ \left\| \left[E_{ij}{}_2^* \right] \right\|_{\xi=1} \left| \frac{\partial X_m}{\partial\xi} Y_n \right|_{\xi=1} \right. \\
&\qquad \left. - \left\| \left[E_{ij}{}_1^* \right] \right\|_{\xi=0} \left| \frac{\partial X_m}{\partial\xi} Y_n \right|_{\xi=0} \right\} d\eta \\
&\qquad + \sum_{i=1}^{M}\sum_{j=1}^{N} w_{ij} \sum_{m=1}^{M}\sum_{n=1}^{N} \int \left\{ \left\| \left[E_{ij}{}_4^* \right] \right\|_{\eta=1} \left| X_m \frac{\partial Y_n}{\partial\eta} \right|_{\eta=1} \right. \\
&\qquad \left. - \left\| \left[E_{ij}{}_3^* \right] \right\|_{\eta=0} \left| X_m \frac{\partial Y_n}{\partial\eta} \right|_{\eta=0} \right\} d\xi = 0
\end{aligned} \tag{35}$$

The dimensionless error between bending moments is defined in the section 3.1.3.4. as it is necessary to decide first on the linear set of functions to represent the out-of-plane shape.

To arrive to the final eigenvalue problem it is necessary to perform a change of variable (to work with square matrices). Let:

$$p = (i-1)N + j, \qquad q = (m-1)N + n \tag{36}$$

Then the system matrices to calculate the eigenvalue problem can be defined as:

$$\boldsymbol{K_{pq}} = \sum_{p=1}^{MN}\sum_{q=1}^{MN}\int\int\left\{\left[\frac{\partial^4 X_i}{\partial\xi^4}Y_j + a_1\frac{\partial^3 X_i}{\partial\xi^3}\frac{\partial Y_j}{\partial\eta} + a_2\frac{\partial^2 X_i}{\partial\xi^2}\frac{\partial^2 Y_j}{\partial\eta^2} + a_3\frac{\partial X_i}{\partial\xi}\frac{\partial^3 Y_j}{\partial\eta^3} + a_4 X_i\frac{\partial^4 Y_j}{\partial\eta^4}\right]X_m Y_n\right\}d\xi\, d\eta \tag{37}$$

$$\boldsymbol{K_{B_{pq}}} = \sum_{p=1}^{MN}\sum_{q=1}^{MN}\left\{\int\left\{\left|\left[E_{ij}{}^{*}_{2}\right]\right|_{\xi=1}\left|\frac{\partial X_m}{\partial\xi}Y_n\right|_{\xi=1} - \left|\left[E_{ij}{}^{*}_{1}\right]\right|_{\xi=0}\left|\frac{\partial X_m}{\partial\xi}Y_n\right|_{\xi=0}\right\}d\eta + \int\left\{\left|\left[E_{ij}{}^{*}_{4}\right]\right|_{\eta=1}\left|X_m\frac{\partial Y_n}{\partial\eta}\right|_{\eta=1} - \left|\left[E_{ij}{}^{*}_{3}\right]\right|_{\eta=0}\left|X_m\frac{\partial Y_n}{\partial\eta}\right|_{\eta=0}\right\}d\xi\right\} \tag{38}$$

$$\boldsymbol{R_{pq}} = \sum_{p=1}^{MN}\sum_{q=1}^{MN}\left\{\left[-c_1\frac{\partial^2 X_i}{\partial\xi^2}Y_j - c_2\frac{\partial X_i}{\partial\xi}\frac{\partial Y_j}{\partial\eta} - c_3 X_i\frac{\partial^2 Y_j}{\partial\eta^2}\right]X_m Y_n\right\} \tag{39}$$

Arriving finally to the eigenvalue problem:

$$\left[\boldsymbol{K_{pq}} + \boldsymbol{K_{B_{pq}}}\right]\{\boldsymbol{W_p}\} - N_o[\boldsymbol{R_{pq}}]\{\boldsymbol{W_p}\} = 0 \rightarrow \det\left[\boldsymbol{K_{pq}} + \boldsymbol{K_{B_{pq}}} - N_o\boldsymbol{R_{pq}}\right] = 0 \tag{40}$$

3.1.3.3. The Ritz method

To examine which method is more accurate, the problem has also been solved using the Ritz method. The solution obtained requires more integration terms but shows also some advantages. The Ritz method only needs to satisfy the essential boundary conditions, the natural boundary conditions related to the moments at the edges can be agreed approximately. Therefore, there is no need to include additional boundary terms to correct the natural boundary conditions as in the Galerkin approach.

The total potential energy is minimized with respect to the linear approximation of the assumed out-of-plane function which would give a minimum (the better the solution approximates to reality the closer it is to the minimum).

$$\frac{\partial \Pi}{\partial w_{mn}} = 0 \tag{41}$$

The previous expressions lead to for the M times N system of equations of the eigenvalue problem. The total potential energy has been calculated in the previous section as:

$$\begin{aligned}
\Pi &= U_b + U_k + V + C \\
&= \frac{1}{2}\iint \left\{ D_{11}\left(\frac{\partial^2 w}{\partial x^2}\right)^2 + 2D_{12}\frac{\partial^2 w}{\partial x^2}\frac{\partial^2 w}{\partial y^2} + D_{22}\left(\frac{\partial^2 w}{\partial y^2}\right)^2 \right. \\
&+ \left. 4\left(D_{16}\frac{\partial^2 w}{\partial x^2} + D_{26}\frac{\partial^2 w}{\partial y^2}\right)\frac{\partial w^2}{\partial x \partial y} + 4D_{66}\left(\frac{\partial w^2}{\partial x \partial y}\right)^2 \right\} dx\, dy \\
&+ \frac{1}{2}\int \left\{ k_1 \left(\frac{\partial w}{\partial x}\right)^2 \Big|_{x=0} + k_2 \left(\frac{\partial w}{\partial x}\right)^2 \Big|_{x=a} \right\} dy \\
&+ \frac{1}{2}\int \left\{ k_3 \left(\frac{\partial w}{\partial y}\right)^2 \Big|_{y=0} + k_4 \left(\frac{\partial w}{\partial y}\right)^2 \Big|_{y=b} \right\} dx \\
&+ \frac{1}{2}\iint \left\{ -N_x \left(\frac{\partial w}{\partial x}\right)^2 - N_y \left(\frac{\partial w}{\partial y}\right)^2 + 2N_{xy}\frac{\partial w}{\partial x}\frac{\partial w}{\partial y} \right\} dx\, dy + C
\end{aligned} \tag{42}$$

Then, it is necessary to substitute the same out-of-plane function (eq. 28) and minimize. Moreover, the same dimensionless procedure and coefficients, as in the Galerkin approach, have been applied (eq. 31-34) plus the non-dimensionalized torsional stiffness:

$$k_{1,2}^* = \frac{k_{1,2}a}{D_{11}} = \frac{k_{1,2}a}{D_{11}^* A_{22} h^2}, \qquad k_{3,4}^* = \frac{k_{3,4}b}{D_{22}} = \frac{k_{3,4}b}{D_{22}^* A_{22} h^2} \tag{43}$$

$$
\begin{aligned}
\frac{\partial \Pi}{\partial \mathrm{W_{mn}}} = W_{mn} \Bigg(& \iint \Bigg\{ \frac{\partial^2 X_i}{\partial \xi^2} \frac{\partial^2 X_m}{\partial \xi^2} Y_j Y_n \\
& + \frac{a_1}{2} \left[\frac{\partial^2 X_i}{\partial \xi^2} \frac{\partial X_m}{\partial \xi} Y_j \frac{\partial Y_n}{\partial \eta} + \frac{\partial X_i}{\partial \xi} \frac{\partial^2 X_m}{\partial \xi^2} \frac{\partial Y_j}{\partial \eta} Y_n \right] \\
& + \frac{a_{2a}}{2} \left[\frac{\partial^2 X_i}{\partial \xi^2} X_m Y_j \frac{\partial^2 Y_n}{\partial \eta^2} + X_i \frac{\partial^2 X_m}{\partial \xi^2} \frac{\partial Y_j^2}{\partial \eta^2} Y_n \right] \\
& + a_{2b} \frac{\partial X_i}{\partial \xi} \frac{\partial X_m}{\partial \xi} \frac{\partial Y_j}{\partial \eta} \frac{\partial Y_n}{\partial \eta} \\
& + \frac{a_3}{2} \left[X_i \frac{\partial X_m}{\partial \xi} \frac{\partial Y_j^2}{\partial \eta^2} \frac{\partial Y_n}{\partial \eta} + \frac{\partial X_i}{\partial \xi} X_m \frac{\partial Y_j}{\partial \eta} \frac{\partial^2 Y_n}{\partial \eta^2} \right] \\
& + a_4 X_i X_m \frac{\partial Y_j^2}{\partial \eta^2} \frac{\partial^2 Y_n}{\partial \eta^2} \\
& - N_o \Bigg(c_1 \frac{\partial X_i}{\partial \xi} \frac{\partial X_m}{\partial \xi} Y_j Y_n \\
& + \frac{c_2}{2} \left[\frac{\partial X_i}{\partial \xi} X_m Y_j \frac{\partial Y_n}{\partial \eta} \right. \\
& \left. + X_i \frac{\partial X_m}{\partial \xi} \frac{\partial Y_j}{\partial \eta} Y_n \right] + c_3 X_i X_m \frac{\partial Y_j}{\partial \eta} \frac{\partial Y_n}{\partial \eta} \Bigg) \Bigg\} d\xi \, d\eta \\
& + \int \left\{ k_1^* \frac{\partial X_i}{\partial \xi} \frac{\partial X_m}{\partial \xi} Y_j Y_n \Big|_{\xi=0} + k_2^* \frac{\partial X_i}{\partial \xi} \frac{\partial X_m}{\partial \xi} Y_j Y_n \Big|_{\xi=1} \right\} d\eta \\
& + \frac{\lambda^4 D_{22}^*}{D_{11}^*} \int \Bigg\{ k_3^* X_i X_m \frac{\partial Y_j}{\partial \eta} \frac{\partial Y_n}{\partial \eta} \Big|_{\eta=0} \\
& + k_4^* X_i X_m \frac{\partial Y_j}{\partial \eta} \frac{\partial Y_n}{\partial \eta} \Big|_{\eta=1} \Bigg\} d\xi \Bigg)
\end{aligned}
\tag{44}
$$

The eigenvalue problem is built similarly as in Galerkin.

Arriving finally to the eigenvalue problem:

$$
p = (i-1)N + j, \qquad q = (m-1)N + n \tag{45}
$$

$$\begin{aligned}\boldsymbol{K_{pq}} = \sum_{p=1}^{MN}\sum_{q=1}^{MN}\int\int\Bigg\{&\frac{\partial^2 X_i}{\partial\xi^2}\frac{\partial^2 X_m}{\partial\xi^2}Y_jY_n\\ &+\frac{a_1}{2}\left[\frac{\partial^2 X_i}{\partial\xi^2}\frac{\partial X_m}{\partial\xi}Y_j\frac{\partial Y_n}{\partial\eta}+\frac{\partial X_i}{\partial\xi}\frac{\partial^2 X_m}{\partial\xi^2}\frac{\partial Y_j}{\partial\eta}Y_n\right]\\ &+\frac{a_{2a}}{2}\left[\frac{\partial^2 X_i}{\partial\xi^2}X_mY_j\frac{\partial^2 Y_n}{\partial\eta^2}+X_i\frac{\partial^2 X_m}{\partial\xi^2}\frac{\partial Y_j^2}{\partial\eta^2}Y_n\right]\\ &+a_{2b}\frac{\partial X_i}{\partial\xi}\frac{\partial X_m}{\partial\xi}\frac{\partial Y_j}{\partial\eta}\frac{\partial Y_n}{\partial\eta}\\ &+\frac{a_3}{2}\left[X_i\frac{\partial X_m}{\partial\xi}\frac{\partial Y_j^2}{\partial\eta^2}\frac{\partial Y_n}{\partial\eta}+\frac{\partial X_i}{\partial\xi}X_m\frac{\partial Y_j}{\partial\eta}\frac{\partial^2 Y_n}{\partial\eta^2}\right]\\ &+a_4X_iX_m\frac{\partial Y_j^2}{\partial\eta^2}\frac{\partial^2 Y_n}{\partial\eta^2}\Bigg\}d\xi\,d\eta\end{aligned} \tag{46}$$

$$\begin{aligned}\boldsymbol{K_{B_{pq}}} = \sum_{p=1}^{MN}\sum_{q=1}^{MN}\Bigg\{&\int\left\{k_1^*\frac{\partial X_i}{\partial\xi}\frac{\partial X_m}{\partial\xi}Y_jY_n\Big|_{\xi=0}+k_2^*\frac{\partial X_i}{\partial\xi}\frac{\partial X_m}{\partial\xi}Y_jY_n\Big|_{\xi=1}\right\}d\eta\\ &+\frac{\lambda^4D_{22}^*}{D_{11}^*}\int\left\{k_3^*X_iX_m\frac{\partial Y_j}{\partial\eta}\frac{\partial Y_n}{\partial\eta}\Big|_{\eta=0}+k_4^*X_iX_m\frac{\partial Y_j}{\partial\eta}\frac{\partial Y_n}{\partial\eta}\Big|_{\eta=1}\right\}d\xi\Bigg\}\end{aligned} \tag{47}$$

$$\begin{aligned}\boldsymbol{R_{pq}} = \sum_{p=1}^{MN}\sum_{q=1}^{MN}\int\int\Bigg\{&c_1\frac{\partial X_i}{\partial\xi}\frac{\partial X_m}{\partial\xi}Y_jY_n\\ &+\frac{c_2}{2}\left[\frac{\partial X_i}{\partial\xi}X_mY_j\frac{\partial Y_n}{\partial\eta}\right.\\ &\left.+X_i\frac{\partial X_m}{\partial\xi}\frac{\partial Y_j}{\partial\eta}Y_n\right]+c_3X_iX_m\frac{\partial Y_j}{\partial\eta}\frac{\partial Y_n}{\partial\eta}\Bigg\}d\xi d\eta\end{aligned} \tag{48}$$

3.1.3.4. Mode Shape

To solve the remaining eigenvalue problem it is necessary to define the linear combination to be used. It is very important that the function chosen is able to reproduce the real buckled shape as accurately as possible. The different solutions proposed in the studied literature have some points in common, all of them attempt to split the out-of-plane displacement in two independent terms in order to uncouple *x* and *y* directions. This simplifies greatly the formulation of the problem. This is the reason it has already been included in both proposed Galerkin and Ritz formulations, even when the exact shape function has been left out to have a more general solution.

Another important fact is that the proposed solution needs to match the essential boundary conditions to guarantee the numerical methods will work. Under the assumptions exposed, this means that the out-of-plane displacement must be exactly zero at the edges.

Some simple configurations have exact solutions, which is the case of specially orthotropic, simply supported plates under uniaxial or biaxial compression. Then the buckling shape of the different modes is simply given by the double sine function (using only the term that contains the required half-waves).

$$w = w_{mn} \sin\left(\frac{m\pi x}{a}\right) \sin\left(\frac{n\pi y}{b}\right) \tag{49}$$

For such simple cases the solution of the differential governing equation can be solved exactly, arriving to well-known exact closed-form solutions. To be able to approximate more complex cases it is only possible to approximate the shape with a linear combination. If the set of functions is complete and satisfies the geometric, then the result will converge to the exact solution. Most popular sets of functions are based on orthogonalized polynomials or trigonometric functions.

The chosen solution is based on the eigenbeam value functions restrained by two arbitrary torsional springs. Most solutions based on trigonometric functions rely on the linear combination of simply supported and clamped solutions to reproduce all the intermediate configurations. However, this does not allow for asymmetric boundary conditions, which will be needed in chapter 5.

The eigenbeam value functions follow the following form:

$$X_m = C_{m_1} \cosh(\alpha_m x) + C_{m_2} \sinh(\alpha_m x) + C_{m_3} \cos(\alpha_m x) + C_{m_4} \sin(\alpha_m x) \tag{50}$$

By imposing the geometric boundary conditions it is possible to solve the shape mode α_m and find de dependencies between the 4 constants C_{m_i} leaving the solution as a function of the amplitude (shape is completely defined). To be able to impose the boundary conditions it is necessary to define the bending moments at the edges of the plate. From the ABD matrix:

$$\begin{Bmatrix} \boldsymbol{N} \\ \boldsymbol{M} \end{Bmatrix} = \begin{bmatrix} \boldsymbol{A} & \boldsymbol{B} \\ \boldsymbol{B} & \boldsymbol{D} \end{bmatrix} \begin{Bmatrix} \boldsymbol{\varepsilon_o} \\ \boldsymbol{\kappa} \end{Bmatrix} \tag{51}$$

Under the assumption of symmetric lay-up, the moments uncouple from the strains. Substituting the curvatures by the correspondent derivatives of the out-of-plane displacements, the moments can be written as:

$$\begin{cases} M_x = -D_{11} \dfrac{\partial^2 w}{\partial x^2} - 2D_{16} \dfrac{\partial^2 w}{\partial x \partial y} - D_{12} \dfrac{\partial^2 w}{\partial y^2} \\ M_y = -D_{12} \dfrac{\partial^2 w}{\partial x^2} - 2D_{26} \dfrac{\partial^2 w}{\partial x \partial y} - D_{22} \dfrac{\partial^2 w}{\partial y^2} \\ M_{xy} = -D_{16} \dfrac{\partial^2 w}{\partial x^2} - 2D_{66} \dfrac{\partial^2 w}{\partial x \partial y} - D_{26} \dfrac{\partial^2 w}{\partial y^2} \end{cases} \tag{52}$$

On the other hand, the use of torsional springs also relates the moments with the out-of-plane displacements through the torsion spring constants:

$$\begin{cases} M_x|_{x=0} = -k_1 \left.\dfrac{\partial w}{\partial x}\right|_{x=0} = \left.-D_{11}\dfrac{\partial^2 w}{\partial x^2} - 2D_{16}\dfrac{\partial^2 w}{\partial x \partial y} - D_{12}\dfrac{\partial^2 w}{\partial y^2}\right|_{x=0} \\ M_x|_{x=a} = k_2 \left.\dfrac{\partial w}{\partial x}\right|_{x=a} = \left.-D_{11}\dfrac{\partial^2 w}{\partial x^2} - 2D_{16}\dfrac{\partial^2 w}{\partial x \partial y} - D_{12}\dfrac{\partial^2 w}{\partial y^2}\right|_{x=a} \\ M_y\big|_{y=0} = -k_3 \left.\dfrac{\partial w}{\partial y}\right|_{y=0} = \left.-D_{12}\dfrac{\partial^2 w}{\partial x^2} - 2D_{26}\dfrac{\partial^2 w}{\partial x \partial y} - D_{22}\dfrac{\partial^2 w}{\partial y^2}\right|_{y=0} \\ M_y\big|_{y=b} = k_4 \left.\dfrac{\partial w}{\partial y}\right|_{y=b} = \left.-D_{12}\dfrac{\partial^2 w}{\partial x^2} - 2D_{26}\dfrac{\partial^2 w}{\partial x \partial y} - D_{22}\dfrac{\partial^2 w}{\partial y^2}\right|_{y=b} \end{cases} \quad (53)$$

It is possible then to join the different equations together to find the out-of-plane function that fulfils the geometric boundary conditions. However, eq. 53 couples *x* and *y* directions, so further simplifications are required.

The assumption that the edges keep straight after the deformation allows for the simplification of the derivative against the perpendicular direction to the edge (D_{12} term). For specially orthotropic materials, that would already be enough, however, D_{16} and D_{26} terms are still carrying the cross derivatives. Several authors [31, 34] working with torsional springs drop those terms in order to keep independent the X and Y directions. That means that the natural boundary conditions are only approximately satisfied. The possibility of this approximation has been already accounted for in both the Galerkin and Ritz formulations.

The next step is matching the bending moments given by the torsional springs with the approximate bending moment (without cross derivatives):

$$\begin{cases} -D_{11}\left.\dfrac{\partial^2 w}{\partial x^2}\right|_{x=0} = -k_1 \left.\dfrac{\partial w}{\partial x}\right|_{x=0}, & -D_{11}\left.\dfrac{\partial^2 w}{\partial x^2}\right|_{x=a} = k_2 \left.\dfrac{\partial w}{\partial x}\right|_{x=a} \\ -D_{22}\left.\dfrac{\partial^2 w}{\partial y^2}\right|_{y=0} = -k_3 \left.\dfrac{\partial w}{\partial y}\right|_{y=0}, & -D_{22}\left.\dfrac{\partial^2 w}{\partial y^2}\right|_{y=b} = k_4 \left.\dfrac{\partial w}{\partial y}\right|_{y=b} \end{cases} \quad (54)$$

It is convenient to work with dimensionless expression for both the boundary conditions and the eigenbeam value functions. After following the same criteria as previous sections the next results are obtained:

$$\begin{cases} \left.\dfrac{\partial^2 W}{\partial \xi^2}\right|_{\xi=0} = k_1^* \left.\dfrac{\partial W}{\partial \xi}\right|_{\xi=0}, & -\left.\dfrac{\partial^2 W}{\partial \xi^2}\right|_{\xi=1} = k_2^* \left.\dfrac{\partial W}{\partial \xi}\right|_{\xi=1} \\ \left.\dfrac{\partial^2 W}{\partial \eta^2}\right|_{\eta=0} = k_3^* \left.\dfrac{\partial W}{\partial \eta}\right|_{\eta=0}, & -\left.\dfrac{\partial^2 W}{\partial \eta^2}\right|_{\eta=1} = k_4^* \left.\dfrac{\partial W}{\partial \eta}\right|_{\eta=1} \end{cases} \quad (55)$$

And,

$$X_m = C_{m_1}\cosh(\alpha_m \xi) + C_{m_2}\sinh(\alpha_m \xi) + C_{m_3}\cos(\alpha_m \xi) + C_{m_4}\sin(\alpha_m \xi) \quad (56)$$

The out-of-plane displacement is then given by:

$$W = \sum_{m=1}^{M} \sum_{n=1}^{N} W_{mn} X_m Y_n \tag{57}$$

Notice that Y_n is analogous to X_m but in y direction. Therefore, the procedure to define the different coefficients of the eigenbeam functions enforcing the essential and (approximate) natural boundary conditions is only developed for X_m.

$$\begin{cases} X_m|_{\xi=0} = 0 \rightarrow C_{m_1} + C_{m_3} = 0 \\ \left.\frac{\partial X_m}{\partial \xi}\right|_{\xi=0} = \frac{1}{k_1^*}\left.\frac{\partial^2 X_m}{\partial \xi^2}\right|_{\xi=0} \rightarrow C_{m_2} + C_{m_4} = \frac{\alpha_m}{k_1^*}\left(C_{m_1} - C_{m_3}\right) \\ X_m|_{\xi=1} = 0 \rightarrow C_{m_1}\cosh(\alpha_m) + C_{m_2}\sinh(\alpha_m) + C_{m_3}\cos(\alpha_m) + C_{m_4}\sin(\alpha_m) = 0 \\ \left.\frac{\partial X_m}{\partial \xi}\right|_{\xi=1} = -\frac{1}{k_2^*}\left.\frac{\partial^2 X_m}{\partial \xi^2}\right|_{\xi=1} \rightarrow \end{cases} \tag{58}$$

$$\begin{aligned} &C_{m_1}\sinh(\alpha_m) + C_{m_2}\cosh(\alpha_m) - C_{m_3}\sin(\alpha_m) + C_{m_4}\cos(\alpha_m) \\ &\quad = -\frac{\alpha_m}{k_2^*}\left[C_{m_1}\cosh(\alpha_m) + C_{m_2}\sinh(\alpha_m) - C_{m_3}\cos(\alpha_m) - C_{m_4}\sin(\alpha_m)\right] \end{aligned}$$

The main problem of the proposed development is that the mode value α_m must be solved numerically from the following non-linear equation:

$$\begin{aligned} &[\sinh(\alpha_m) - sin(\alpha_m)]\left[sinh\,(\alpha_m) + \frac{2\alpha_m}{k_1^*}\cosh(\alpha_m)\right. \\ &\quad \left. + \sin(\alpha_m) + \frac{\alpha_m}{k_2^*}\left(\cosh(\alpha_m) + \frac{2\alpha_m}{k_1^*}\sinh(\alpha_m) + \cos(\alpha_m)\right)\right] \\ &\quad - \left[\cos(\alpha_m) - \cosh(\alpha_m) - \frac{2\alpha_m}{k_1^*}\sinh(\alpha_m)\right]\left[\cos(\alpha_m)\right. \\ &\quad \left. - \cosh(\alpha_m) - \frac{\alpha_m}{k_2^*}(\sinh(\alpha_m) + \sin(\alpha_m))\right] = 0 \end{aligned} \tag{59}$$

The lowest α_m value corresponds to the solution with only one half-wave. Successive solutions can be obtained by solving the following mode values. It is important to solve α_m up to a certain degree of accuracy to obtain proper results.

The different C_{m_i} constants are calculated then from the α_m numerical results.

$$\begin{cases} C_{m_1} = -\dfrac{\sinh(\alpha_m) - \sin(\alpha_m)}{\cos(\alpha_m) - \cosh(\alpha_m) - \dfrac{2\alpha_m}{k_1^*}\sinh(\alpha_m)} C_{m_4} = -\gamma_m C_{m_4} \\ C_{m_2} = -\left(1 + \dfrac{2\gamma_m \alpha_m}{k_1^*}\right) C_{m_4} \\ C_{m_3} = \gamma_m C_{m_4} \end{cases} \tag{60}$$

As it has been mentioned, one of the constants cannot be solved, otherwise the amplitude of the shape would have already been fixed. The dimensionless shape function is then

given for $C_{m_4} = 1$, using the undetermined W_{mn} coefficient to give the corresponding amplitude.

$$\begin{aligned} W &= \sum_{m=1}^{M}\sum_{n=1}^{N} W_{mn} X_m Y_n \\ &= \sum_{m=1}^{M}\sum_{n=1}^{N} W_{mn}\left[-\gamma_m \cosh(\alpha_m\xi) - \left(1+\frac{2\gamma_m\alpha_m}{k_1^*}\right)\sinh(\alpha_m\xi)\right. \\ &\left. + \gamma_m \cos(\alpha_m\xi) + \sin(\alpha_m\xi)\right]\left[-\gamma_n \cosh(\alpha_n\eta)\right. \\ &\left. - \left(1+\frac{2\gamma_n\alpha_n}{k_3^*}\right)\sinh(\alpha_n\eta) + \gamma_n \cos(\alpha_n\eta) + \sin(\alpha_n\eta)\right] \end{aligned} \tag{61}$$

Once the linear set of functions has been chosen and the required approximations for the natural boundary conditions are made, it is possible to determine the E_i coefficients in Galerkin method.

$$\begin{aligned} E_1 = |M_x - \bar{M}_x|_{x=0} &= \left|-D_{11}\frac{\partial^2 w}{\partial x^2} - 2D_{16}\frac{\partial^2 w}{\partial x \partial y} - D_{12}\frac{\partial^2 w}{\partial y^2} - \bar{M}_x\right|_{x=0} \\ &= -2D_{16}\left.\frac{\partial^2 w}{\partial x \partial y}\right|_{x=0} \end{aligned} \tag{62}$$

The rest of the coefficients can be obtained following the same procedure. In dimensionless[5] form, they all are:

$$\begin{aligned} {E_{ij}}_1^* &= \left.\frac{a_1}{2}\frac{\partial X_i}{\partial \xi}\frac{\partial Y_j}{\partial \eta}\right|_{\xi=0} \quad {E_{ij}}_2^* = \left.\frac{a_1}{2}\frac{\partial X_i}{\partial \xi}\frac{\partial Y_j}{\partial \eta}\right|_{\xi=1} \\ {E_{ij}}_3^* &= \left.\frac{a_3}{2}\frac{\partial X_i}{\partial \xi}\frac{\partial Y_j}{\partial \eta}\right|_{\eta=0} \quad {E_{ij}}_4^* = \left.\frac{a_3}{2}\frac{\partial X_i}{\partial \xi}\frac{\partial Y_j}{\partial \eta}\right|_{\eta=1} \end{aligned} \tag{63}$$

Therefore, using the proposed solution to approximate the out-of-plane displacement, the boundary terms (eq.38) in Galerkin solution could be specified as:

[5] Apart from the non-dimensionalization, $E^*_{ij_k}$ also accounts for the set of linear functions that represent the out-of-plane displacement (therefore there is one term for each combination). Furthermore, the dimensionless amplitude of the out-of-plane displacement is taken out.

$$\boldsymbol{K_{B_{pq}}} = \sum_{p=1}^{MN}\sum_{q=1}^{MN}\left\{\int\left\{\frac{a_1}{2}\frac{\partial X_i}{\partial \xi}\frac{\partial Y_j}{\partial \eta}\bigg|_{\xi=1}\left|\frac{\partial X_m}{\partial \xi}Y_n\right|_{\xi=1}\right.\right.$$
$$\left.-\frac{a_1}{2}\frac{\partial X_i}{\partial \xi}\frac{\partial Y_j}{\partial \eta}\bigg|_{\xi=0}\left|\frac{\partial X_m}{\partial \xi}Y_n\right|_{\xi=0}\right\}d\eta$$
$$+\int\left\{\frac{a_3}{2}\frac{\partial X_i}{\partial \xi}\frac{\partial Y_j}{\partial \eta}\bigg|_{\eta=1}\left|X_m\frac{\partial Y_n}{\partial \eta}\right|_{\eta=1}\right.$$
$$\left.\left.-\frac{a_3}{2}\frac{\partial X_i}{\partial \xi}\frac{\partial Y_j}{\partial \eta}\bigg|_{\eta=0}\left|X_m\frac{\partial Y_n}{\partial \eta}\right|_{\eta=0}\right\}d\xi\right\} \tag{64}$$

3.1.3.5. The Eigenvalue problem

After developing both the Galerkin and Ritz solution methods and having approximated the buckled shape, it is necessary to build the system matrices and solve the generalized eigenvalue problem.

A generalized eigenvalue problem is a system of equation that shows the following form:

$$(\boldsymbol{A} - \lambda \boldsymbol{B})\boldsymbol{v} = 0 \tag{65}$$

Where *A* and *B* are square matrices, λ is the eigenvalue and v is the eigenvector. The objective is obtaining the different eigenvalues that allow non-trivial solutions of the system (therefore $\boldsymbol{v} \neq 0$).

3.1.3.5.1. Solving the system matrices

Before solving the eigenvalue problem it is necessary to determine *A* and *B*. The different terms in the matrix are obtained from the multiplication of several coefficients with the results of integrals coming either from the energy minimization in the Ritz solution or the residual error minimization in the Galerkin solution. Depending on how that integral has been solved, two different methods are distinguished:

- The first consists in solving analytically the required integrals. To obtain those the symbolic solver of Matlab has been used.
- The second method consists in solving the integrals numerically. The best results in terms of performance and accuracy have been obtained using a Gauss Legendre algorithm. Different ones have also been tested, such as Romberg´s method, but have shown poorer time performance.

The main advantage of using analytical integration is the speed at which all the integrals can be solved. However, an important problem has been encountered. The use of hyperbolic functions has resulted on the appearance of numerical problems such as catastrophic cancellation.

This problem is caused when two very similar numbers are subtracted. Due to the limited precision used by computers to store and operate on numbers, this can result in an important reduction in the number of accurate digits of the solution. A simplified example is presented:

$$\begin{aligned} x_{1_{real}} &= 205.3217, \quad & x_{1_{computer}} &= 205.3 \\ x_{2_{real}} &= 205.3976, \quad & x_{2_{computer}} &= 205.3 \\ (x_1 - x_2)_{real} &= 0.0759, \quad & (x_1 - x_2)_{computer} &= 0 \end{aligned} \tag{66}$$

For instance, if a computer can only store 4 meaningful digits, the result of the previous operation is very different from the real solution. Double float precision allows for much better accuracy in the storage of numbers, however, hyperbolic functions (sinh(x) and cosh(x)) tend to infinite when the absolute value of x gets bigger. This means that the individual integration of those functions can result in very big numbers.

It is possible to avoid this numerical issue by using numerical integration instead. The main drawback then, is that it is necessary to execute the numeric algorithm for every integration, which reduces the performance in comparison with analytical solutions.

In section 3.3 it is studied when those numerical issues arise and numerical integration is required.

3.1.3.5.2. Solving the Eigenvalue problem

Due to the size of the square system matrices (two times M by N), it is necessary to numerically evaluate the critical eigenvalues of the Eigenvalue problem. Multitude of algorithms are available for that purpose, but it is interesting to determine first the characteristics of the Eigenvalue system and what solutions are required in order to choose the best algorithm.

The system matrices ought to be symmetric, therefore a solver for symmetric eigenvalue systems should be sufficient. However, it has been observed that due to numerical errors in the evaluation of the systems matrix terms, sometimes the matrices are not perfectly symmetric. In fact, the symmetry of the system is used to assess if catastrophic cancellation takes place when using analytical integration. Therefore, the adopted solution checks the degree of asymmetry and switches to numerical integration if necessary. Moreover, if there is only a small degree of asymmetry this is corrected by adding the matrix to its transpose and divided by two. This can speed up eigenvalue algorithm solvers.

It is convenient to obtain not only the smallest (critical) eigenvalue, since the subsequent modes can also be interesting in plates. Moreover, the corresponding eigenvector can be used to plot the buckling solution and compare it with the solution obtained from other methods.

The eig function of Matlab (Cholesky factorization and Schur decomposition) has been used as it easily returns all the eigenvalues and correspondent eigenvectors without an observed important difference in performance from other methods.

3.2. FE model

The main verification of the solutions obtained by the proposed semi-analytical model has been done running equivalent models in FEM with the commercial software package ABAQUS. The FEM model is built from a script written in Python, which is able to automatically set the parameters of the model to the requested configuration.

3.2.1. Model basics

The model consists of a single rectangular flat plate, declared as a 3D deformable body to allow for the out-of-plane deformation during buckling. The thickness and properties are introduced by a composite lay-up definition and the corresponding material lamina properties.

3.2.2. Mesh

A structured mesh has been used. After some preliminary convergence studies it has been concluded that 20 elements should be used in the shorter edge, making sure that every half-wave has at least half this number of elements to be properly modeled (to stay on the safe side). The number of elements per edge is doubled when shear loading is present to cope with the more complex mode shapes. Two different mesh and element combinations are used. The first consists in rectangular S4R shell elements with reduced integration. Moreover, STRI3 elements have been used with its required triangular mesh. The advantage of using those elements is that Kirchhoff thin plate hypothesis is already imposed in the element formulation, neglecting transverse shear effects (thick plates).

3.2.3. Boundary conditions and loads

Several boundary conditions are applied to the FE model. First of all the out-of-plane displacement of all the edges is set to zero. To avoid free body translations the first corner has its translation fixed. Rotation is also limited by fixing the perpendicular movement of the other corner on the bottom edge. The in-plane displacement of the rest of the edges is completely free, so no zero in-plane displacement is imposed (only forces). These are shown in figure 6:

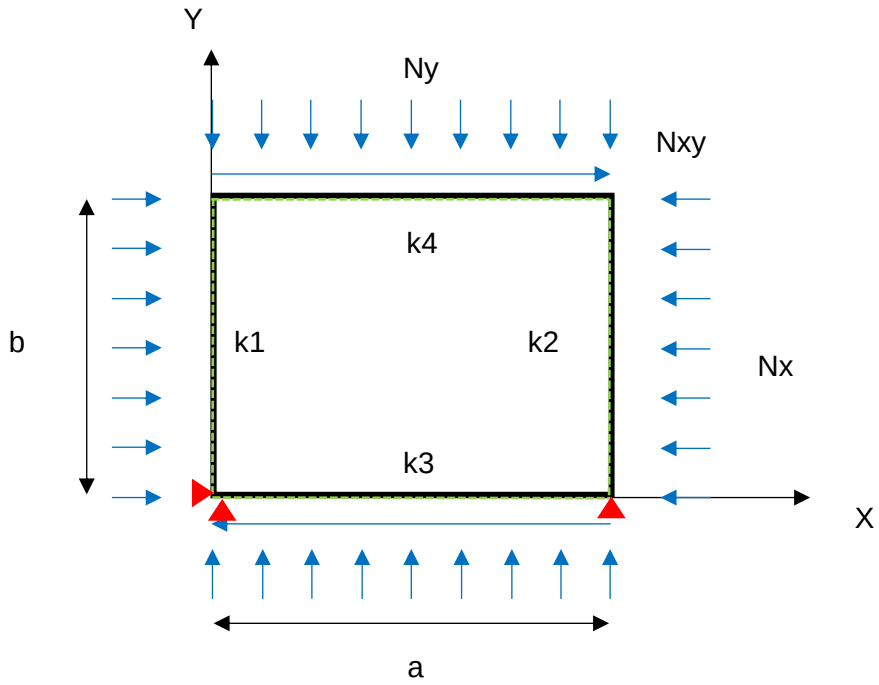

Figure 6: Boundary conditions and loads FE model

The elastic torsion restrain is modeled through the use of spring elements connected to ground. Those elements are present around all the edges connecting every node. Since they have discrete values per element it is necessary to convert their values:

$$k_{i_{FEM}} = \frac{k_i \, lengthside_i}{numberofelements_i} \tag{67}$$

The load is applied uniformly distributed along the edges. The only difference is that the FE model is under simple shear instead of pure shear. Since the boundary conditions does not allow the rotation of the plate, it does not make any difference.

The loads applied are normalized (as shown in the first two terms of eq. 32) in order to obtain the eigenvalue with the critical load.

3.2.4. Analysis and results

The buckling load is obtained through a linear buckling analysis (perturbation). Several buckling modes are required to be able to check successive modes, and also to discard negative eigenvalues when the plate is under shear.

Apart from the eigenvalue, the out-of-plane displacements are also requested, so it is possible to check that the buckling mode is equivalent to the one obtained from the semi-analytical model. The results obtained from Abaqus are then output in .txt files for further post-processing.

3.3. Solution and verification

Both the semi-analytical and FE models have been implemented, so they can be executed automatically from a Matlab program. This program can run though several configurations to compare the results given from the proposed semi-analytical model and FEM.

Additionally, the results obtained have also been compared with closed-form solutions currently used by Fokker in preliminary design. These simpler closed form solutions are developed only for specially orthotropic laminates, ideal boundary conditions and up to dual load combinations. However, it is interesting to see how the proposed solution improves both the accuracy and possibilities of the current tools used for preliminary design.

The semi-analytical model requires certain approximations to make the mathematical formulations manageable. Therefore, it has been found necessary to make a detailed verification in order to assess how well do the approximation work.

The variables of the semi-analytical model are:

- **Geometry**: the model geometry is controlled by modifying the length 'a', therefore changing the aspect ratio of the plate.
- **Lay-up and material**: different lay-ups are tested to verify the results. Most of the solutions will focus on three main lay-ups: predominant 0s (541)[6], predominant 45s (181) and quasi isotropic (343). These laminates have been selected based on the typical design space used by Fokker. Studying the following figure, it might be seen that the three laminates represent the vertices of the Fokker design space triangle:

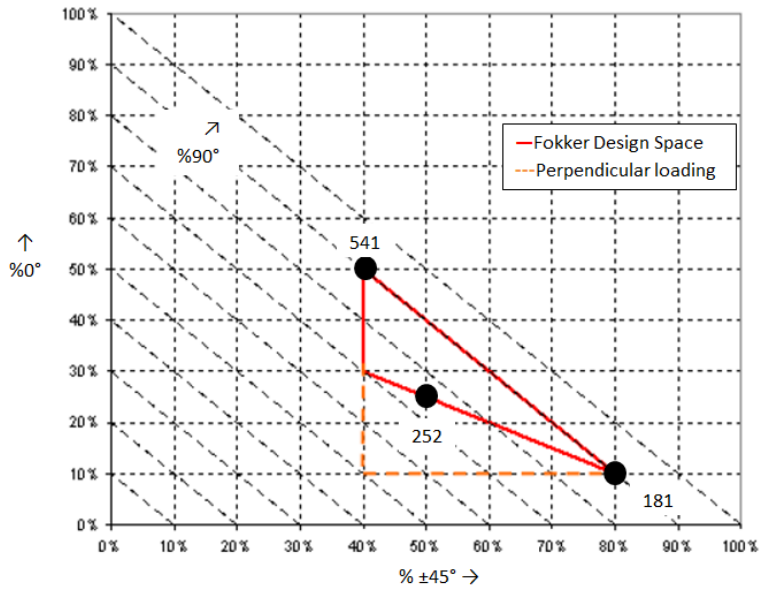

Figure 7: Fokker laminate design space

The sequence of the main laminates is described on the following table.

[6] This number defines the number of plies with the three standard orientations. The first digit is the number of 0s, the second is the number of ±45s and the thirds is the number of 90s. Additionally, those lay-ups are symmetric and balanced.

Table 1: Fokker layups

Laminate name	Layup
Predominant 0s (541)	[0,45,0,90,0,-45,0,45,0,-45]s
Predominant 45s (181)	[45,-45,0,45,-45,90,45,-45,45,-45]s
QI (343)	[-45,0,0,45,90,90,-45,0,45,90]s

Typical Fokker carbon fiber material properties are used. Additional lay-ups are used as well to cover other typical Fokker designs or to cope with special laminates.

- **Thickness**: according to thin plate theory, the results are proportional to t^3. However, if transverse shear is taken into account, thick plates do not follow this rule. Different thicknesses are tested in order to assess which are the maximum thicknesses for which thin plate theory still gives reliable results.
- **Boundary conditions**: The proposed formulation allows to independently set every edge torsional restrain making it possible to have simply supported conditions, clamped or anything in between on any edge. Several configuration are tested to verify the validity of the proposed formulation.
- **Load**: The semi-analytical solution allows for any combination of constant in-plane loads. Individual loads and combinations are used to verify the accuracy of each of them.

Additionally, the number of terms, used to reproduce the out-of-plane shape in the semi-analytical model, is very important. The performance of the method depends greatly on this number, so several tests are carried out to assess which are the minimum number required and the correspondent accuracy to be expected.

The lamina properties used are the following:

Table 2: Lamina properties

Lamina properties	
Longitudinal Young modulus (E_x)	135 GPa
Transverse Young modulus (E_y)	8.84 GPa
Shear modulus (G_{xy})	4.94 GPa
Poisson coefficient (ν_{xy})	0.3

3.3.1. Summary of results

The results obtained from both the semi-analytical, Fokker closed form and FE models are saved into Excel documents. These documents gather the solutions of all the configurations tested and allow a fast visualization (through cell color) of the error in

between the different solutions. Due to the amount of solutions, it has been decided to include all the solutions in a digital annex and present the most important results grouped in figures.

3.3.2. Convergence of semi-analytical model

It is difficult to define an exact rule for the convergence of the semi-analytical model. Clearly, the number of functions necessary to have a proper solution depends on:

- **The number of half-waves (aspect ratio)**. It has been seen that every term in the linear set of functions, (which represents the out-of-plane displacement) is the solution estimated for its correspondent combination of half-waves. Therefore plates with a critical mode consisting in several waves would need more terms to be properly solved.
- **Loading**. The chosen linear set of functions has two independent terms for the x and y directions. This is suitable to represent buckled shapes when there is axial loading. However, under shear, the waves have diagonal shape. Those shapes can only be created by the combination of different terms, making it necessary to use a higher number to obtain an accurate solution.
- **Laminate properties**. The properties and material complexity have an important effect on the number of terms required. When laminates are specially orthotropic, the natural boundary conditions are perfectly satisfied and convergence is faster. It has been observed that non-balanced laminates are the ones presenting more problems.

The following figures present convergence analysis of the semi-analytical model for different cases. Both are for plates with clamped boundary conditions (simply supported typically have faster convergence). Moreover, the predominant 45s laminate has been chosen because of the most important effect of D_{16} and D_{26} terms. For simplicity, symmetric[7] number of terms are used. Other strategies could be considered to improve the performance, such as using more terms in one direction to cope with the aspect ratio, or using specific half-waves.

The first figure studies the convergence under uniaxial compression for different aspect ratios.

[7] The same number of terms is used in both directions. Therefore using 16 terms means the use of 4 in each direction.

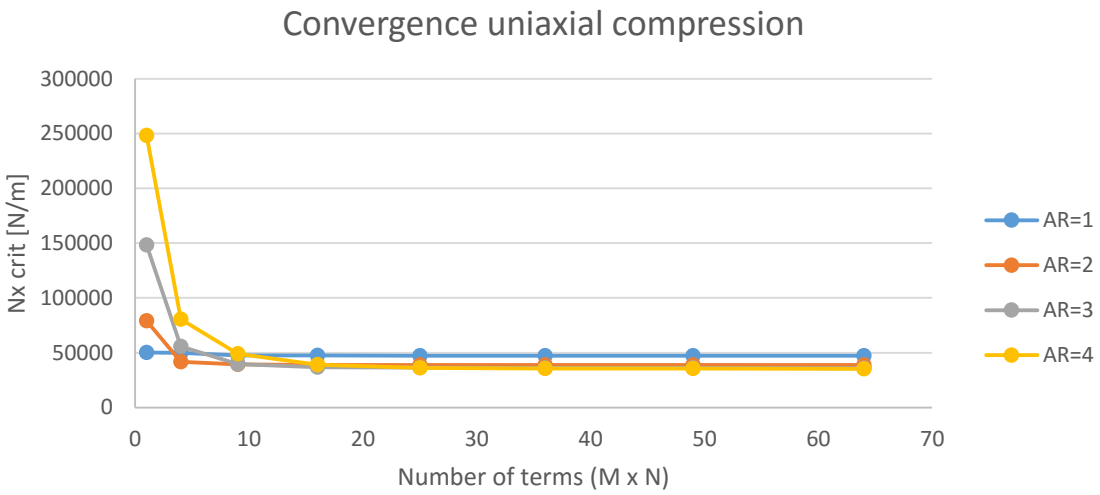

Figure 8: Convergence study uniaxial compression

The second figure shows the convergence analysis under shear loading.

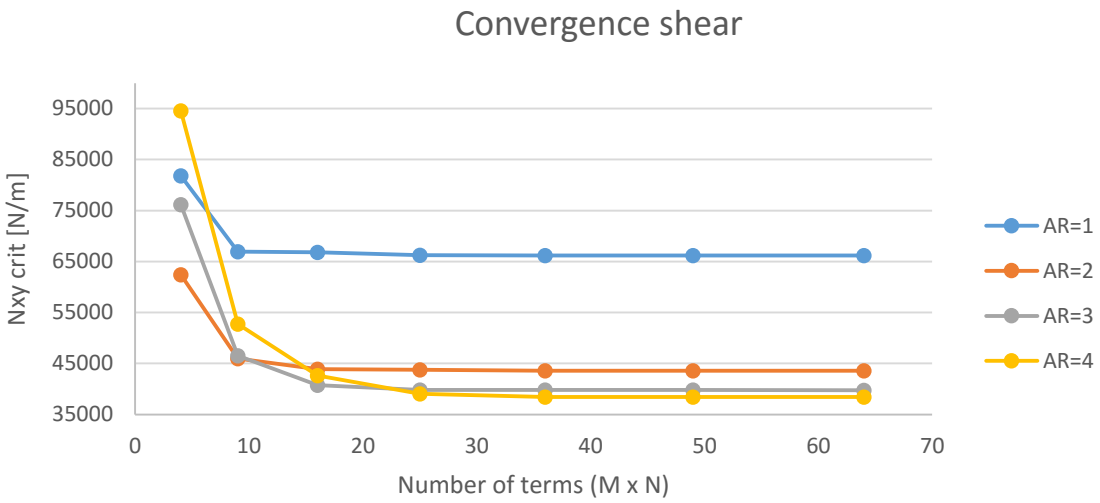

Figure 9: Convergence study shear

In uniaxial compression, it is clear that the main problem is having enough terms to capture the solution (plate with aspect ratio 1 buckles with one half-wave, so one term already gives a good approximation). As has been mentioned, shear presents more problems because the diagonal buckling shape cannot be properly approximated with one term (it is started with four). In the cases presented, convergence is obtained at 16 terms, except for a plate of aspect ratio 4 under shear, were 25 terms are required.

3.3.3. Verification with FEM

The main verification consists in a comparison between the solutions given by both semi-analytical and FE models. Aside from the Excel files included in the annex, it has been decided to present several cases to demonstrate that the accuracy of the solutions can be easily assessed for a limited number of representative cases.

The fact that there are 5 different variables (aspect ratio, thickness, boundary conditions, load case and lay-up) that can take multiple values, makes the amount of possible cases difficult to present. The following cases have been chosen:

Verifications will involve the three main lay-ups previously defined. Every one of them will be tested in uniaxial compression, shear and a combination of the previous two (one to one ratio). The verification of the selected load cases should give confidence in that any combination of compression and shear might be included in the design space.

The geometry has been fixed, the length of the shorter side *b* is 100mm and the thickness of the laminate is 1mm (ensuring thin plate behaviour).

The verification of the previous configuration include buckling load against aspect ratio curves for different boundary conditions (simply supported, constant elastic restrain of 200N and clamped). This boundary conditions should guarantee that both ideal and intermediate cases can be solved with the developed formulation. The maximum aspect ratio tested is 4.6. From the verifications it can be observed that the results remain fairly constant for the higher aspect ratios, resulting less interesting to test much higher aspect ratios. The results obtained by the FE software package are introduced as discrete dots over the curves. All loads are given in N/m (in combined loading, the result given is for the Nx component).

The results of the semi-analytical model are obtained using 36 terms and the Ritz method with numeric integration. In case of discrepancies between Ritz and Galerkin, these are outlined.

3.3.3.1. Predominant 45s

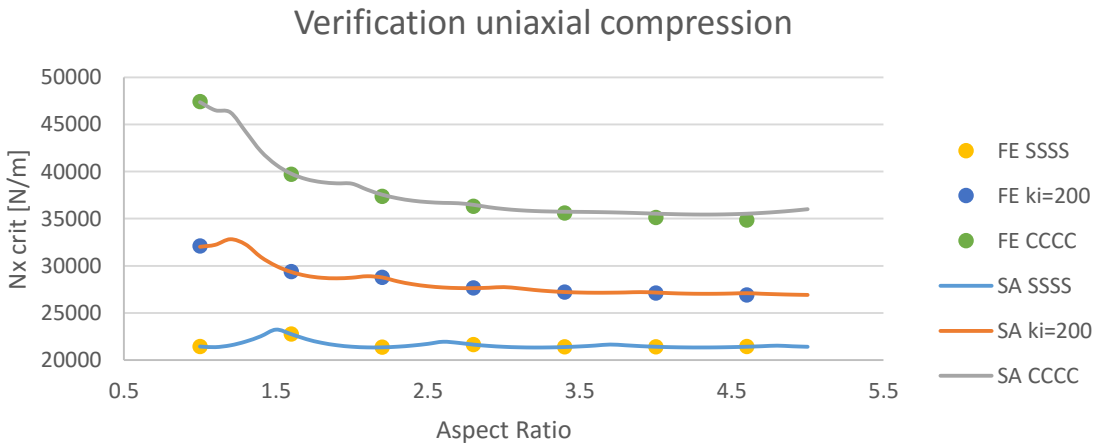

Figure 10: Verification predominant 45s under uniaxial compression

The results show excellent agreement between the semi-analytical solution and FEM. The error is below 1% except for the last two results of the clamped curve (1.2 and 1.4%). Plates with clamped boundary conditions buckle in a higher number of half-waves, so it seems clear that the problem is that more terms are required to properly predict the buckling load for higher aspect ratios. Using more terms might not be a practical solution, as the performance of the calculations is affected, however, the solution for high aspect ratio plates tends to go towards a constant value. Therefore, it is not necessary to solve

high aspect ratio plates, very good results for the critical buckling load are obtained assuming a constant buckling value after 5-6 half-waves. For a more efficient calculation an infinite plate formulation could be developed.

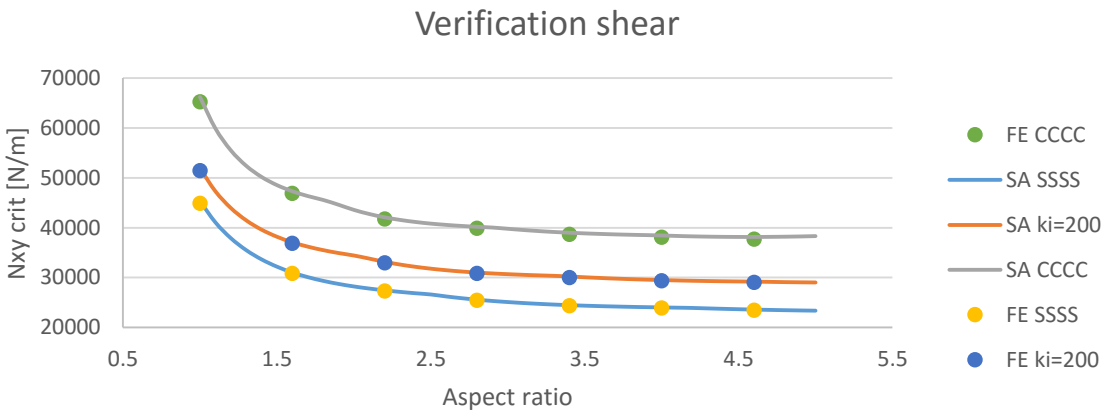

Figure 11: Verification predominant 45s under shear

The agreement between FE and semi-analytical is also excellent for shear with a maximum error of 1.4%. Shear shows less spikes so it is more difficult to see the aspect ratio where there is a change in the number of half-waves. On the other hand, there appears to be less problems to solve the higher aspect ratios of the clamped solution.

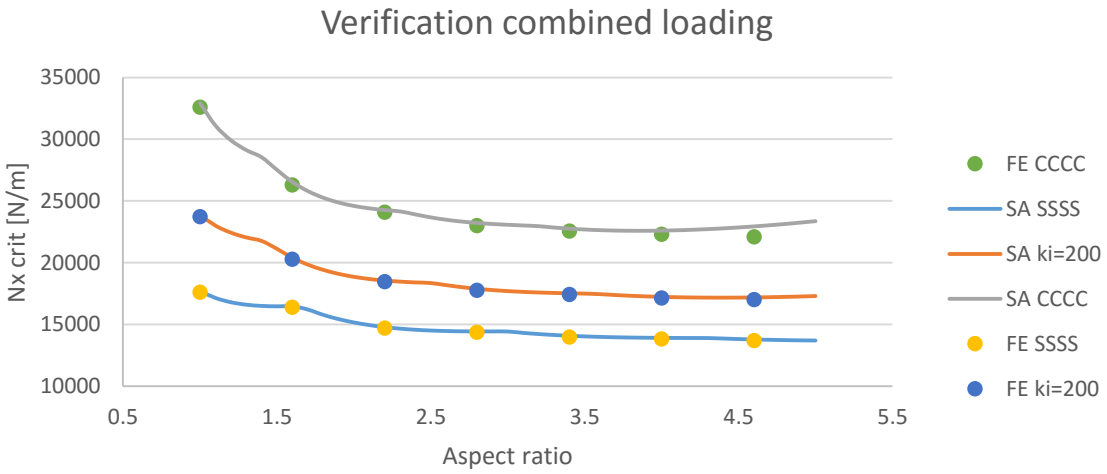

Figure 12: Verification predominant 45s under combined loading

Combined loading also shows a very good agreement between solutions. Similarly to compression, some problems arise to reproduce the clamped buckling mode for the highest aspect ratio data point (3.7%). The rest of the results have errors below 1.3%, so it is clear that the semi-analytical solution does not have any problem to handle combined loading.

Differences between the Galerkin and Ritz methods are negligible for all the load cases (below 0.2%).

3.3.3.2. Predominant 0s

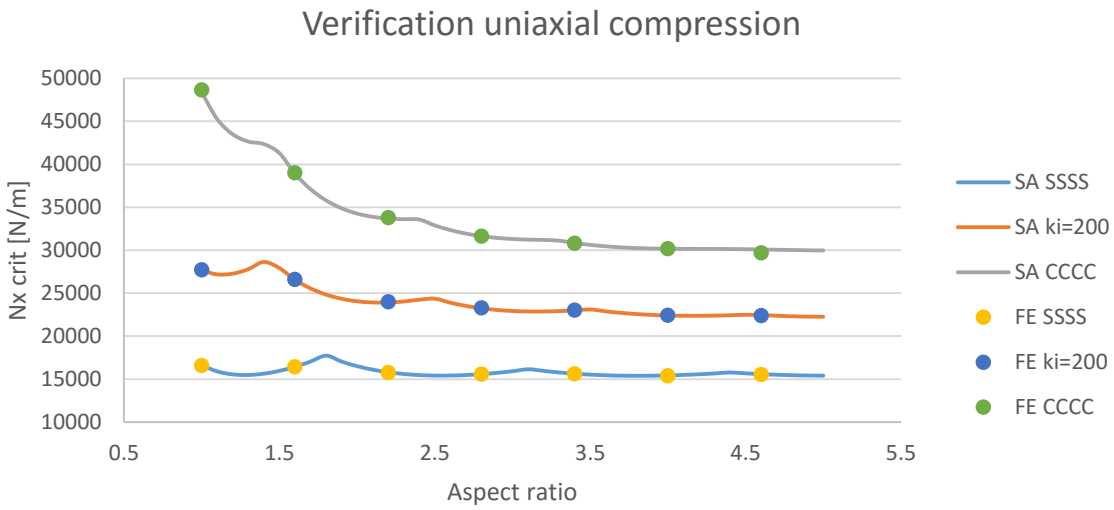

Figure 13: Verification predominant 0s under uniaxial compression

The predominantly 0s laminate shows even a better agreement than previous cases with a maximum error of 1.3%. The reason is the lesser importance of D_{16} and D_{26} terms (laminate is more orthotropic) and also the fewer number of half-waves. Mittelstedt [44] uses the modified aspect ratio parameter to account for the effect of D_{11} and D_{22}:

$$\alpha = \frac{a}{b}\sqrt[4]{\frac{D_{22}}{D_{11}}} \tag{68}$$

The modified aspect ratio parameter can be a good approach to avoid misestimating the number of terms required for the higher aspect ratios, however it must be remembered that other factors, such as loading and boundary conditions, are important as well.

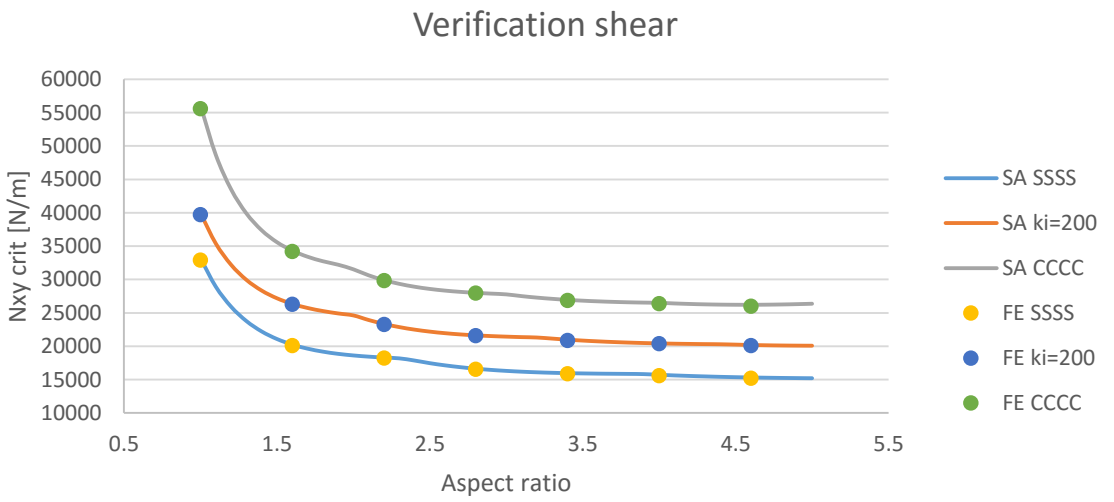

Figure 14: Verification predominant 0s under shear

Shear also shows an excellent agreement with FEM results, with all the errors below 1%.

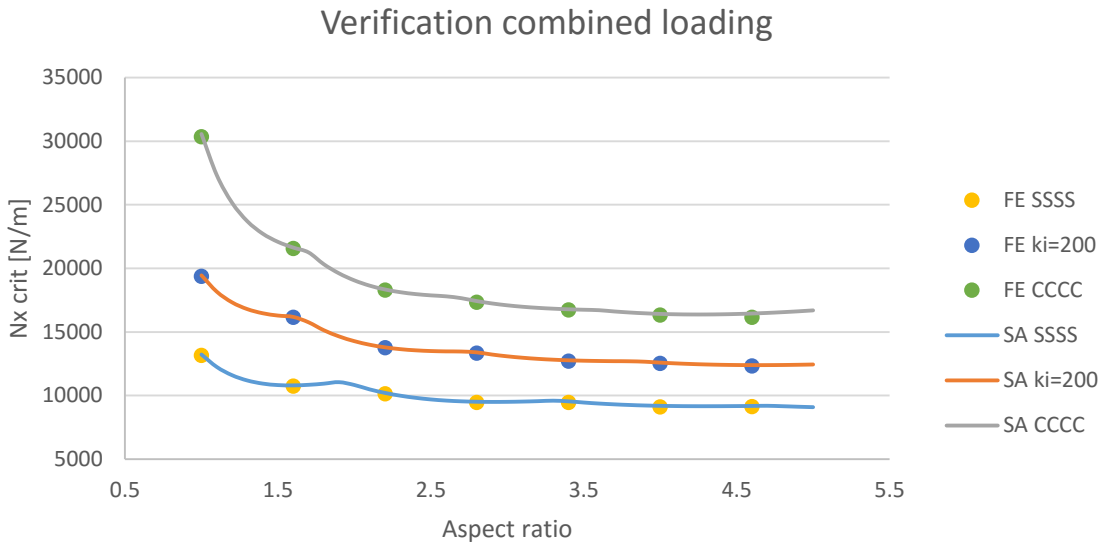

Figure 15: Verification predominant 0s under combined loading

Again, combined loading seems to be the more susceptible to have more half-waves and therefore present problems before with the lack of terms for high aspect ratios. However, the maximum error is only 1.8% (for the last result of the clamped solution) and all the rest are below 1%.

There has been also a good agreement between Ritz and Galerkin for all the different cases (below 0.75%). Moreover, this error does not affect the clamped results (where the errors have been more important) because in those cases the natural boundary conditions are satisfied exactly despite bending-twisting coupling (zero error between Ritz and Galerkin).

3.3.3.3. Quasi isotropic

Quasi isotropic laminates have a similar behaviour to isotropic materials, and the presence of less 45s reduce the D_{16} and D_{26} coupling in comparison with other layups. In such cases, the natural boundary conditions are satisfied and the results tend to the exact solution for a small number of terms. However, high aspect ratio plates will require enough terms to represent the number of half-waves.

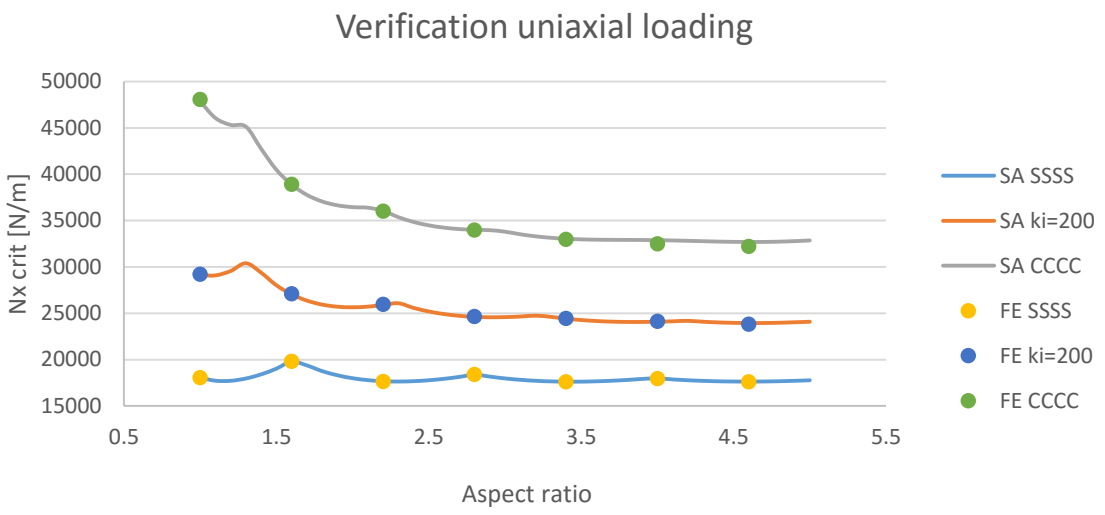

Figure 16: Verification QI under uniaxial compression

As expected, there is an excellent agreement between the two models, with a maximum error below 1.5%.

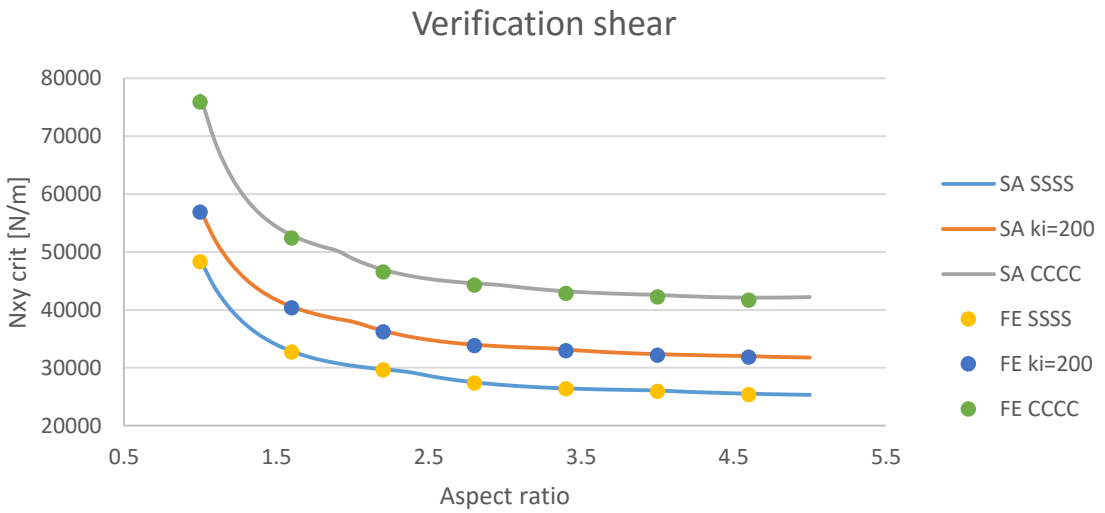

Figure 17: Verification QI under shear

Shear also gives a similar accuracy as uniaxial compression, with a maximum error of 1.5%

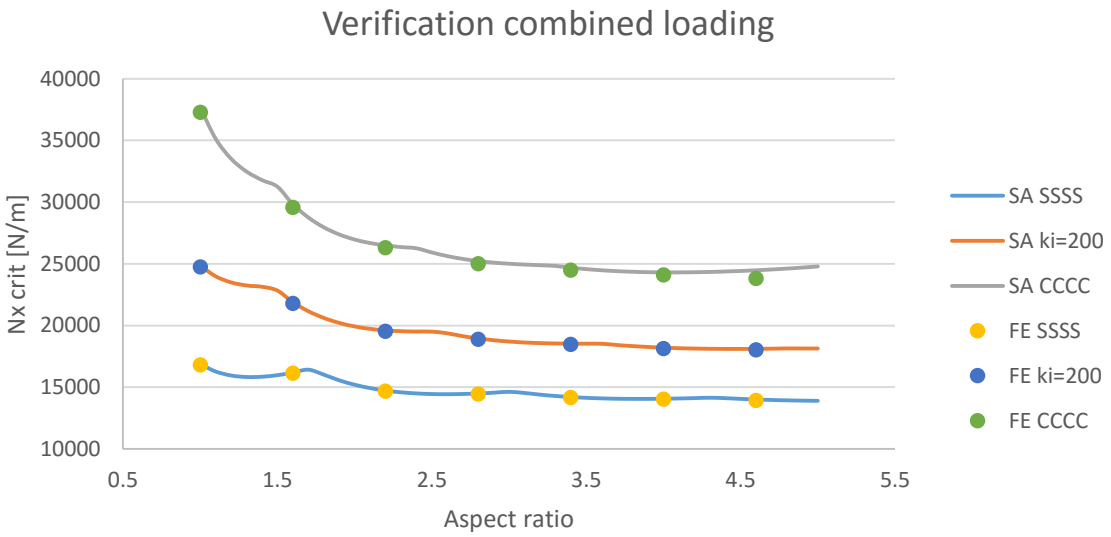

Figure 18: Verification QI under combined loading

Combined loading shows again higher sensibility to the lack of terms for the clamped solution at the highest aspect ratio (error 2.8%). Despite this value the agreement between solutions is still very good (rest of errors below 1.1%).

Again, there is no important differences between Galerkin and Ritz, so both methods might be used.

3.3.4. Special cases

Additional verifications have been performed to assess some special cases.

3.3.4.1. Thickness verification

The developed thin plate formulation is only valid when thickness is much smaller than the other dimensions. However, it is more difficult to specify a limit value above which thin plate theory is no longer valid.

The following figures give the evolution of the error between results given by the semi-analytical model and the FE results using shell elements. The buckling results for symmetric thin plate plates are proportional to the *D* matrix, and this is proportional to t^3, therefore there is no need to calculate results for every thickness. The x axis shows the results as a function of t^3/b in order to show this proportionality. The FE results diverge from the semi-analytical when thickness is increased (the % error is included next to every data point).

With these results it is possible to assess the limitations of thin plate theory and visualize the cases that will require a more advanced plate formulation.

The thickness to side length ratios used in the figures are (from left to right) 1/100, 1/50, 1/33 and 1/25.

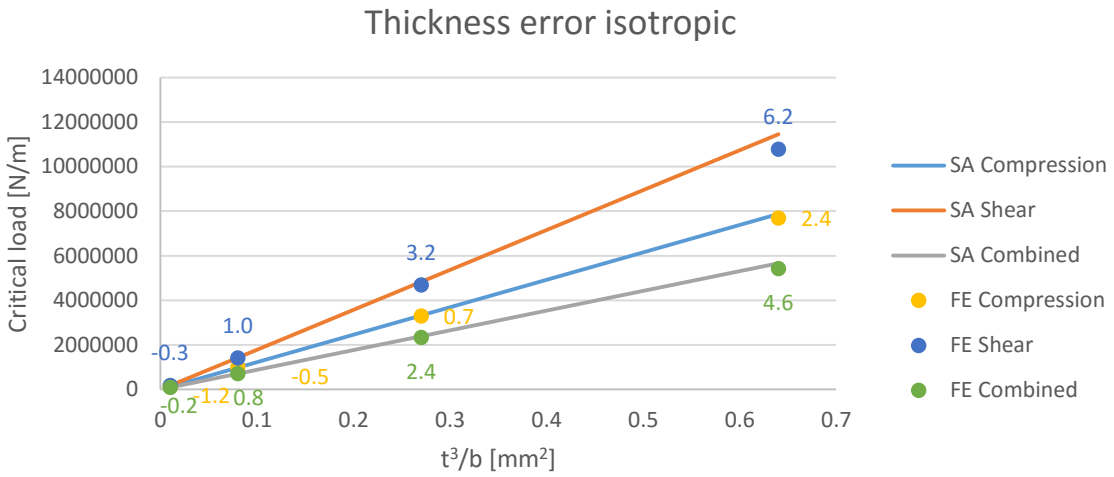

Figure 19: Error due to thickness effects for an isotropic laminate

For isotropic laminates, thickness effect are relevant for ratios below 1/50 or 1/33. Before that, errors are in the same order as calculated for the previous verifications. Compression is clearly less affected by thickness effects while shear gives a 6.2% error for a 1/25 ratio.

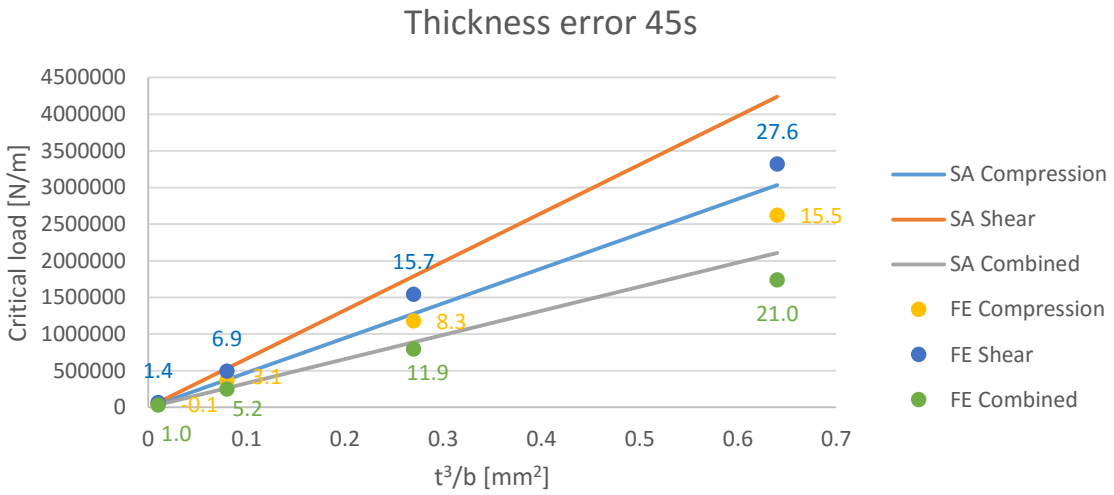

Figure 20: Error due to thickness effects for a predominant 45s laminate

Composite laminates are more affected by the thickness effects. Chapter 10 of Whitney [15] states that the high ratio between in-plane Young modulus to interlaminar shear modulus is the main reason of the higher sensitivity of composites.

For the predominant 45s laminate, thickness effects are already significant for a 1/50 ratio, which reduces the application of the thin plate theory. Again compression is less affected than shear. Notice that semi-analytical solutions are unconservative, so it might be necessary to use safety margins for ratios below 1/100 or 1/50. If it is necessary to typically work on smaller ratios it might be interesting to adapt the formulation to higher order theories for moderately thick plates.

It must be taken into account that the aspect ratio, boundary conditions and lay-up affect the importance of thickness effects:

- High aspect ratio plates show less thickness effects as the ratio between surface and thickness is higher in those cases. The results given (figures 18 and 19) are for the least favorable case (square plate).
- The results given are for a clamped plate. This has shown to be the least favorable case among the ones tested.
- The predominant 45s laminate has shown to be one of the most sensitive to thickness effects. So once again, the case presented is one the least favorable.

3.4. Conclusions buckling

The verifications performed show excellent agreement for typical laminates used at Fokker aerospace under the different conditions tested and using a much reduced number of degrees of freedom compared to FE. The different numeric methods used (Galerkin and Ritz) have provided almost identical results once the surface boundary terms are taken into account in the Galerkin method solution. Therefore, there are no clear reasons to conclude which method is recommended, further implementations of the formulation in high performance programs might be used to decide based on computational efficiency.

The main limitation observed is the rigorous implication of thin plate theory assumptions for typical lamina properties. As commented by Whitney in section 10.1 of [15] the high ratio of in-plane Young modulus to transverse shear modulus can result in important divergences (unconservative) of the results for relatively thin plates. This tendency has been confirmed and more conservative margins are given to validate when thin plate theory is applicable for such materials.

Moreover, it has been studied the different aspects that control the number of terms required to obtain accurate buckling solutions. The results obtained confirmed the conclusions reached during the convergence study and showed how some errors started to appear for higher aspect ratios for the cases determined as more critical. Therefore, the use of similar strategies might be used to determine the minimum number of terms when different plates are under study. Furthermore, more advanced automated approaches can be developed to avoid the necessity of performing preliminary convergence studies. Factors to be considered in future developments are the use of term that are more meaningful to the solution (using custom terms instead of a series ranging from one to M) and the use of dissimilar number of terms in each direction. Such developments would allow an optimization of the required time.

On the same line, it has already been mentioned that the current approach cannot efficiently solve high aspect ratio plates due to the high amount of terms required. The advantage of such cases is that the buckling load quickly converges to a constant value when multiple half-waves are present. The studied solutions clearly showed this behaviour for aspect ratios around or over four. This fact can be exploited by using an infinite plate theory. Such simplified formulation would provide the constant value at which the solution converges using a reduced computational effort.

Numerical problems have been identified in some cases when using analytical integration. The issue has been solved by using numerical integration algorithms instead but the

performance for such cases is reduced. Additional or alternative measures could be taken such as using different shape functions that might not show this sensitivity, for example using polynomials or linear interpolation between simply supported and clamped solutions.

In conclusion, the developed formulation yields excellent results for the required design space, with the only limitation being that it is necessary to verify that the ratio thickness to side length allows the application of thin plate theory. The proposed 36 terms has shown to perfectly work up to aspect ratio 4 for any load case or boundary condition. Higher aspect ratios can be achieved as well by using more terms, however the results suggest that it can be useful to use infinite plate formulations to optimize the results of higher aspect ratios. The current Fokker analytical solutions (See Annex\Buckling\Verification1) are less accurate and valid for a much reduced design space (no elastic restrains). The results for axial loads are acceptable, with errors up to 5 %, but shear is poorly solved due to the neglected of D_{16} and D_{26} terms, with error on buckling load estimation above 20%.

4. Post-buckling of plates

This chapter continues with the development of the post-buckling solution for plates. The implemented solution follows the same approach as buckling, aiming to solve a wide range of different configurations. The increasing complexity of the equations further encourages coming up with convenient approximations capable of reproducing the post-buckling phenomena.

The structure of the chapter is very similar to the previous one. After developing the semi-analytical solution, a brief explanation of the equivalent FE model is introduced. The last section gathers the solutions obtained by the semi-analytical solution and the comparison with FE results.

4.1. Semi-analytical model

4.1.1. Introduction

The semi-analytical model for post-buckling is based on the same thin plate theory. Therefore the main assumptions used in the section 3.1.1.1 are the same. Minor changes are introduced in the additional assumptions to cope with the particularities of post-buckling:

- The plate is allowed to have imperfections. In fact the imperfection is necessary so non-trivial solutions are obtained when solving the equilibrium path. The imperfection can be introduced as a linear combination of buckling modes with an arbitrary amplitude. In order to simplify the imperfection it has been decided to use Qiao's approach [34] to reduce the linear combination to a critical term using sinusoidal waves with the same number of half-waves as the first buckling mode. The formulation can be extended to use the arbitrary linear combinations if required.
- In post-buckling it is impossible to keep both the edges straight and the applied load on the edge constant. Due to the out-of-plane deformation there is a redistribution of loads from the center of the plate to the edges. Therefore, two different options are given:
    - **Keep the applied load constant**: In this case the edges are no longer straight after buckling.
    - **Keep the edges straight**: In this case the load is applied as a constant displacement at the edges.

4.1.2. Governing equations

The introduction of imperfections in the plate and the fact that the force distribution inside the plate is no longer constant results on the use of non-linear partial differential equations. These new equations were derived by Marguerre [9] and are known as Von Kármán-Marguerre equations. The equilibrium equation becomes:

$$\frac{\partial^2 M_x}{\partial x^2} + 2\frac{\partial^2 M_{xy}}{\partial x \partial y} + \frac{\partial^2 M_y}{\partial y^2} + N_x \frac{\partial^2 w}{\partial x^2} + 2N_{xy}\frac{\partial^2 w}{\partial x \partial y} + N_y \frac{\partial^2 w}{\partial y^2} + N_x \frac{\partial^2 w_o}{\partial x^2} + 2N_{xy}\frac{\partial^2 w_o}{\partial x \partial y} + N_y \frac{\partial^2 w_o}{\partial y^2} = 0 \tag{69}$$

Where w_o is the plate initial imperfection. The non-constant value of N_x, N_y and N_{xy} makes necessary to use also the compatibility equation in order to completely define the problem. According to Marguerre, the compatibility equation for imperfect plates is:

$$\frac{\partial^2 \varepsilon_x^0}{\partial y^2} + \frac{\partial^2 \varepsilon_y^0}{\partial x^2} - \frac{\partial^2 \varepsilon_{xy}^0}{\partial x \partial y} + \frac{\partial^2 w}{\partial x^2}\frac{\partial^2 w}{\partial y^2} - \left(\frac{\partial^2 w}{\partial x \partial y}\right)^2 + \frac{\partial^2 w}{\partial x^2}\frac{\partial^2 w_o}{\partial y^2} + \frac{\partial^2 w_o}{\partial x^2}\frac{\partial^2 w}{\partial y^2} - 2\frac{\partial^2 w}{\partial x \partial y}\frac{\partial^2 w_o}{\partial x \partial y} = 0 \tag{70}$$

Where ε^0 is the plate strain at the mid-plane. To apply these equations to laminated plates it is necessary to introduce the ABD matrix, which for mid-plane symmetric plates can be simplified to:

$$\boldsymbol{N} = \boldsymbol{A}\boldsymbol{\varepsilon}^{\boldsymbol{0}}, \quad \boldsymbol{M} = \boldsymbol{D}\boldsymbol{\kappa} \tag{71}$$

Inverting the A matrix ($\boldsymbol{a} = \boldsymbol{A}^{-1}$) and substituting the curvatures by the out-of-plate displacement derivatives the following relations are obtained.

$$\begin{pmatrix} \varepsilon_x^0 \\ \varepsilon_y^0 \\ \varepsilon_{xy}^0 \end{pmatrix} = \begin{bmatrix} a_{11} & a_{12} & a_{16} \\ a_{12} & a_{22} & a_{26} \\ a_{16} & a_{26} & a_{66} \end{bmatrix} \begin{pmatrix} N_x \\ N_y \\ N_{xy} \end{pmatrix} \tag{72}$$

$$\begin{pmatrix} M_x \\ M_y \\ M_{xy} \end{pmatrix} = \begin{bmatrix} D_{11} & D_{12} & D_{16} \\ D_{12} & D_{22} & D_{26} \\ D_{16} & D_{26} & D_{66} \end{bmatrix} \begin{pmatrix} \frac{\partial^2 w}{\partial x^2} \\ \frac{\partial^2 w}{\partial y^2} \\ -2\frac{\partial^2 w}{\partial x \partial y} \end{pmatrix} \tag{73}$$

The Marguerre equations for mid-plane symmetric plates are obtained substituting eq. 73 and 72 into 68 and 69. Moreover, it is preferable to introduce the Airy stress function. The Airy stress function (ϕ) is a scalar potential function used to represent 2D stress fields (or force) which satisfies the equilibrium in the absence of body forces. It allows to combine the different forces or stresses into a single term. Then, the different forces are obtained from the derivatives of the Airy function. In the absence of distributed forces, the in-plane forces are:

$$N_x = \frac{\partial^2 \phi}{\partial y^2}, \qquad N_y = \frac{\partial^2 \phi}{\partial x^2}, \qquad N_{xy} = -\frac{\partial^2 \phi}{\partial x \partial y} \tag{74}$$

Substituting also eq. 74 is obtained:

$$D_{11}\frac{\partial^4 w}{\partial x^4}+4D_{16}\frac{\partial^4 w}{\partial x^3\partial y}+2(D_{12}+2D_{66})\frac{\partial^4 w}{\partial x^2\partial y^2}+4D_{26}\frac{\partial^4 w}{\partial x\partial y^3}+D_{22}\frac{\partial^4 w}{\partial y^4}$$
$$-\frac{\partial^2\phi}{\partial y^2}\left(\frac{\partial^2 w}{\partial x^2}+\frac{\partial^2 w_o}{\partial x^2}\right)+2\frac{\partial^2\phi}{\partial x\partial y}\left(\frac{\partial^2 w}{\partial x\partial y}+\frac{\partial^2 w_o}{\partial x\partial y}\right) \tag{75}$$
$$-\frac{\partial^2\phi}{\partial x^2}\left(\frac{\partial^2 w}{\partial y^2}+\frac{\partial^2 w_o}{\partial y^2}\right)=0$$

$$a_{22}\frac{\partial^4\phi}{\partial x^4}-2a_{26}\frac{\partial^4\phi}{\partial x^3\partial y}+(a_{66}+2a_{12})\frac{\partial^4\phi}{\partial x^2\partial y^2}-2a_{16}\frac{\partial^4\phi}{\partial x\partial y^3}+a_{11}\frac{\partial^4\phi}{\partial y^4}$$
$$+\frac{\partial^2 w}{\partial x^2}\frac{\partial^2 w}{\partial y^2}-\left(\frac{\partial^2 w}{\partial x\partial y}\right)^2+\frac{\partial^2 w}{\partial x^2}\frac{\partial^2 w_o}{\partial y^2}+\frac{\partial^2 w_o}{\partial x^2}\frac{\partial^2 w}{\partial y^2} \tag{76}$$
$$-2\frac{\partial^2 w}{\partial x\partial y}\frac{\partial^2 w_o}{\partial x\partial y}=0$$

The next step is to non-dimentionalize the previous equations and define several coefficients in order to simplify the notation. The dimensionless relations are:

$$W=\frac{w}{h},\qquad W_o=\frac{w_o}{h},\qquad \xi=\frac{x}{a},\qquad \eta=\frac{y}{b},\qquad \lambda=\frac{a}{b},\qquad \boldsymbol{D}^*=\frac{\boldsymbol{D}}{A_{22}h^2}, \tag{77}$$
$$\boldsymbol{a}^*=A_{22}\boldsymbol{A}^{-1}=A_{22}\boldsymbol{a},\qquad F=\frac{\phi}{A_{22}h^2}$$

The coefficients used are:

$$a_1=\frac{4D_{16}^*}{D_{11}^*}\lambda,\qquad a_{2a}=\frac{2D_{12}^*}{D_{11}^*}\lambda^2,\qquad a_{2b}=\frac{4D_{66}^*}{D_{11}^*}\lambda^2,\qquad a_2=a_{2a}+a_{2b}, \tag{78}$$
$$a_3=\frac{4D_{26}^*}{D_{11}^*}\lambda^3,\qquad a_4=\frac{D_{22}^*}{D_{11}^*}\lambda^4,\qquad a_5=\frac{\lambda^2}{D_{11}^*}$$

$$b_1=-2\lambda\frac{a_{26}^*}{a_{22}^*},\qquad b_2=\frac{a_{66}^*+2a_{12}^*}{a_{22}^*}\lambda^2,\qquad b_3=\frac{-2a_{16}^*}{a_{22}^*}\lambda^3,\qquad b_4=\frac{a_{11}^*}{a_{22}^*}\lambda^4, \tag{79}$$
$$b_5=\frac{\lambda^2}{a_{22}^*}$$

Notice the difference between the plate length a, the compliance $\boldsymbol{a}$ and the equilibrium coefficients a_i.

Substituting eq. 77-79 into 75 and 76:

$$\frac{\partial^4 W}{\partial\xi^4}+a_1\frac{\partial^4 W}{\partial\xi^3\partial\eta}+a_2\frac{\partial^4 W}{\partial\xi^2\partial\eta^2}+a_3\frac{\partial^4 W}{\partial\xi\partial\eta^3}+a_4\frac{\partial^4 W}{\partial\eta^4}$$
$$-a_5\left[\frac{\partial^2 F}{\partial\eta^2}\left(\frac{\partial^2 W}{\partial\xi^2}+\frac{\partial^2 W_o}{\partial\xi^2}\right)-2\frac{\partial^2 F}{\partial\xi\partial\eta}\left(\frac{\partial^2 W}{\partial\xi\partial\eta}+\frac{\partial^2 W_o}{\partial\xi\partial\eta}\right)\right. \tag{80}$$
$$\left.+\frac{\partial^2 F}{\partial\xi^2}\left(\frac{\partial^2 W}{\partial\eta^2}+\frac{\partial^2 W_o}{\partial\eta^2}\right)\right]=0$$

$$\frac{\partial^4 F}{\partial \xi^4} + b_1 \frac{\partial^4 F}{\partial \xi^3 \partial \eta} + b_2 \frac{\partial^4 F}{\partial \xi^2 \partial \eta^2} + b_3 \frac{\partial^4 F}{\partial \xi \partial \eta^3} + b_4 \frac{\partial^4 F}{\partial \eta^4} + b_5 \left[\frac{\partial^2 W}{\partial \xi^2} \frac{\partial^2 W}{\partial \eta^2} - \left(\frac{\partial^2 W}{\partial \xi \partial \eta} \right)^2 + \frac{\partial^2 W}{\partial \xi^2} \frac{\partial^2 W_o}{\partial \eta^2} + \frac{\partial^2 W_o}{\partial \xi^2} \frac{\partial^2 W}{\partial \eta^2} - 2 \frac{\partial^2 W}{\partial \xi \partial \eta} \frac{\partial^2 W_o}{\partial \xi \partial \eta} \right] = 0 \tag{81}$$

Different authors [17, 27] split the problem of solving the previous equations. First, the compatibility equation is used to directly solve the coefficients in the Airy Stress function. It is necessary to work with simple out-of-plane functions in order to make the calculations manageable. Therefore, this approach has been used mainly for simply supported specially orthotropic laminates. Since solutions are also available for clamped configurations, it is possible to interpolate solutions for elastically restrained plates.

However, the use of eigenbeam value functions and a mid-plane symmetric formulation increase significantly the complexity of the calculations. Since it is no longer possible to exactly solve for the Airy Stress function in the compatibility equation, it is decided to solve approximately both equilibrium and compatibility in one go using the Galerkin method[8].

4.1.3. The Galerkin method

In order to apply the Galerkin method it is necessary to define both the out-of-plane displacement and the Airy Stress function:

$$W = \sum_{m=1}^{M} \sum_{n=1}^{N} W_{mn} X_m(\xi) Y_n(\eta) \tag{82}$$

$$F = -N_x^* \frac{\eta^2}{2} - N_y^* \lambda^2 \frac{\xi^2}{2} - N_{xy}^* \lambda \xi \eta + \sum_{p=1}^{P} \sum_{q=1}^{Q} \chi_{pq} X_p^c(\xi) Y_q^c(\eta) \tag{83}$$

The out-of-plane deformation follows the same generic form used in buckling. The Airy Stress function will be explained in detail in the next section, but the current form allows also for generic formulations, so the following formulation is still valid for the different cases implemented.

Additionally, the imperfection is also introduced as a one term combination of *X* and *Y* functions.

$$W = W_o X_o Y_o \tag{84}$$

[8] Ritz method is also an option, but since both methods have given almost identical results for buckling (once the natural boundary conditions are corrected) it has been decided to develop only the first.

A double sine function (with the number of half-waves of the first buckling mode) is used to model the imperfection. Further shapes might also be used without modifying the formulation. If multiple combinations are required, then it would be possible to update the formulation and include an additional summatory for such terms.

Instead of developing the Galerkin method from the variations of the total potential energy, it will be directly applied multiplying both the equilibrium and compatibility equations by trial functions in order to minimize the error. The procedure is similar to the one followed by Qiao in [34] and some of the nomenclature used is kept for convenience.

4.1.3.1. Equilibrium equation

Starting with the equilibrium equation, eq. 82 is substituted into 80 and multiplied by the trial function:

$$\begin{aligned}\int\int\Bigg\{&\sum_{i=1}^{M}\sum_{j=1}^{N}W_{ij}\left[\frac{\partial^4 X_i}{\partial\xi^4}Y_j+a_1\frac{\partial^3 X_i}{\partial\xi^3}\frac{\partial Y_j}{\partial\eta}+a_2\frac{\partial^2 X_i}{\partial\xi^2}\frac{\partial^2 Y_j}{\partial\eta^2}+a_3\frac{\partial X_i}{\partial\xi}\frac{\partial^3 Y_j}{\partial\eta^3}\right.\\&\left.+a_4X_i\frac{\partial^4 Y_j}{\partial\eta^4}\right]\\&-a_5\left[\sum_{i=1}^{M}\sum_{j=1}^{N}W_{ij}\left\{\sum_{p=1}^{P}\sum_{q=1}^{Q}\chi_{pq}\left[X_p^c\frac{\partial^2 Y_q^c}{\partial\eta^2}\frac{\partial^2 X_i}{\partial\xi^2}Y_j\right.\right.\right.\\&\left.+\frac{\partial X_p^c}{\partial\xi}Y_q^c\,X_i\frac{\partial^2 Y_j}{\partial\eta^2}-2\frac{\partial X_p^c}{\partial\xi}\frac{\partial Y_q^c}{\partial\eta}\frac{\partial X_i}{\partial\xi}\frac{\partial Y_j}{\partial\eta}\right]-N_x^*\frac{\partial^2 X_i}{\partial\xi^2}Y_j\\&\left.-N_y^*\lambda^2X_i\frac{\partial^2 Y_j}{\partial\eta^2}+2N_{xy}^*\lambda\frac{\partial X_i}{\partial\xi}\frac{\partial Y_j}{\partial\eta}\right\}\\&+W_o\left\{\sum_{p=1}^{P}\sum_{q=1}^{Q}\chi_{pq}\left[X_p^c\frac{\partial^2 Y_q^c}{\partial\eta^2}\frac{\partial^2 X_o}{\partial\xi^2}Y_o+\frac{\partial X_p^c}{\partial\xi}Y_q^c\,X_o\frac{\partial^2 Y_o}{\partial\eta^2}\right.\right.\\&\left.-2\frac{\partial X_p^c}{\partial\xi}\frac{\partial Y_q^c}{\partial\eta}\frac{\partial X_o}{\partial\xi}\frac{\partial Y_o}{\partial\eta}\right]-N_x^*\frac{\partial^2 X_o}{\partial\xi^2}Y_o-N_y^*\lambda^2X_o\frac{\partial^2 Y_o}{\partial\eta^2}\\&\left.\left.+2N_{xy}^*\lambda\frac{\partial X_o}{\partial\xi}\frac{\partial Y_o}{\partial\eta}\right\}\right]\Bigg\}X_mY_n\,d\xi\,d\eta=0\;\;\forall\,m,n\;\in M,N\end{aligned}\tag{85}$$

The current solution does not account for the mismatch of the natural boundary conditions observed during the development of the equilibrium equation from the first variation of the total potential energy (chapter 3). If the effect of the imperfection is neglected then it is possible to add the same correction terms used in buckling.

$$\sum_{i=1}^{M}\sum_{j=1}^{N} W_{ij}\int\left\{\left|\left[E_{ij}{}_2^*\right]\right|_{\xi=1}\left|\frac{\partial X_m}{\partial\xi}Y_n\right|_{\xi=1}-\left|\left[E_{ij}{}_1^*\right]\right|_{\xi=0}\left|\frac{\partial X_m}{\partial\xi}Y_n\right|_{\xi=0}\right\}d\eta$$
$$+\sum_{i=1}^{M}\sum_{j=1}^{N} W_{ij}\int\left\{\left|\left[E_{ij}{}_4^*\right]\right|_{\eta=1}\left|X_m\frac{\partial Y_n}{\partial\eta}\right|_{\eta=1}\right. \tag{86}$$
$$\left.-\left|\left[E_{ij}{}_3^*\right]\right|_{\eta=0}\left|X_m\frac{\partial Y_n}{\partial\eta}\right|_{\eta=0}\right\}d\xi$$

Where the E terms were given by eq. 25.

The equilibrium equation is finally rewritten in matrix form for conciseness:

$$\boldsymbol{V}_{EL}^{mn}\boldsymbol{\Phi}+\mathbf{V}_{\mathrm{S}}^{mn}\boldsymbol{\Phi}-\boldsymbol{\Phi}^T\boldsymbol{K}_{ENL}^{\mathrm{mn}}\boldsymbol{\Phi}-\mathbf{V}_{\mathrm{ENLO}}^{mn}\boldsymbol{\Phi}-\boldsymbol{V}_{ELP}^{mn}\boldsymbol{\Phi}-con^{mn}=0 \tag{87}$$

Where,

$$\boldsymbol{\Phi}=\left[W_{11}W_{12}\dots W_{m+(n-1)M}\dots W_{MN-1}W_{MN}\chi_{11}\chi_{12}\cdots\chi_{p+(q-1)P}\cdots\chi_{PQ-1}\chi_{PQ}\right]^T \tag{88}$$

And the matrix terms are:

$$\boldsymbol{V}_{EL}^{mn}=\left[\boldsymbol{V}_{1}{}_{EL}^{mn}\quad\boldsymbol{V}_{2}{}_{EL}\right]\rightarrow\ \boldsymbol{V}_{1}{}_{EL}^{mn}=\left[d_{i+(j-1)M}^{mn}\right]_{1\,x\,MN}\ \ \&\ \ \boldsymbol{V}_{2}{}_{EL}=[0]_{1\,x\,PQ}$$
$$d_{i+(j-1)M}^{mn}=\int_0^1\int_0^1\left[\frac{\partial^4X_i}{\partial\xi^4}Y_j+a_1\frac{\partial^3X_i}{\partial\xi^3}\frac{\partial Y_j}{\partial\eta}+a_2\frac{\partial^2X_i}{\partial\xi^2}\frac{\partial^2Y_j}{\partial\eta^2}+a_3\frac{\partial X_i}{\partial\xi}\frac{\partial^3Y_j}{\partial\eta^3}\right. \tag{89}$$
$$\left.+a_4X_i\frac{\partial^4Y_j}{\partial\eta^4}\right]X_mY_nd\xi d\eta$$

$$\boldsymbol{V}_{S}^{mn}=\left[\boldsymbol{V}_{1}{}_{S}^{mn}\quad\boldsymbol{V}_{2}{}_{S}\right]\rightarrow\ \boldsymbol{V}_{1}{}_{S}^{mn}=\left[z_{i+(j-1)M}^{mn}\right]_{1\,x\,MN}\ \ \&\ \ \boldsymbol{V}_{2}{}_{S}=[0]_{1\,x\,PQ}$$
$$z_{i+(j-1)M}^{mn}=\frac{a_1}{2}\int_0^1\left[\frac{\partial Y_j}{\partial\eta}Y_n\right]d\eta\left[\frac{\partial X_i}{\partial\xi}\bigg|_{\xi=1}\frac{\partial X_m}{\partial\xi}\bigg|_{\xi=1}-\frac{\partial X_i}{\partial\xi}\bigg|_{\xi=0}\frac{\partial X_m}{\partial\xi}\bigg|_{\xi=0}\right] \tag{90}$$
$$+\frac{a_3}{2}\int_0^1\left[\frac{\partial X_i}{\partial\xi}X_m\right]d\xi\left[\frac{\partial Y_j}{\partial\eta}\bigg|_{\eta=1}\frac{\partial Y_n}{\partial\eta}\bigg|_{\eta=1}-\frac{\partial Y_j}{\partial\eta}\bigg|_{\eta=0}\frac{\partial Y_n}{\partial\eta}\bigg|_{\eta=0}\right]$$

$$\boldsymbol{K}_{ENL}^{mn}=\begin{bmatrix}\boldsymbol{K}_{11_{ENL}} & \boldsymbol{K}_{12_{ENL}}\\ \boldsymbol{K}_{21}{}_{ENL}^{mn} & \boldsymbol{K}_{22_{ENL}}\end{bmatrix}\rightarrow\ \boldsymbol{K}_{11_{ENL}}=[0]_{MNx\,MN}\ \ \&\ \ \boldsymbol{K}_{12_{ENL}}$$
$$=[0]_{MN\,x\,PQ} \tag{91}$$
$$\&\ \ \boldsymbol{K}_{21}{}_{ENL}^{mn}=\left[g_{p+(q-1)P,\ i+(j-1)M}^{mn}\right]_{PQ\ x\,MN}\ \ \&\ \ \boldsymbol{K}_{22_{ENL}}=[0]_{PQ\,x\,PQ}$$

$$g^{mn}_{p+(q-1)P,\ i+(j-1)M} = a_5 \int_0^1 \int_0^1 \left[X_p^c \frac{\partial^2 Y_q^c}{\partial \eta^2} \frac{\partial^2 X_i}{\partial \xi^2} Y_j + \frac{\partial X_p^c}{\partial \xi} Y_q^c \, X_i \frac{\partial^2 Y_j}{\partial \eta^2} - 2 \frac{\partial X_p^c}{\partial \xi} \frac{\partial Y_q^c}{\partial \eta} \frac{\partial X_i}{\partial \xi} \frac{\partial Y_j}{\partial \eta} \right] X_m Y_n d\xi d\eta$$

$$\boldsymbol{V}^{mn}_{ENLO} = \left[\boldsymbol{V}_{1_{ENLO}} \quad \boldsymbol{V}_{2}{}^{mn}_{ENLO} \right] \rightarrow \ \boldsymbol{V}_{1_{ENLO}} = [0]_{1\,x\,MN} \ \ \& \ \ \boldsymbol{V}_{2}{}^{mn}_{ENLO} = \left[l^{mn}_{i+(j-1)M} \right]_{1\,x\,PQ}$$

$$l^{mn}_{p+(q-1)P} = a_5 W_o \int_0^1 \int_0^1 \left[X_p^c \frac{\partial^2 Y_q^c}{\partial \eta^2} \frac{\partial^2 X_o}{\partial \xi^2} Y_o + \frac{\partial X_p^c}{\partial \xi} Y_q^c \, X_o \frac{\partial^2 Y_o}{\partial \eta^2} - 2 \frac{\partial X_p^c}{\partial \xi} \frac{\partial Y_q^c}{\partial \eta} \frac{\partial X_o}{\partial \xi} \frac{\partial Y_o}{\partial \eta} \right] X_m Y_n d\xi d\eta \tag{92}$$

$$\boldsymbol{V}^{mn}_{ELP} = \left[\boldsymbol{V}_{1}{}^{mn}_{ELP} \quad \boldsymbol{V}_{2_{ELP}} \right] \rightarrow \ \boldsymbol{V}_{1}{}^{mn}_{ELP} = \left[e^{mn}_{i+(j-1)M} \right]_{1\,x\,MN} \ \ \& \ \ \boldsymbol{V}_{2_{ELP}} = [0]_{1\,x\,PQ}$$

$$e^{mn}_{i+(j-1)M} = a_5 \int_0^1 \int_0^1 \left[-N_x^* \frac{\partial^2 X_i}{\partial \xi^2} Y_j - N_y^* \lambda^2 X_i \frac{\partial^2 Y_j}{\partial \eta^2} + 2 N_{xy}^* \lambda \frac{\partial X_i}{\partial \xi} \frac{\partial Y_j}{\partial \eta} \right] X_m Y_n d\xi d\eta \tag{93}$$

$$con_{mn} = a_5 W_o \int_0^1 \int_0^1 \left[-N_x^* \frac{\partial^2 X_o}{\partial \xi^2} Y_o - N_y^* \lambda^2 X_o \frac{\partial^2 Y_o}{\partial \eta^2} + 2 N_{xy}^* \lambda \frac{\partial X_o}{\partial \xi} \frac{\partial Y_o}{\partial \eta} \right] X_m Y_n d\xi d\eta \tag{94}$$

The increasing complexity of the integrals to be performed (multiplication of up to three terms) makes it more convenient to use numerical integration to obtain the different matrix terms.

4.1.3.2. Compatibility equation

The same procedure is applied to the compatibility equation:

$$\int\int\left\{\sum_{i=1}^{P}\sum_{j=1}^{Q}\chi_{ij}\left[\frac{\partial^4 X_i^c}{\partial\xi^4}Y_j^c+b_1\frac{\partial^3 X_i^c}{\partial\xi^3}\frac{\partial Y_j^c}{\partial\eta}+b_2\frac{\partial^2 X_i^c}{\partial\xi^2}\frac{\partial^2 Y_j^c}{\partial\eta^2}+b_3\frac{\partial X_i^c}{\partial\xi}\frac{\partial^3 Y_j^c}{\partial\eta^3}\right.\right.$$
$$\left.+b_4 X_i^c\frac{\partial^4 Y_j^c}{\partial\eta^4}\right]$$
$$+b_5\left[\sum_{i=1}^{M}\sum_{j=1}^{N}W_{mn}\left\{\sum_{m=1}^{M}\sum_{n=1}^{N}W_{ij}\left[\frac{\partial^2 X_m}{\partial\xi^2}Y_nX_i\frac{\partial^2 Y_j}{\partial\eta^2}\right.\right.\right.$$
$$\left.-\frac{\partial X_m}{\partial\xi}\frac{\partial Y_n}{\partial\eta}\frac{\partial X_i}{\partial\xi}\frac{\partial Y_j}{\partial\eta}\right]$$
$$+W_o\left[\frac{\partial^2 X_o}{\partial\xi^2}Y_oX_m\frac{\partial^2 Y_n}{\partial\eta^2}+X_o\frac{\partial^2 Y_o}{\partial\eta^2}\frac{\partial^2 X_m}{\partial\xi^2}Y_n\right.$$
$$\left.\left.\left.\left.-2\frac{\partial X_o}{\partial\xi}\frac{\partial Y_o}{\partial\eta}\frac{\partial X_m}{\partial\xi}\frac{\partial Y_n}{\partial\eta}\right]\right\}\right]\right\}X_p^c\,Y_q^c\,d\xi\,d\eta=0\ \ \forall\,p,q\ \in P,Q \tag{95}$$

In matrix form:

$$\boldsymbol{V}_{CL}^{pq}\boldsymbol{\Phi}-\boldsymbol{\Phi}^T\boldsymbol{K}_{CNL}^{pq}\boldsymbol{\Phi}-\boldsymbol{V}_{CNLO}^{pq}\boldsymbol{\Phi}=0 \tag{96}$$

Where the various terms are:

$$\boldsymbol{V}_{CL}^{pq}=\left[\boldsymbol{V}_{1_{CL}}\quad\boldsymbol{V}_{2_{CL}}^{pq}\right]\rightarrow\ \boldsymbol{V}_{1_{CL}}=[0]_{1\,x\,MN}\ \ \&\ \ \ \boldsymbol{V}_{2_{CL}}^{pq}=\left[q_{i+(j-1)P}^{pq}\right]_{1\,x\,PQ}$$

$$q_{i+(j-1)P}^{pq}=\int_0^1\int_0^1\left[\frac{\partial^4 X_i^c}{\partial\xi^4}Y_j^c+b_1\frac{\partial^3 X_i^c}{\partial\xi^3}\frac{\partial Y_j^c}{\partial\eta}+b_2\frac{\partial^2 X_i^c}{\partial\xi^2}\frac{\partial^2 Y_j^c}{\partial\eta^2}+b_3\frac{\partial X_i^c}{\partial\xi}\frac{\partial^3 Y_j^c}{\partial\eta^3}\right.$$
$$\left.+b_4X_i^c\frac{\partial^4 Y_j^c}{\partial\eta^4}\right]X_p^c\,Y_q^c\,d\xi\,d\eta \tag{97}$$

$$\boldsymbol{K}_{CNL}^{mn}=\begin{bmatrix}\boldsymbol{K}_{11}^{pq}{}_{CNL} & \boldsymbol{K}_{12_{CNL}}\\ \boldsymbol{K}_{21_{CNL}} & \boldsymbol{K}_{22_{CNL}}\end{bmatrix}\rightarrow\ \boldsymbol{K}_{11}^{pq}{}_{CNL}=\left[h_{n+(m-1)M,\ i+(j-1)M}^{pq}\right]_{MNx\,MN}$$
$$\boldsymbol{K}_{12_{CNL}}=[0]_{MN\,x\,PQ}\ \ \&\ \ \boldsymbol{K}_{21_{CNL}}=[0]_{PQ\,x\,MN}\ \ \&\ \ \boldsymbol{K}_{22_{CNL}}=[0]_{PQ\,x\,PQ} \tag{98}$$
$$h_{n+(m-1)M,\ i+(j-1)M}^{pq}=b_5\int_0^1\int_0^1\left[\frac{\partial^2 X_m}{\partial\xi^2}Y_nX_i\frac{\partial^2 Y_j}{\partial\eta^2}-\frac{\partial X_m}{\partial\xi}\frac{\partial Y_n}{\partial\eta}\frac{\partial X_i}{\partial\xi}\frac{\partial Y_j}{\partial\eta}\right]X_p^c\,Y_q^c d\xi d\eta$$

$$\boldsymbol{V}_{CNLO}^{pq}=\left[\boldsymbol{V}_{1_{CNLO}}\quad\boldsymbol{V}_{2_{CNLO}}^{pq}\right]\rightarrow\ \boldsymbol{V}_{\boldsymbol{1}_{CNLO}}=[0]_{1\,x\,MN}\ \ \&\ \ \boldsymbol{V}_{2_{CNLO}}^{pq}$$
$$=\left[s_{i+(j-1)P}^{pq}\right]_{1\,x\,PQ} \tag{99}$$

$$s_{m+(n-1)P}^{pq} = b_5 W_o \int_0^1 \int_0^1 \left[\frac{\partial^2 X_o}{\partial \xi^2} Y_o X_m \frac{\partial^2 Y_n}{\partial \eta^2} + X_o \frac{\partial^2 Y_o}{\partial \eta^2} \frac{\partial^2 X_m}{\partial \xi^2} Y_n - 2 \frac{\partial X_o}{\partial \xi} \frac{\partial Y_o}{\partial \eta} \frac{\partial X_m}{\partial \xi} \frac{\partial Y_n}{\partial \eta} \right] X_p^c \, Y_q^c d\xi \, d\eta$$

Then, both equilibrium and compatibility equations are formulated in matrix form using the same independent variable Φ.

4.1.4. Solving the non-linear system of equations

The resulting nonlinear system of equations is solved using the Newton-Raphson method. This method has been chosen due to its simplicity, especially in its applications to systems of equations expressed in matrix form. The procedure followed is based on Qiao's work [34].

However, Newton-Raphson can present limitations when compared to more advanced methods. For example, it has difficulties tracing the equilibrium path when the post-buckling stiffness tends to zero or to negative values (snap through). This results in discrepancies in the resolution of cases with mode jumping. This phenomenon was not the focus of this Thesis, however for such phenomena it might be interesting to adopt more capable Arc length methods to solve the equilibrium path.

The Newton-Raphson method for nonlinear system of equations is based on the following expression:

$$\boldsymbol{\Phi}_{n+1} = \boldsymbol{\Phi}_n + \Delta \boldsymbol{\Phi}_n = \boldsymbol{\Phi}_n - \boldsymbol{J}^{-1} \boldsymbol{f} \tag{100}$$

Where J is the Jacobian of the system to be solved and f are the residues of the system.

$$\begin{cases} g_1^{mn} = \boldsymbol{V}_{EL}^{mn} \boldsymbol{\Phi} + \mathbf{V}_{\mathrm{S}}^{mn} \boldsymbol{\Phi} - \boldsymbol{\Phi}^T \boldsymbol{K}_{ENL}^{\mathrm{mn}} \boldsymbol{\Phi} - \mathbf{V}_{\mathrm{ENLO}}^{mn} \boldsymbol{\Phi} - \boldsymbol{V}_{ELP}^{mn} \boldsymbol{\Phi} - con^{mn} \\ \boldsymbol{g}_2^{pq} = \boldsymbol{V}_{CL}^{pq} \boldsymbol{\Phi} - \boldsymbol{\Phi}^T \boldsymbol{K}_{CNL}^{pq} \boldsymbol{\Phi} - \boldsymbol{V}_{CNLO}^{pq} \boldsymbol{\Phi} \end{cases} \tag{101}$$

$$\boldsymbol{f} = \left[g_1^{11} g_1^{12} \dots g_1^{mn} \dots g_1^{MN-1} g_1^{MN} g_2^{11} g_2^{12} \dots g_2^{pq} \dots g_2^{PQ-1} g_2^{PQ} \right]^T \tag{102}$$

$$\begin{cases} \boldsymbol{\psi}_1^{mn} = \boldsymbol{V}_{EL}^{mn\,\mathrm{T}} + \mathbf{V}_{\mathrm{S}}^{mn\,T} - \left(\boldsymbol{K}_{ENL}^{\mathrm{mn}\ \mathrm{T}} + \boldsymbol{K}_{ENL}^{\mathrm{mn}} \right) \boldsymbol{\Phi} - \mathbf{V}_{\mathrm{ENLO}}^{mn\ \mathrm{T}} - \boldsymbol{V}_{ELP}^{mn\ \mathrm{T}} \\ \boldsymbol{\psi}_2^{pq} = \boldsymbol{V}_{CL}^{pq\,\mathrm{T}} - \left(\boldsymbol{K}_{CNL}^{pq\ \mathrm{T}} + \boldsymbol{K}_{CNL}^{pq} \right) \boldsymbol{\Phi} - \boldsymbol{V}_{CNLO}^{pq\ \mathrm{T}} \end{cases} \tag{103}$$

$$\boldsymbol{J} = \left[\psi_1^{11} \psi_1^{12} \dots \psi_1^{mn} \dots \psi_1^{MN-1} \psi_1^{MN} \psi_2^{11} \psi_1^{12} \dots \psi_2^{pq} \dots \psi_2^{PQ-1} \psi_2^{PQ} \right]^T \tag{104}$$

For every load step chosen, eq. 100 is iterated until the convergence criterion is satisfied.

$$\frac{|\Delta \boldsymbol{\Phi}_n|}{|\boldsymbol{\Phi}_{n+1}|} \leq tolerance \tag{105}$$

The initial guess for the first load step in a zero vector, while for the rest of load steps, the previous solution is taken. It can be seen that, during iterations, the matrix terms either

remain constant or are directly proportional to the load applied. Therefore, the expensive step of solving the matrix terms is only done once. Further details are given in section 4.1.6.

4.1.5. Airy stress function

The solution obtained is based on a generic Airy Stress function. In it we can distinguish two parts: the first responds to the constant load distribution, given by the in-plane loads applied and is already known:

$$F_c = -N_x^* \frac{\eta^2}{2} - N_y^* \lambda^2 \frac{\xi^2}{2} - N_{xy}^* \lambda \xi \eta \tag{106}$$

The second corresponds to the load redistribution due to the out-of-plane deformation. This is modelled through a linear combination of function similarly what was done for the out of plane function:

$$F_r = \sum_{p=1}^{P} \sum_{q=1}^{Q} \chi_{pq} X_p^c(\xi) Y_q^c(\eta) \tag{107}$$

Remembering that:

$$F = F_c + F_r \tag{108}$$

Where P and Q, analogously to M and N in the out-of-plane shape, give the number of functions to represent the stress redistribution in each direction.

Two different solutions are presented depending on how the load is applied to the plate.

4.1.5.1. Constant load distribution

The first solution is based on applying the in-plane loads as constant distributions along the edges. This solution has already been used by Romeo and Frulla [28] and Qiao [34].

Since the load at the edges has to match the constant load applied, the force redistribution terms must vanish at the edges:

$$\begin{aligned} N_{x_r}^*\big|_{\xi=0,1} &= \sum_{p=1}^{P} \sum_{q=1}^{Q} \chi_{pq} X_p^c(\xi)\big|_{\xi=0,1} \frac{\partial^2 Y_q^c(\eta)}{\partial \eta^2} = 0 \\ N_{y_r}^*\Big|_{\eta=0,1} &= \sum_{p=1}^{P} \sum_{q=1}^{Q} \chi_{pq} \frac{\partial^2 X_p^c(\xi)}{\partial \xi^2} Y_q^c(\eta)\big|_{\eta=0,1} = 0 \\ N_{xy_r}^*\Big|_{\xi=0,1\ \eta=0,1} &= \sum_{p=1}^{P} \sum_{q=1}^{Q} \chi_{pq} \frac{\partial X_p^c(\xi)}{\partial \xi}\Big|_{\xi=0,1} \frac{\partial Y_q^c(\eta)}{\partial \eta}\Big|_{\eta=0,1} = 0 \end{aligned} \tag{109}$$

To ensure the previous boundary conditions are satisfied, the following terms must be zero:

$$X_p^c(\xi)\big|_{\xi=0,1} = \left.\frac{\partial X_p^c(\xi)}{\partial \xi}\right|_{\xi=0,1} = 0$$
$$Y_q^c(\eta)\big|_{\eta=0,1} = \left.\frac{\partial Y_q^c(\eta)}{\partial \eta}\right|_{\eta=0,1} = 0 \quad (110)$$

Such conditions have been fulfilled by choosing eigenbeam value functions to model the load redistribution. Then, the approach is completely analogous to the one followed to find the shape functions for clamped-clamped boundary conditions. Therefore, for more details review section 3.1.3.4.

4.1.5.2. Constant displacement

The main interest in developing a semi-analytical solution for composite plates is to implement a fast tool to solve stiffened panels. However, in stiffened panels the load is typically introduced as a constant displacement, due to the relatively high bending stiffness of the reinforcing beam members.

Romeo and Frulla already realised that the constant load distribution was not consistent with test results involving stiffened plates. Therefore in [29] they switched to a new Airy Stress function able to represent the load redistribution for constant displacement. This new function is based on the exact solution of the compatibility equation for simply supported specially orthotropic plates under bi-axial loading using a linear combination dependent on the number of half-waves.

$$F_r = \sum_{p=1}^{P}\sum_{q=1}^{Q} \chi_{pq}\cos(2p\pi\xi)\cos(2q\pi\eta), \qquad \chi_{11} = 0 \quad (111)$$

Since the function is obtained under some ideal conditions, in the rest of cases it can only work as an approximation. The main limitation of such function is related to the incapacity of solving the stress redistribution under shear loading.

Shear loading was not a priority feature in the proposal of this Thesis but nevertheless it has been attempted to incorporate (really successfully in the case of buckling). Work is still required to properly capture the load redistribution under shear. However, the results presented in section 4.4.3 show that this function captures accurately predict out-of-plane displacements and maximum and minimum forces in the plate, therefore the approach is still of interest for such cases. Further analysis is performed in section 4.3.

4.1.6. Algorithm flowchart

The following chart is presented to further clarify the process followed to solve the post-buckling problem.

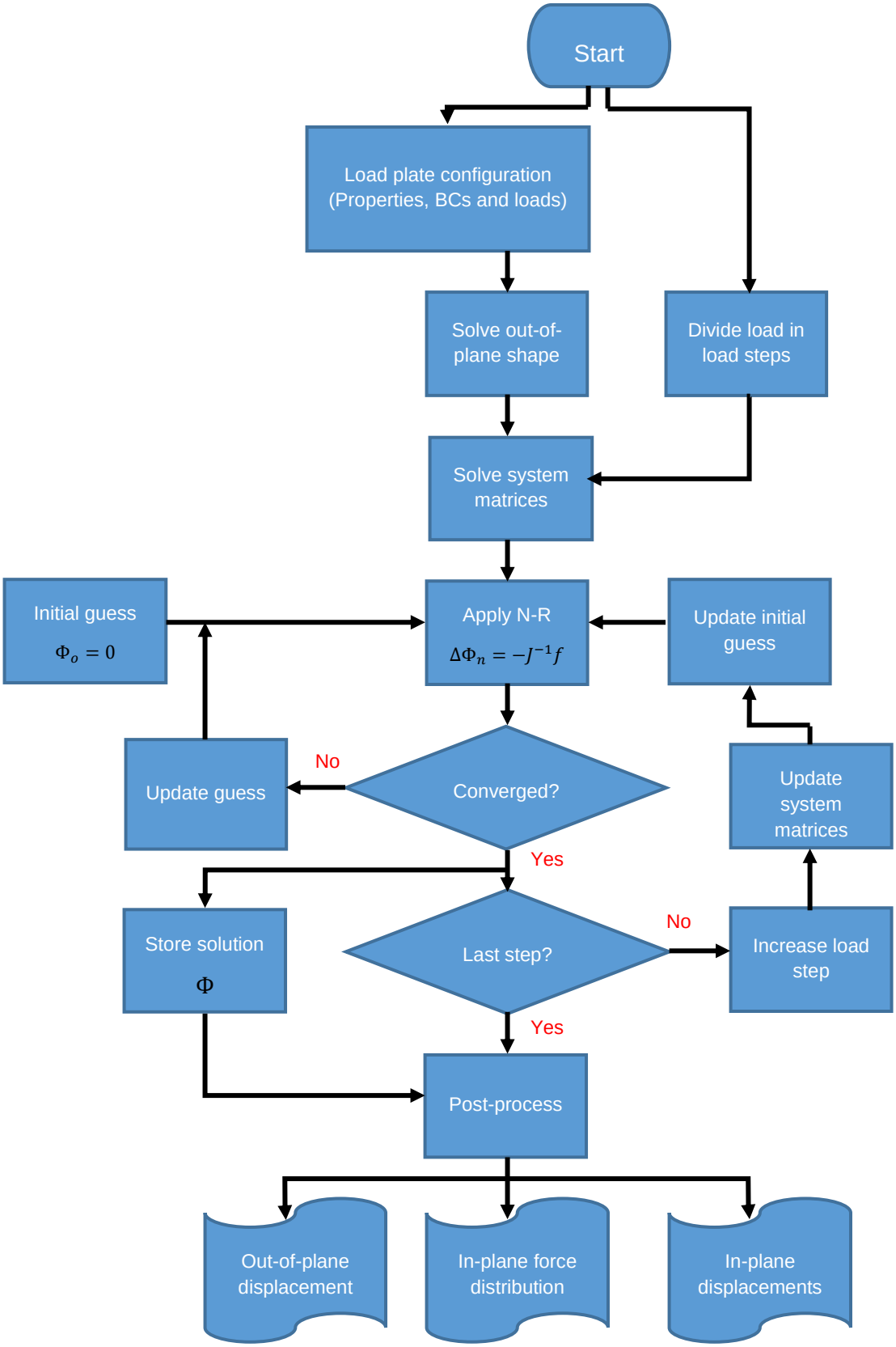

Figure 21: Flowchart post-buckling plate solution

4.1.7. Post-process

The post-buckling analysis involves more variables than buckling. In the latter, eigenvalues and eigenvectors were directly obtained and the only post-processing that might be required was transforming the eigenvector into the buckling shape.

On the other hand, post-buckling seeks the solution of the equilibrium path of the plate, from zero load up to a specified post-buckling ratio. Moreover, variables like the in-plane force distribution and the in-plane displacements become relevant.

4.1.7.1. Out-of-plane displacement

The out-of-plane displacement is obtained through the first part of the Φ solution. This vector gives the amplitude for every combination of shape functions, so all of them are summed together multiplied by their amplitudes and evaluated at specific points (like a mesh) to obtain a 2D mapping of the out-of-plane displacement. This 2D distribution is stored for every load step so it is possible to reproduce an animation of the deformation taking every load step as a frame, or taking the maximum at every load step in order to create the curve of the maximum out-of-plane displacement against post-buckling ratio.

4.1.7.2. In-plane force distribution

The in-plane force distribution is obtained identically as the out-of-plane displacement, but from the second part of the Φ solution. The amplitudes are multiplied by the corresponding derivatives of the Airy Stress function to obtain the distribution of in-plane forces for the selected points (mesh). Aside from the 2D distribution at every load step, the maxima and minima of every in-plane force are stored to be able to plot them as curves against the post-buckling ratio.

4.1.7.3. In-plane displacements

The in-plane displacements are not solved in the governing equation of the plate. Going back to the assumptions, it was assumed it was possible to uncouple in-plane and out-of-plane behaviour simplifying the solution process. However, once the out-of-plane displacement and the in-plane force distributions are solved, it is possible to explicitly derive the in-plane displacement from them.

According to the plate theory used, the in-plane displacements depend on the mid-plane strain and out-of-plane displacements:

$$\begin{cases} \dfrac{\partial u}{\partial x} = \varepsilon_x^o - \dfrac{1}{2}\left(\dfrac{\partial w}{\partial x}\right)^2 \\ \dfrac{\partial v}{\partial y} = \varepsilon_y^o - \dfrac{1}{2}\left(\dfrac{\partial w}{\partial y}\right)^2 \\ \gamma = \varepsilon_{xy}^0 - \dfrac{\partial w}{\partial x}\dfrac{\partial w}{\partial y} \end{cases} \tag{112}$$

Moreover, for mid-plane symmetric plates, the mid-plane strain are only dependent on the in-plane force distribution (or Airy Stress function).

$$\begin{cases} \varepsilon_x^0 = a_{11}\dfrac{\partial^2\phi}{\partial y^2} + a_{12}\dfrac{\partial^2\phi}{\partial x^2} - a_{16}\dfrac{\partial^2\phi}{\partial x\partial y} \\ \varepsilon_y^0 = a_{12}\dfrac{\partial^2\phi}{\partial y^2} + a_{22}\dfrac{\partial^2\phi}{\partial x^2} - a_{26}\dfrac{\partial^2\phi}{\partial x\partial y} \\ \varepsilon_{xy}^0 = a_{16}\dfrac{\partial^2\phi}{\partial y^2} + a_{26}\dfrac{\partial^2\phi}{\partial x^2} - a_{66}\dfrac{\partial^2\phi}{\partial x\partial y} \end{cases} \tag{113}$$

The displacement increments are obtained by integrating the result of substituting eq. 113 into 112 over all the plate. For the x direction:

$$\int\int \frac{\partial u}{\partial x}\,dx\,dy = \int\int \left\{ a_{11}\frac{\partial^2\phi}{\partial y^2} + a_{12}\frac{\partial^2\phi}{\partial x^2} - a_{16}\frac{\partial^2\phi}{\partial x\partial y} - \frac{1}{2}\left(\frac{\partial w}{\partial x}\right)^2 \right\} dx\,dy \tag{114}$$

$$\Delta u = \frac{\int\int \left\{ a_{11}\dfrac{\partial^2\phi}{\partial y^2} + a_{12}\dfrac{\partial^2\phi}{\partial x^2} - a_{16}\dfrac{\partial^2\phi}{\partial x\partial y} - \dfrac{1}{2}\left(\dfrac{\partial w}{\partial x}\right)^2 \right\} dx\,dy}{b} \tag{115}$$

It is clear then that the in-plane displacement can be obtained directly from the Airy Stress function and out-of-plane displacement. The result obtained is the average relative displacement between one edge and the other, which is especially suitable when solving post-buckling under applied displacement (keeping the edges straight).

The non-dimensionalized solution is then:

$$\begin{aligned} \Delta u^* = -\int_0^1\int_0^1 \Bigg\{ & \left[\frac{1}{2}\frac{h}{a}\sum_{m=1}^{M}\sum_{n=1}^{N}\left(W_{MN}\frac{\partial X_m}{\partial \xi}Y_n \right)^2 \right] \\ & + \left[-\frac{h}{b}\lambda a_{11}^* N_x^* - \frac{h}{a}\lambda^2 a_{12}^* N_y^* + \frac{h}{a}\lambda^2 a_{16}^* N_{xy}^* \right] \\ & + \left[\sum_{p=1}^{P}\sum_{q=1}^{Q}\chi_{pq}\left(\frac{h}{b}\lambda a_{11}^* X_p^c \frac{\partial^2 Y_q^c}{\partial \eta^2} + \frac{h}{a}\lambda^2 a_{12}^* \frac{\partial^2 X_p^c}{\partial \xi^2} Y_q^c \right.\right. \\ & \left.\left. - \frac{h}{a}\lambda^2 a_{16}^* \frac{\partial X_p^c}{\partial \xi}\frac{\partial Y_q^c}{\partial \eta} \right) \right] \Bigg\} d\xi d\eta \end{aligned} \tag{116}$$

$$\Delta v^* = -\int_0^1 \int_0^1 \left\{ \left[\frac{1}{2}\frac{h}{b} \sum_{m=1}^{M} \sum_{n=1}^{N} \left(W_{MN} X_m \frac{\partial Y_n}{\partial \eta} \right)^2 \right] + \left[-\frac{h}{b} a_{12}^* N_x^* - \frac{h}{a} \lambda a_{22}^* N_y^* + \frac{h}{a} \lambda a_{26}^* N_{xy}^* \right] + \left[\sum_{p=1}^{P} \sum_{q=1}^{Q} \chi_{pq} \left(\frac{h}{b} a_{12}^* X_p^c \frac{\partial^2 Y_q^c}{\partial \eta^2} + \frac{h}{a} a_{22}^* \frac{\partial^2 X_p^c}{\partial \xi^2} Y_q^c - \frac{h}{a} a_{26}^* \frac{\partial X_p^c}{\partial \xi} \frac{\partial Y_q^c}{\partial \eta} \right) \right] \right\} d\xi d\eta \tag{117}$$

The in-plane rotation can only be obtained similarly:

$$\gamma = -\int_0^1 \int_0^1 \left\{ \left[\frac{1}{2}\frac{h^2}{ab} \sum_{m=1}^{M} \sum_{n=1}^{N} W_{MN}^2 \frac{\partial X_m}{\partial \xi} Y_n X_m \frac{\partial Y_n}{\partial \eta} \right] + \left[-\frac{h^2}{b^2} a_{16}^* N_x^* - \frac{h}{a^2} \lambda^2 a_{26}^* N_y^* + \frac{h}{ab} \lambda a_{66}^* N_{xy}^* \right] + \left[\sum_{p=1}^{P} \sum_{q=1}^{Q} \chi_{pq} \left(\frac{h^2}{b^2} a_{16}^* X_p^c \frac{\partial^2 Y_q^c}{\partial \eta^2} + \frac{h^2}{a^2} a_{26}^* \frac{\partial^2 X_p^c}{\partial \xi^2} Y_q^c - \frac{h^2}{ab} a_{66}^* \frac{\partial X_p^c}{\partial \xi} \frac{\partial Y_q^c}{\partial \eta} \right) \right] \right\} d\xi d\eta \tag{118}$$

The non-dimensionalizations have been done following the same criteria as in previous chapters. Additionally, for the in-plane displacements:

$$\Delta u^* = \frac{\Delta u}{a}, \qquad \Delta v^* = \frac{\Delta v}{b} \tag{119}$$

4.2. FE model

The approach followed to verify the semi-analytical solution against a FE model in post-buckling is basically the same as used in buckling. The same software package is used and also the process of building the FE model is automated by means of a Python script.

The main changes applied are explained in the following subsections.

4.2.1. Mesh

The deformations on post-buckling adopt more complex shapes so the preliminary convergence studies have shown the necessity to increase the number of elements to 40 (per short side) to stay on the safe side during the verifications.

4.2.2. Boundary conditions and loads

The first difference with the buckling analysis is that post-buckling requires an imperfection to solve the proper equilibrium path. This imperfection should be equivalent to the one considered in the semi-analytical model in order to get comparable results. Therefore, it has been decided to execute in first step a buckling analysis (the same as presented in chapter 3), and use the buckling mode (deformation), multiplied by an amplitude factor, as the imperfection in the post-buckling solution. This approach requires modifying the keyword editor of the buckling and post-buckling models in order to generate and reload the .fil file with the buckling mode. One problem of this approach is that Abaqus applies the imperfection displacement gradually during the loading of the plate, while the semi-analytical model accounts for an imperfection that is already present when the loading starts. This does not affect the validity of the results, but explains slight differences during the linear range (pre-buckling).

The boundary conditions and loads depend on which post-buckling model is used.

4.2.2.1. Constant load

Constant load is the approach followed in all buckling analysis, therefore this means that it is not necessary to modify how the BCs are applied in the FE model with respect to the previous chapter. Mind that for buckling, apply the load constantly or through a constant applied displacement were equivalent cases since the stiffness of the plate before buckling is constant.

4.2.2.2. Constant applied displacement

On the other hand, if the edges are to be kept straight during post-buckling, it is necessary to introduce changes in the FE model, especially on the boundary conditions to impose this new loading case.

The edges of the model are kept straight using equation constraints tying the degrees of freedom of all their nodes. The plate must be able to stretch and also allow simple shear deformations to test results under shear (or non-balanced laminates). The upper and lower edges are kept straight and horizontal by tying the vertical displacement of all the nodes of each edge.

The side edges require a more complex approach as they must be kept straight but being allowed to rotate (cannot be kept vertical). In order to do that, the horizontal displacement of the inner nodes of the edge are expressed as a linear combination of the horizontal displacement of the two corners:

$$u_i = \frac{n-i}{n}u_0 + \frac{i}{n}u_n \tag{120}$$

Where n is the number of elements in the side, u_0 is the horizontal displacement of the bottom corner, u_i is the horizontal displacement of the i-th node and u_n is the horizontal displacement of the upper corner.

In this new model, the displacement is applied at the edges is constrained, so it does not make sense to keep applying the axial loads as distributed forces, as the edges will move together no matter how the load is applied. The following figure shows how the load application has been simplified.

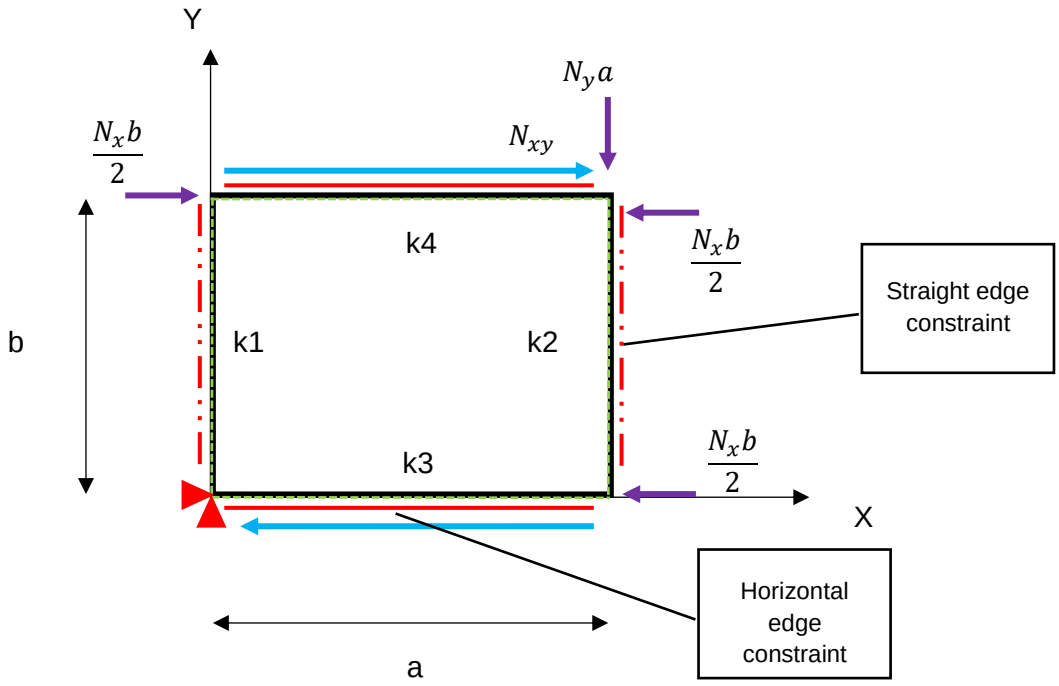

Figure 22: Boundary conditions and load applied displacement FE model

The applied concentrated forces are equivalent to applying constant displacement along the edge but allowing a higher degree of control on the loads applied in each side and especially simplifying the analysis for a specific post-buckling ratio (it is just necessary to multiply the buckling load by the desired ratio and apply it with the concentrated forces).

4.2.3. Analysis and results

The post-buckling solution is obtained using a non-linear static general analysis. The load applied in the model is the buckling load obtained from the semi-analytical solution multiplied by the post-buckling coefficient desired.

The results requested are the ones already calculated by the semi-analytical model. The in-plane force distributions are explicitly requested in the field output (called section forces (SF) in Abaqus) and the results for every node and load step are stored in .txt files for the post-processing of the verification. The results of the out-of-plane displacement are exported in the same way, while the increment of in-plane displacements are obtained subtracting the results of opposite corners.

4.3. Analytical model

In addition to semi-analytical and FEM, an analytical solution has also been implemented in the verification. However, due to the increasing complexity of post-buckling, this solution can only cope with specially orthotropic laminates under bi-axial loading and applied displacement.

The analytical solution is a modification from the one proposed by Kassapoglou in the section 7.1 of [11], which has already been shown during the literature study (eq. and figure 2). The new equation allows for bi-axial loading, buckling in different number of half-waves and discards the fixed edges of the previous, in order to be applicable to the studied configurations.

The solutions obtained are used mainly to highlight the limitations[9] of the pure analytical approach in comparison to the semi-analytical. The results obtained are the out-of-plane (at the centre of the half-wave) and in-plane edge displacements. In-plane load distribution could also be obtained. The corresponding equations are:

$$w_{11} = 4\sqrt{\frac{-D_{11}\left(\frac{m_o}{a}\right)^4 - 2(D_{12}+2D_{66})\frac{m_o^2 n_o^2}{a^2 b^2} - D_{22}\left(\frac{n_o}{b}\right)^4 + N_x\left(\frac{m_o}{a\pi^2}\right)^2 + N_y\left(\frac{n_o}{b\pi^2}\right)^2}{\left(\frac{m_o}{a}\right)^4 \frac{A_{11}A_{22}-A_{12}^2}{A_{22}} + \left(\frac{n_o}{b}\right)^4 \frac{A_{11}A_{22}-A_{12}^2}{A_{11}}}} \tag{121}$$

$$\Delta u = -\frac{A_{22}}{A_{11}A_{22}-A_{12}^2} N_x b\lambda + \frac{A_{12}}{A_{11}A_{22}-A_{12}^2} N_y a - \frac{1}{8} w^2 \frac{m_o^2 \pi^2}{a} \tag{122}$$

$$\Delta v = -\frac{A_{11}}{A_{11}A_{22}-A_{12}^2} \frac{N_y a}{\lambda} + \frac{A_{12}}{A_{11}A_{22}-A_{12}^2} N_x b - \frac{1}{8} w^2 \frac{n_o^2 \pi^2}{b} \tag{123}$$

Where m_o and n_o are the critical number of half-waves in x and y directions.

4.4. Solution and verification

Again, both semi-analytical and FE models have been developed to be automatically executed from a main Matlab program. The purpose of this program consists in solving both models for multiple configurations and post-process the results to facilitate the verification of the developed model and give confidence on the validity of its results. Moreover, the obtained results give a clear view of which are the limitations and the expected accuracy on different cases. It must be reminded that the use of more analytical approaches typically sacrifices accuracy (due to the necessity of applying more approximations) in order to obtain a better performance and therefore create solutions more suitable for preliminary design or optimization.

The number of approximations required to create the semi-analytical model makes it necessary to conduct thoughtful verifications to prove solutions are still valid and investigate the accuracy that could be expected from the different configurations. The verification performed for post-buckling is based on the same configurations tested for buckling (using the same geometries, thicknesses, boundary conditions, loads and

[9] On the other hand, the analytical solution is in closed form and, as such, significantly faster than the semi-analytical one. For a set of limited cases it can be a much better option, but not for stiffened panels.

laminates). The post-buckling solution requires additional variables compared to the ones presented in buckling in section 3.3.

- **PB coefficient:** the post-buckling coefficient is the ratio between the applied load and the critical buckling one. Using the PB coefficient is an efficient way to introduce the loads in the model so different comparisons for different buckling loads can be compared. Most of the cases have been solved until PB coefficient equal to two, this allows for a good analysis of the non-linear effects that ocurr after buckling for values above what is found in typical aerospace applications.
- **Imperfection:** To avoid obtaining the zero out-of-plane displacement equilibrium solution (unstable) it is necessary to introduce an initial imperfection in the plate. The higher the imperfection the more bending behaviour is obtained, while the smaller the more ideal buckling behaviour is achieved. Differente values have been tested in order to use the minimum that allows to capure post-buckling. The results obtained have encouraged using 1% of the thickness as an imperfection.
- **Load step:** In the post-buckling analysis is necessary to select the intervals at which the intermediate solutions are sought. This number is important in the convergence of the solution and also in obtaining a good resolution in the solution curves. The Newton-Raphson iteration is not very computationally expensive, so increasing the step does not have a big impact in the performance. Typical values used are around 100 steps.
- **Newton-Raphson tolerance:** Determines the maximum error allowed inside Newton-Raphson iterations.
- **Post-processing mesh:** The solutions obtained in the semi-analytical model need to be evaluated in the 2D space of the plate. The number of points at which the solutions are evaluated can impact the performance. Values around 20 or 40 have proven to give enough accuracy.

Additionally there is the number of terms to represent the linear combinations. Apart from the out-of-plane displacement (M x N), it is necessary to add the number of terms for the Airy Stress function (P x Q). The number of terms selected has an important effect on both the accuracy and the required time of the semi-analytical solution (See table 2 for execution time examples). Several combinations might be used to optimize the solutions.

4.4.1. Solution format

It has already been mentioned that the number of variables per case is higher than in buckling. This makes the verification process more complex and choosing the relevant information becomes more important. In section 4.1.7 was mentioned that the solutions obtained from the semi-analytical model are the out-of-plane displacement distribution, the averaged in-plane displacement and the three in-plane force distributions (X, Y and shear).

4.4.1.1. Solution curves

The first step to reduce the amount of data is simplifying the distributions into maximums and minimums. Then, it is possible to create curves against the post-buckling coefficient. However, simplifying to a maximum or minimum means losing a lot of information. To keep the most of it, the complete distribution solution is given at specific PB coefficients.

The following set of figures have been created to show the results. Every bullet introduces a figure description and an example for the case of a square simply supported isotropic plate under uniaxial compression. The thickness of the plate is 1 mm as in all the post-buckling cases presented in this chapter to guarantee that thin plate theory is applicable:

- **Out-of-plane displacement**: The first figure shows the evolution of the maximum (in absolute value) of the out-of-plane displacement for the different PB coefficients. The figure superposes the semi-analytical solution (blue), the FE solution (green) and the analytical if available (red). Results are given in meters.

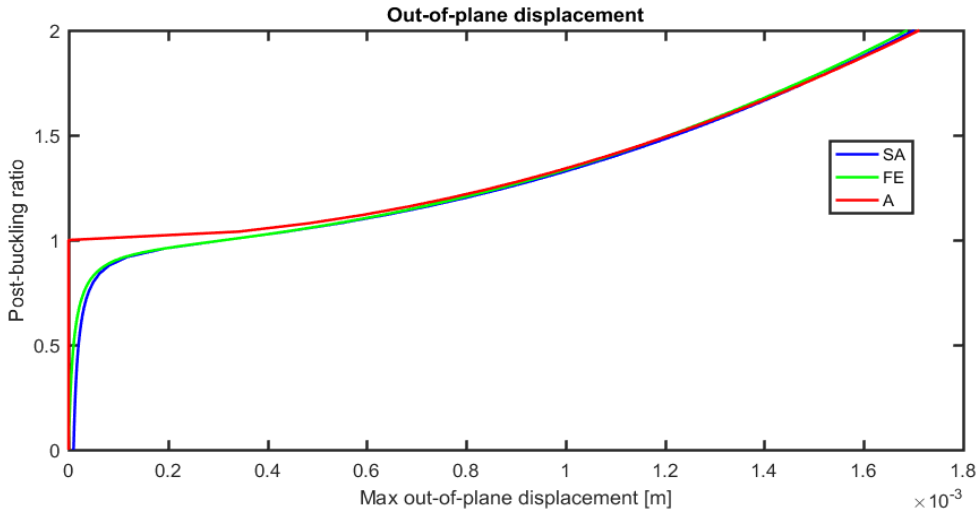

Figure 23: Example out-of-plane displacement

- **Avg Inplane displacements**: The second figure presents the in-plane displacements (how much one edge moves with respect to the other). The figure follows the same colouring criteria but it has been divided into two sub-plots. The upper one shows the results in the x direction while the bottom one shows the results in y. It should be noticed that the slope of the curve gives the stiffness of the plate, which remains fairly constant before and after every mode change. Results are again given in meters.

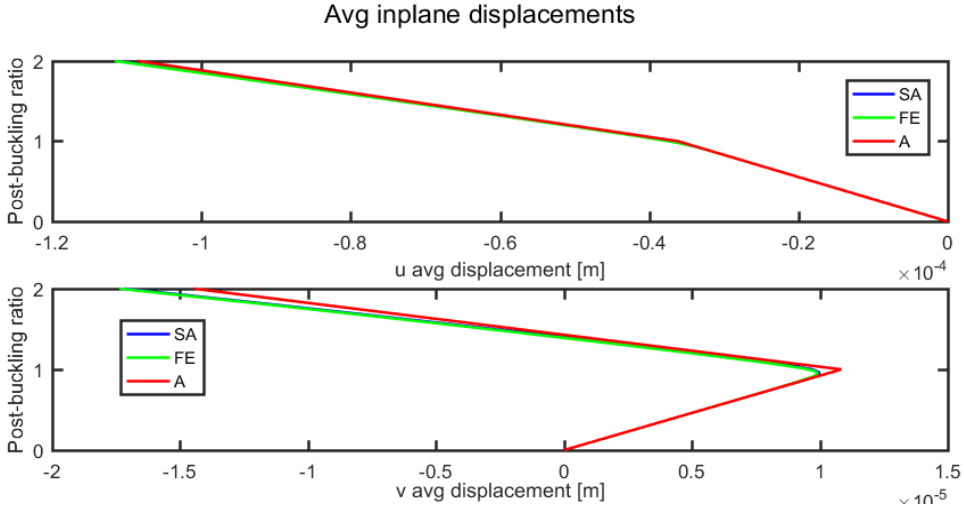

Figure 24: Example averaged in-plane displacements

- **In-plane forces**: The third figure plots the maximum and minimum in-plane force distribution at every load step. The different forces are plotted with different colours and line formats, following these criteria: the minimum of the semi-analytical is plotted with a continuous line, the maximum with a semi-continuous line and the FE solutions (both min and max) with discrete points (with '+' symbol). Regarding the colours, the forces in x are plotted in red, the forces in y in blue and the shear forces in green. Results are given in Newtons divided by meters.

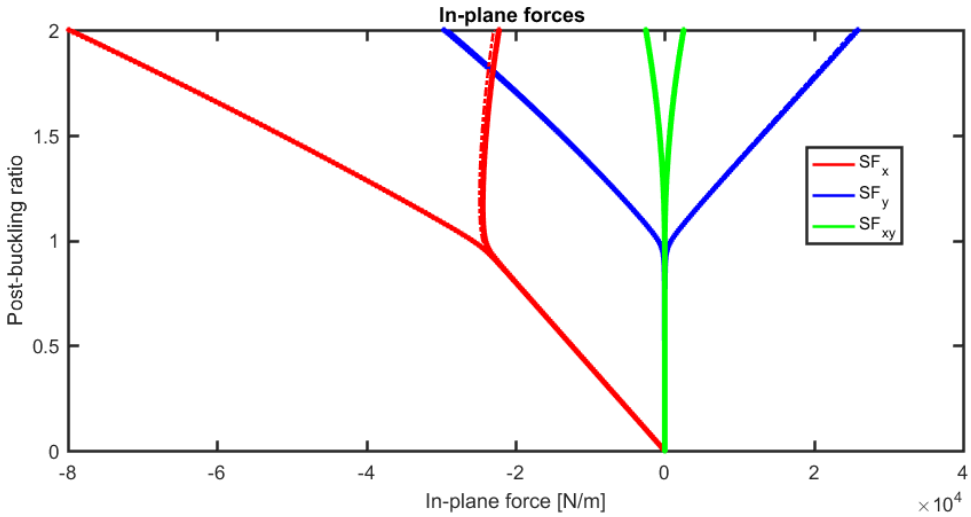

Figure 25: Example max in-plane force distribution

- **In-plane force and out-of-plane displacement distributions:** The corresponding figures contain 4 different subplots each. First one is the force distribution in x, the second the force distribution in y, the third the shear distribution and the last one is the out-of-plane displacement. Every figure shows the results through a 2D colour plot over all the plate geometry (the axis present the dimensions of the plate in meters), and the different values can be interpreted thanks to independent colour legends.

  Four figures are produced for every plate configuration. Two of them show the semi-analytical results, one at half the maximum PB coefficient and the other at the maximum. The other two show the FE results at the same load steps. The following figure presents as example the distributions for the semi-analytical solution at the last PB coefficient:

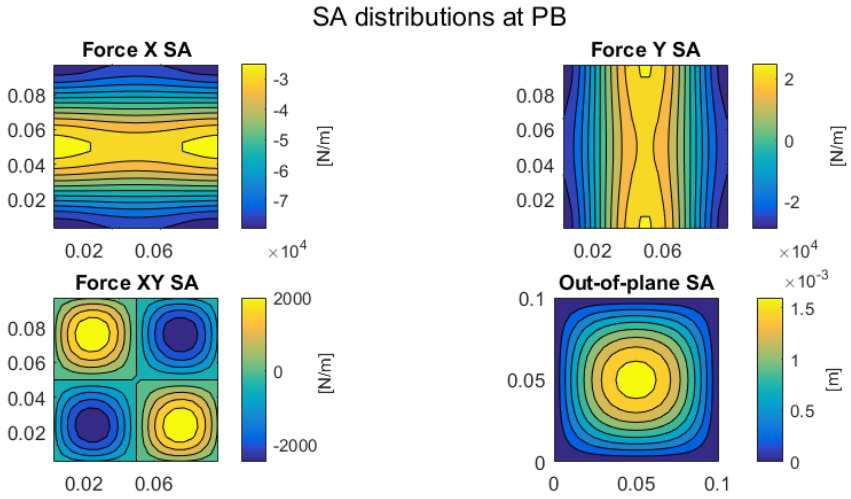

Figure 26: Example distributions (semi-analytical for PB coefficient 2)

As can be seen from figures 23-25, both the analytical and semi-analytical solutions show excellent agreement with FE. Such results can be used as a benchmark before starting with more complex cases.

To distinguish the verification of different plate configurations, a 5 digit code has been implemented. It accounts for the aspect ratio, plate thickness, boundary condition, load case and laminate lay-up. The code is presented in the Appendix A.

4.4.1.2. Solution tables

Apart from the individual figures it makes sense to have the solution error of many different configurations side by side, so it is possible to better assess the accuracy of the semi-analytical solution in a general way. The solution tables follow the same exact format as the ones presented in the buckling chapter. However, they contain more information using Excel files (See Annex\PBuckling).

The solutions covered are a simplification of the figures, the results included are: the out-of-plane displacement, u and v in-plane displacements, in-plane force absolute maximums and pre and post-buckling stiffnesses in x and y. This makes up to 8 variables. The solutions are taken at half the maximum PB coefficient and the maximum, which makes 16 different results per case, organized in different sheets.

Two different files are created. The first one contains the FE solutions. The second contains the error in % between SA and FE results.

The tables group big amounts of data, but using color scales it is possible to quickly asses the differences in accuracy of the different variables, and which plate configurations give lower accuracy.

4.4.2. Convergence study

The number of terms required to properly solve post-buckling depends mainly on the plate configuration. Therefore, it is difficult to perform a convergence study when the results would depend on every case. Therefore, it has been decided to establish a reference configuration for which the convergence study is performed.

The convergence study is also important to understand the significance of the number of terms in both the out-of-plane and Airy Stress function. In an ideal convergence study, the most complex configuration (the one that should require more terms) would be tested to guarantee the proper behaviour of the rest. However, the additional limitations of cases involving shear can make it difficult to assess the importance of the different terms, as the exact convergence is not guaranteed.

Therefore, it has been decided to start with the convergence study of a rectangular plate (aspect ratio 3) with elastic restrains under uniaxial compression with predominant 45s layup. This case includes most of the difficulties for a good convergence, but at the same time the fact that it is under compression gives confidence that convergence will be achieved.

4.4.2.1. Convergence uniaxial compression

Initial tests suggest 3 or more terms are required as the plate buckled in three half-waves under those conditions. Different combinations for both out-of-plane deflection and Airy Stress function are studied:

4.4.2.1.1. Convergence out-of-plane displacement

During the out-of-plane displacement convergence study, the terms of the Airy Stress function are kept constant to 6x6 (6 terms in the x direction and 6 in the y) while the deflection terms are modified to assess their effect. The following figures show the evolution of the out-of-plane displacement for 4x4 (a), 6x6 (b) and 8x8 terms (c).

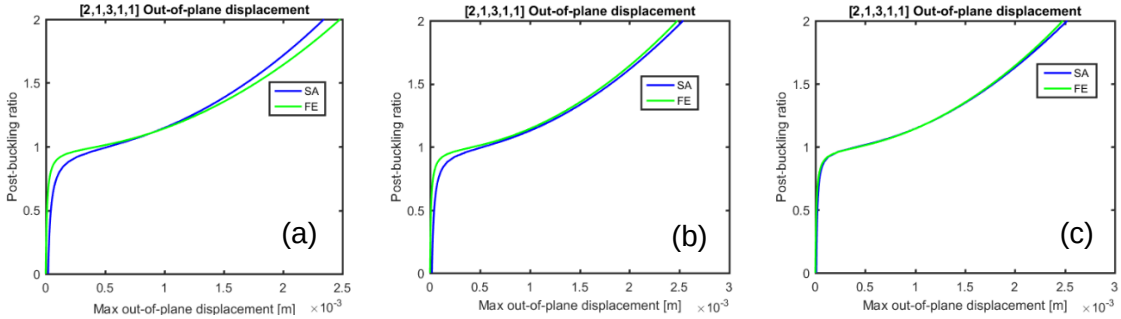

Figure 27: Convergence study out-of-plane displacement under uniaxial compression

The trends clearly show the improvement of the solution by choosing more terms. As expected 4x4 terms is already able to reproduce the proper behaviour, although the accuracy at the beginning and end of the curve is not excellent. 6x6 terms achieves a closer solution especially at higher PB ratios and 8x8 improves the solution near the buckling point, giving a perfect agreement through all the ratios.

Clearly, the number of terms to be used will depend on the required accuracy. Using more terms increases the amount of time required, so both accuracy and speed must be balanced.

4.4.2.1.2. Convergence Airy Stress function

For the convergence study of the Airy Stress function, the out-of-plane terms are fixed to 6x6 and 4x4 (a), 6x6 (b) and 8x8 terms (c) in the Airy Stress function are tested. Results are shown in figure 27:

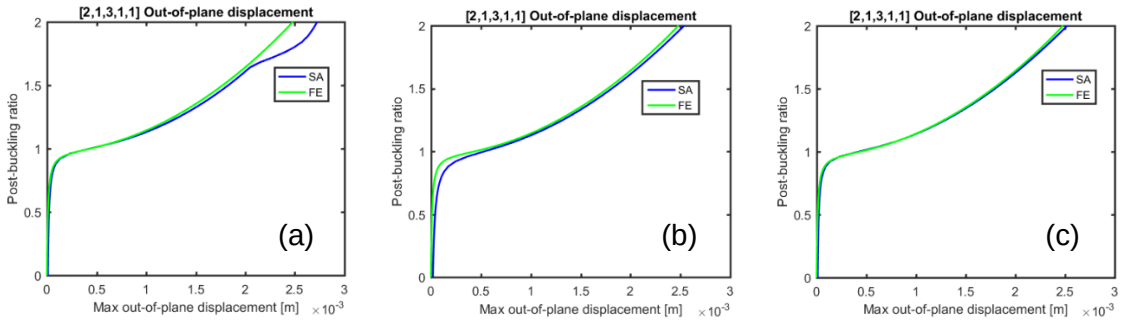

Figure 28: Convergence study Airy Stress function under uniaxial compression

The 4x4 case, surprisingly shows better behaviour than 6x6 for the beginning of the curve (near buckling) but shows mode change for PB ratio 1.6 which makes difficult reaching further conclusions. 8x8 terms is comparable to the last figure obtained for the out-of-plane convergence, so it is difficult to assess which terms are more important.

If the in-plane forces are compared, the use of 6x6 for the displacement and 6x6 terms for the Airy Stress function increases the accuracy of the results over poorer number of terms. Further additional terms almost do not have any effect in the solutions, as shown by figure 29.

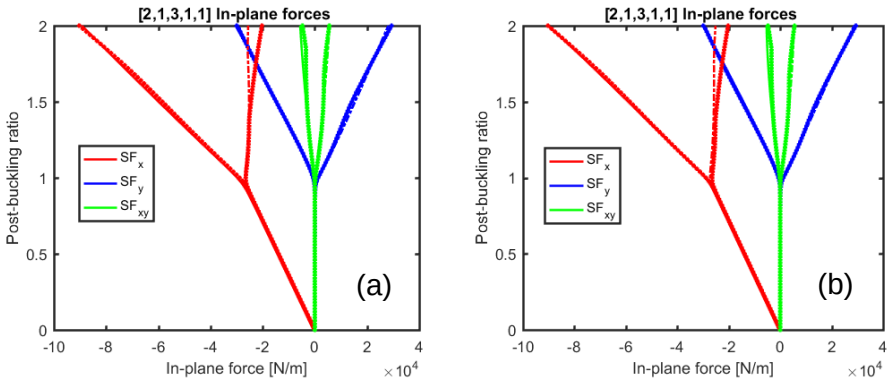

Figure 29: Convergence of the in-plane forces for 6x6-6x6 terms (a) and 8x8-8x8 terms (b) under uniaxial compression

4.4.2.1.3. Conclusions convergence uniaxial compression

From the results obtained it can be concluded that all the combinations are able to predict the post-buckling behaviour. 4x4 terms for the Airy Stress function is the worst case due to the mode change, additional tests suggest that using fewer terms make the solutions more sensitive to mode change. 8x8 terms can slightly improve the behaviour for the out-of-plane displacement, but barely have any effect on the force prediction. Considering also the computational time, is concluded that in this case 6x6-6x6[10] terms is the most balanced solution.

[10] This expression is used to show the number of terms used for each expression. First two number are the terms for the out-of-plane displacement and the last two, the terms for the Airy Stress function. The total number of terms is the multiplication of the first two plus the multiplication of the lasts.

4.4.2.2. Convergence combined loading

Combined loading has proven to be the most difficult case to solve, due to the higher complexity of the out-of-plane displacement shape and force distributions. The convergence study under combined loading is especially interesting as it should show the limitations of the formulation for the most difficult of the cases under study. In this case, the boundary conditions selected are clamped.

The following figures shows the results for the out-of-plane displacement and forces for 4x4-4x4 (a), 6x6-6x6 (b) and 8x8-8x8 terms (c):

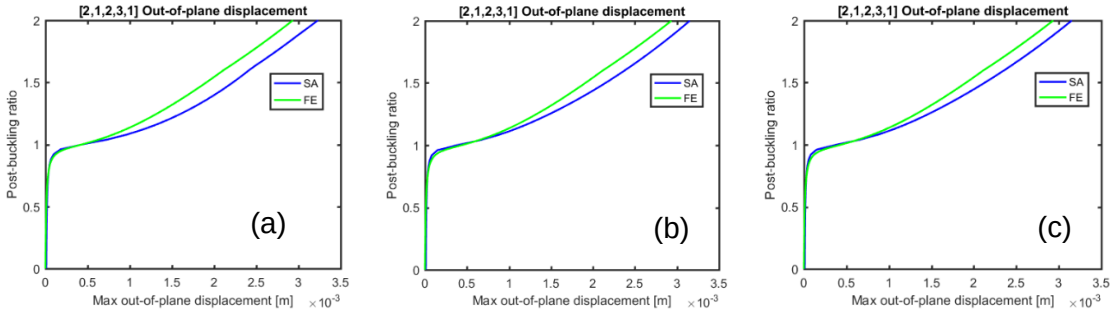

Figure 30: Convergence of the out-of-plane displacement under combined loading

The differences for the out-of-plane displacement are not significant. Some improvement is observed from 4 to 6 terms (per direction and function) in the mid zone of the curve. The most interesting fact is that all solutions present some error, suggesting that the current linear combinations are not able to perfectly reproduce the post-buckling behaviour irrespective of the number of terms. However, the behaviour is approximated in all cases and the error is not big (around 8% at PB ratio two) taking into account the complexity of the case.

For the same cases but comparing the in-plane forces:

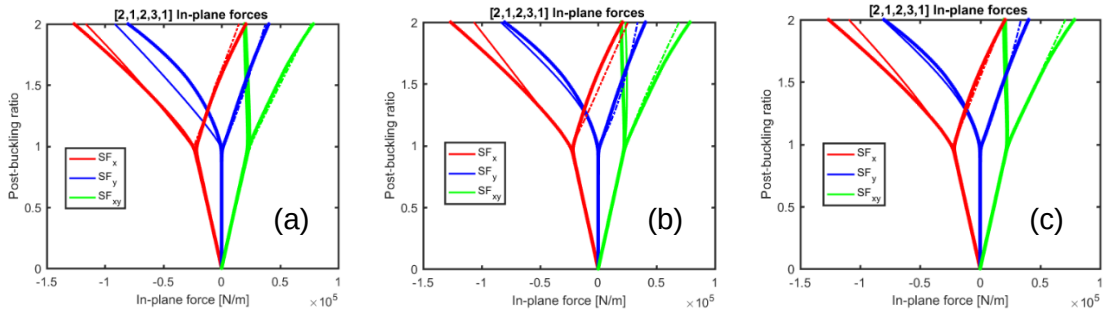

Figure 31: Convergence of the in-plane forces under combined loading

The forces are also difficult to compare, as there isn't a clear convergent behaviour. The force in X and shear present better result when less terms are used, while the force in Y is the other way around. In all the cases, the behaviour is properly approximated, but it seems that the current functions used cannot perfectly solve the case, regardless of the number of terms.

4.4.2.3. Conclusions convergence

The convergence study under compression showed a tendency to converge with the number of terms. The use of 6x6-6x6 terms is recommended as the best balance between

accuracy and computational time. On the other hand, it is difficult to extract conclusions from the combined loading case, as there is no clear convergent behaviour. For the rest of comparisons with FE has been decided to use 6x6-6x6 terms.

The following table introduces an approximate guideline of the required time for the resolution of post-buckling for different number of terms.

Table 3: Time performance of the SA solution for different number of terms

Number of terms	Approximate execution time
4x4-4x4	10 s
6x6-6x6	90 s
8x8-8x8	9 min

However, it must be taken into account that the code implemented can be further optimized. For example Qiao [34] using a similar approach and 5x5-5x5 terms states that the semi-analytical solution requires about 5.5 seconds to complete, being 16 times faster than FEM.

4.4.3. Verification with FEM

The main verification consists in a compilation of different solution figures. All the configurations selected include the out-of-plane displacement curve, as it is the main solution variable. Moreover, additional solutions are distributed among the different configurations in order to show representative results without involving hundreds of figures.

The verifications include combinations of boundary conditions, load combinations and laminates used during the buckling verification. However, not all the possible configurations are presented in this report, since that would mean having too many figures without giving relevant additional information.

The geometry of the plates is the same used in buckling. Most of the results are for square plates, but some results for rectangular (aspect ratio 3) plates are presented as well, to show the capabilities of the method.

The results of the semi-analytical model are obtained using 6x6 terms for the out-of-plane displacement and 6x6 terms for the Airy Stress function. Galerkin method for applied displacement is used if it is not specified otherwise.

4.4.3.1. Predominant 45s

The predominant 45s laminates is the more difficult laminate tested. As has already been discussed, the presence of D_{16} and D_{26} complicate the solution of the natural boundary condition and additionally make the buckling and deformation patterns more complex (introducing rotation of the deflection patter even under uniaxial compression).

4.4.3.1.1. Compression

The following results correspond to a square plate under simply supported boundary conditions. As has already been mentioned, the thickness is 0.1 mm and the short side of the plate 0.1m.

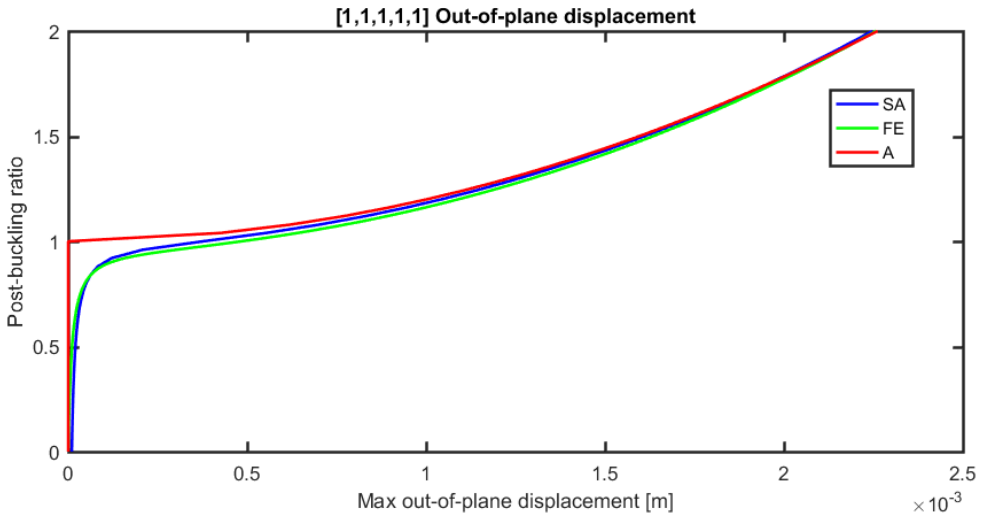

Figure 32: Out-of-plane displacement square simply supported plate under uniaxial compression (Predominant 45s)

The agreement between the different solutions is excellent. Even the analytical solution is able to make a good prediction without accounting for the bending-twisting terms.

In the semi-analytical and FE solutions it is possible to see that there is some out-of-plane displacement before buckling due to the imperfection. This imperfection introduces a more bending like behaviour.

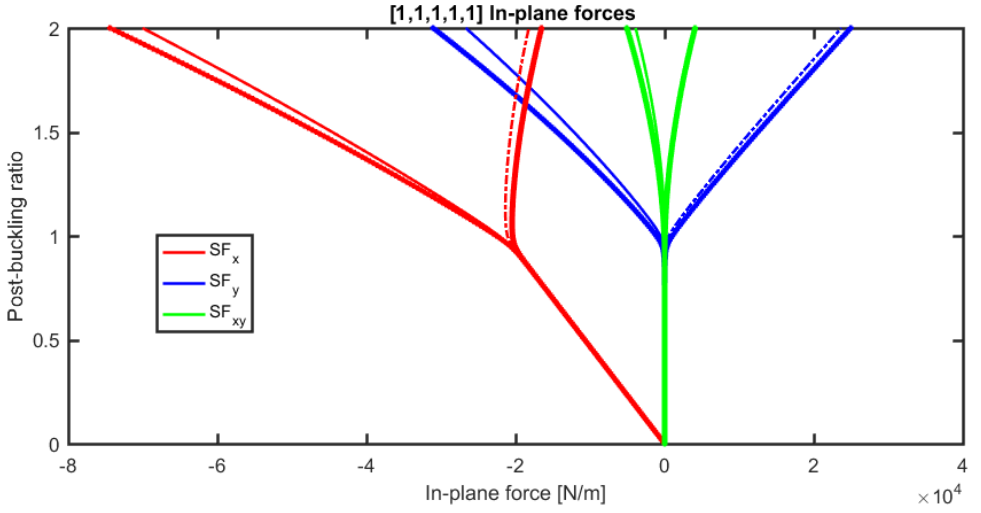

Figure 33: Max stresses square simply supported plate under uniaxial compression (Predominant 45s)

There is a good agreement between all the predicted maximum stresses. The plot also allows to see the load redistribution the plate suffers after the buckling load.

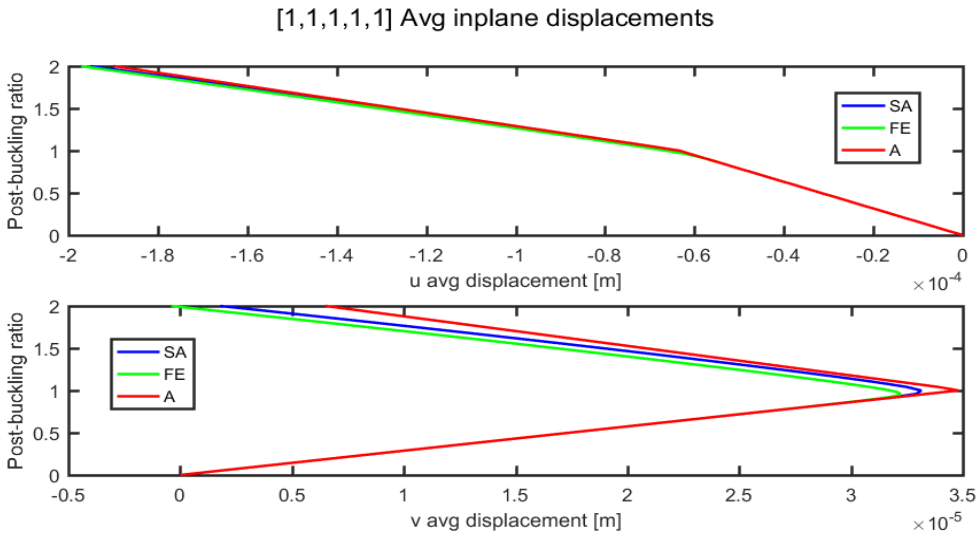

Figure 34: In-plane displacements square simply supported plate under uniaxial compression (Predominant 45s)

In-plane displacements are in perfect agreement for all the solutions. It is really clear how there are two different slopes (which represent the stiffness of the plate) before and after buckling. The v displacement is driven first by the Poisson effect (plate extends in the direction perpendicular to compression) and then by the shrinking produced by the out-of-plane displacement.

4.4.3.1.2. Shear

The next results are for a square clamped plate under shear loading.

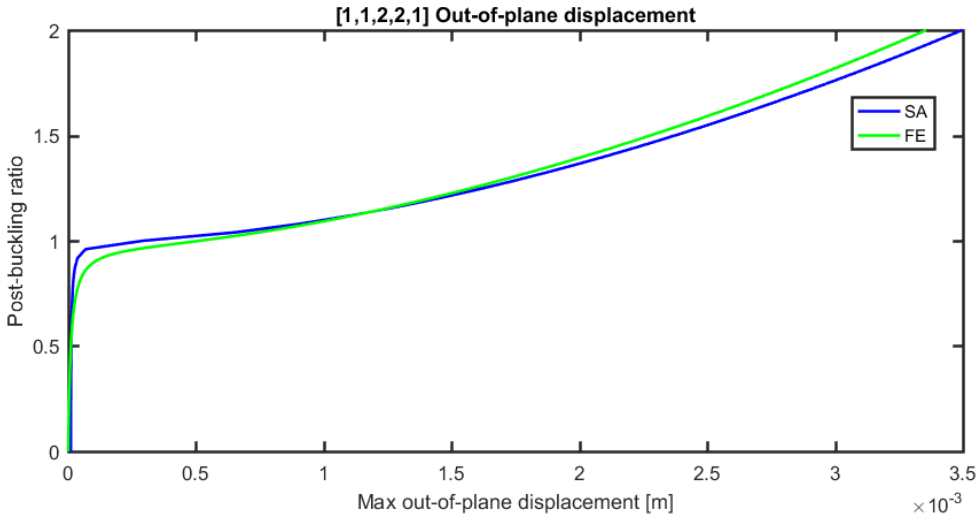

Figure 35: Out-of-plane displacement square clamped plate under shear (Predominant 45s)

Out-of-plane displacement is in very good agreement. The small differences between both curves seem to be driven by a minor discrepancy on the buckling load (FE solution starts to deflect earlier). However, the general behaviour and values are really well captured by the semi-analytical solution.

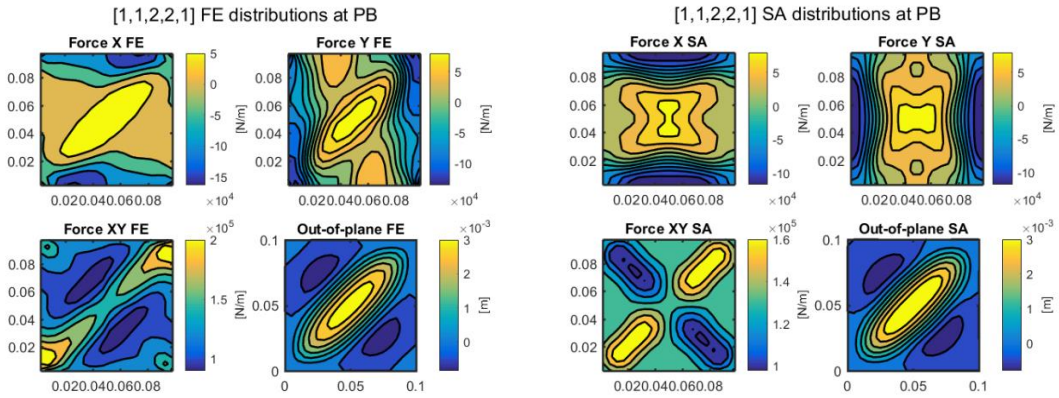

Figure 36: In-plane force and out-of-plane distributions square clamped plate under shear (Predominant 45s). FEM solution on the left, semi-analytical on the right

This figure shows the aforementioned limitations to reproduce the in-plane force distributions when diagonal buckling shapes are present, due to the symmetry of the functions that represent this redistribution. The diagonal behaviour is caused by the diagonal shape of the buckled shape, this is characteristic in shear loading or in 45s dominated laminates. Despite the incapacity to properly predict the redistribution, the maximum and minimum values are approximately matched.

The out-of-plane displacement is able to reproduce the diagonal behaviour and both are in perfect agreement.

4.4.3.1.3. Combined loading

The next results are for a square constant elastically restrained (200N as in buckling verification) plate under combined loading.

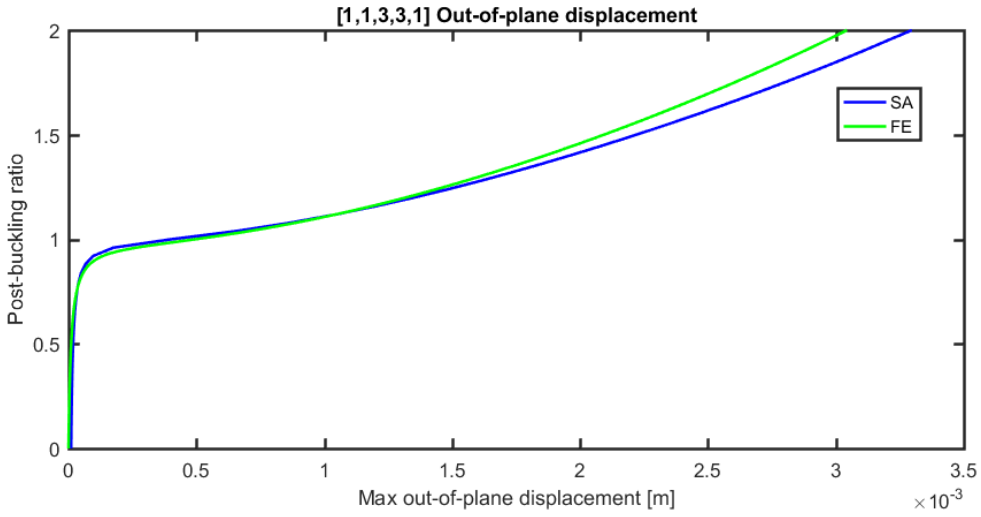

Figure 37: Out-of-plane displacement square elastically restrained plate under combined loading (Predominant 45s)

The results show very good agreement for the initial post-buckling behaviour but with some over prediction of the out-of-plane displacement for PB coefficient above 1.3-1.4. The discrepancies are probably caused by the difficulty to approximate both the complex shape and force distributions as a results of the combined loading and the high PB coefficient.

The following figure shows the result for the same plate configuration but rectangular (aspect ratio three), instead of square, to show the influence of the aspect ratio in the verification.

First results showed mode changing around PB ratio 1.6. To cope with this, the initial imperfection for this case has been increased from 1 to 2% of the thickness, resulting in:

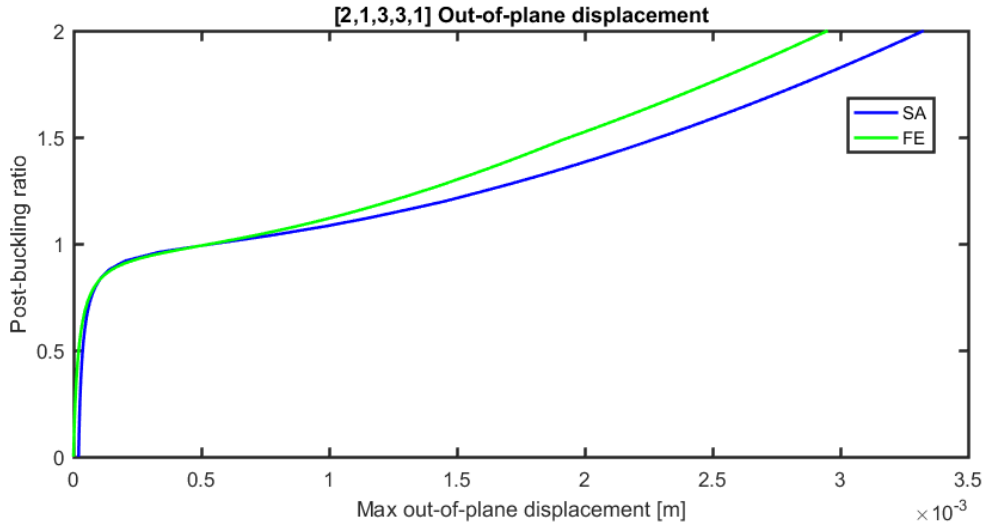

Figure 38: Out-of-plane displacement rectangular elastically restrained plate under combined loading (Predominant 45s)

The results for the higher aspect ratio plate are very similar. The out-of-plane displacement is almost the same and the discrepancies observed in the last verification are still there. The main difference is that the discrepacies start already at PB coefficient 1.1-1.2.

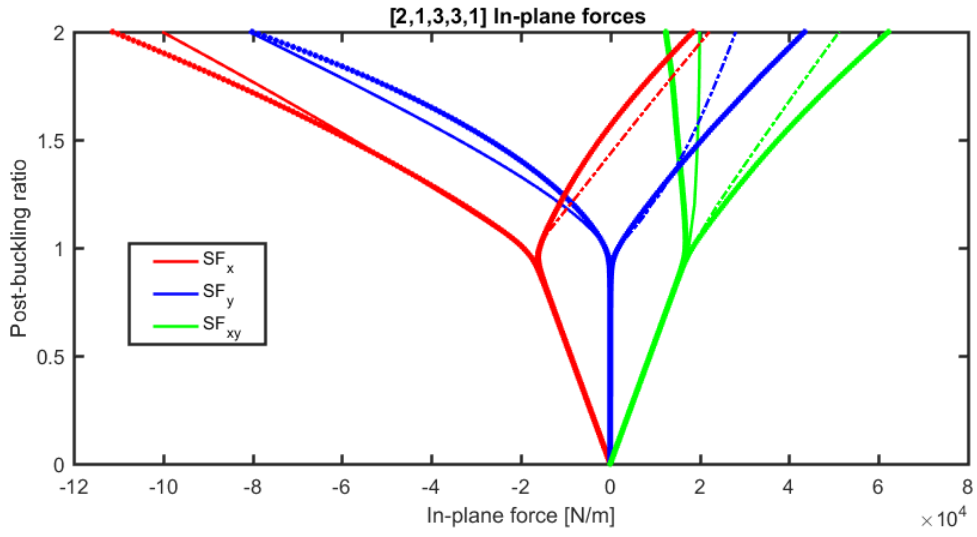

Figure 39: Max stresses rectangular elastically restrained plate under combined loading (Predominant 45s)

The maximum in-plane forces show better agreement in the x direction, but some underestimations of shear and tensile forces in y.

4.4.3.2. Predominant 0s

The predominant 0s laminate have a behaviour closer to a specially orthotropic material due to the use of fewer ±45 layers. Therefore, the results are expected to be in better agreement than in the previous section with the predominant 45s.

4.4.3.2.1. Compression

The following results correspond to a square plate under clamped boundary conditions.

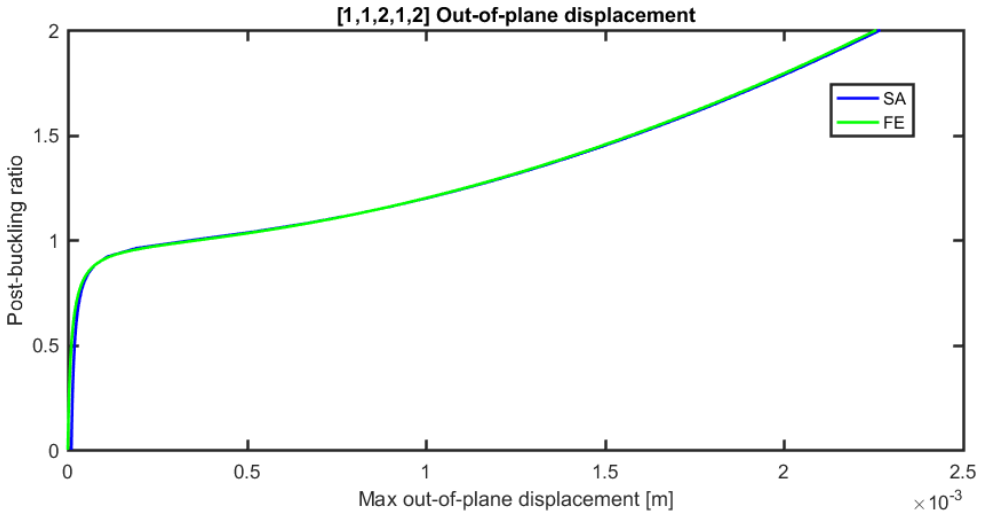

Figure 40: Out-of-plane displacement square clamped plate under uniaxial compression (Predominant 0s)

The results are in excellent agreement through the entire range of PB coefficients. Just notice that there is no analytical solution because the boundary conditions are not simply supported.

4.4.3.2.2. Shear

The next results are for a square plate under elastically restrained conditions.

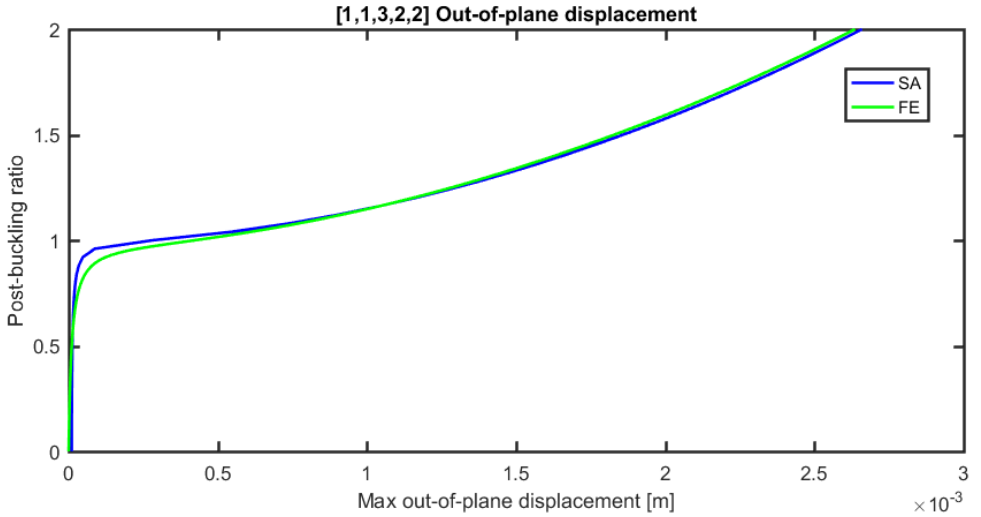

Figure 41: Out-of-plane displacement square elastically restrained plate under shear (Predominant 0s)

The out-of-plane displacement of the elastically restrained plate under shear are also in excellent agreement. There are small discrepancies as the semi-analytical solution shows

a more perfect buckling as if the imperfection was somehow smaller than in the FE case. However this just affect the very beginning of the curve.

Once again, the same case is verified but for a rectangular plate (aspect ratio 3) to check that the results are still valid for rectangular plates.

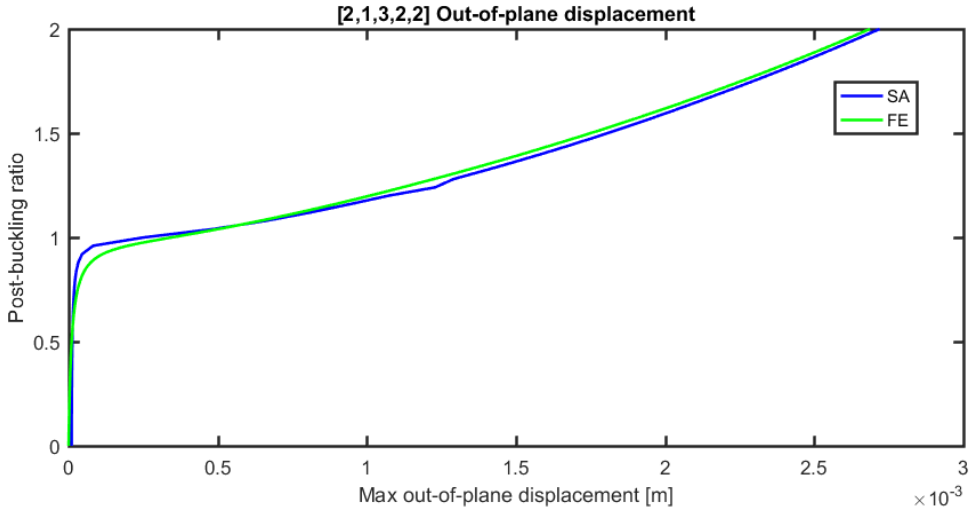

Figure 42: Out-of-plane displacement rectangular elastically restrained plate under shear (Predominant 0s)

The agreement is once again excellent, as for the square plate. There seems to be a small spike on the semi-analytical solution for PB coefficient around 1.25, which is probably caused by some convergence issue in the Newton Raphson algorithm. However, the deviation is minimum (almost imperceptible).

4.4.3.2.3. Combined loading

The next results are for a square simply supported plate under combined loading.

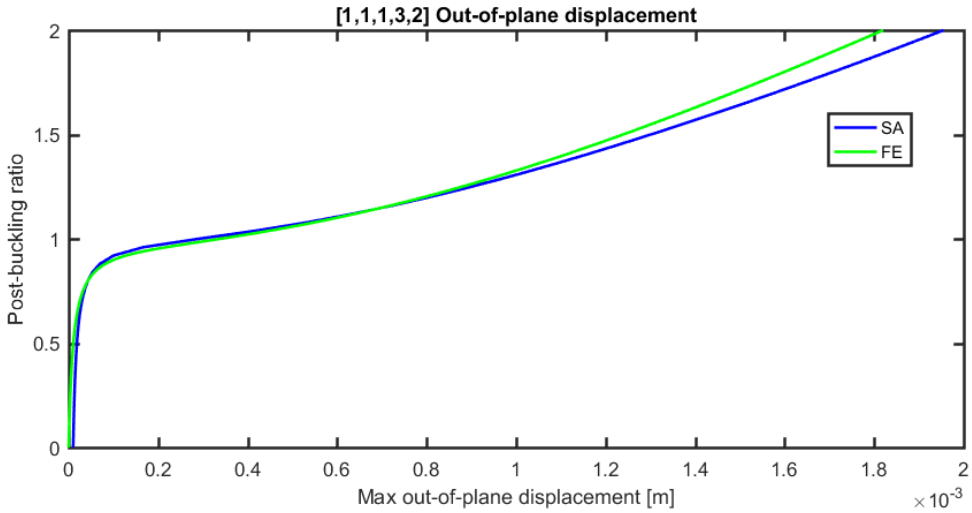

Figure 43: Out-of-plane displacement square simply supported plate under combined loading (Predominant 0s)

The results for the combined loading are very similar to the ones obtained for the predominant 45s despite the different lay-up and boundary conditions. The agreement for

the lower PB coefficients is excellent but some over estimation of the displacement is obtained for the higher ones. Nevertheless the differences do not seem too important as they are conservative and around 6% at the most unfavourable point.

4.4.3.3. Quasi isotropic

The quasi isotropic laminate has the same number of ±45s as the predominant 0s, but with the same number of 0s and 90s. It is not clear that the results should be better for this laminate as it will tend to buckle on more half-waves than the predominant 0s while having comparable D_{16} and D_{26} terms.

4.4.3.3.1. Compression

The following results correspond to a square plate under elastically restrained boundary conditions.

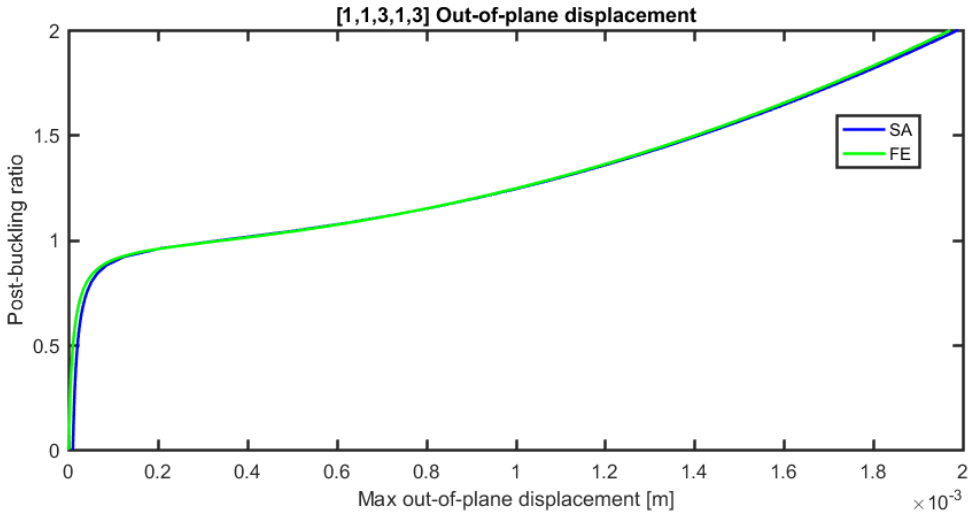

Figure 44: Out-of-plane displacement square elastically restrained plate under uniaxial compression (Quasi isotropic)

The results show excellent agreement between FE and semi-analytical solution.

4.4.3.3.2. Shear

The next results are for a square plate under simply supported boundary conditions.

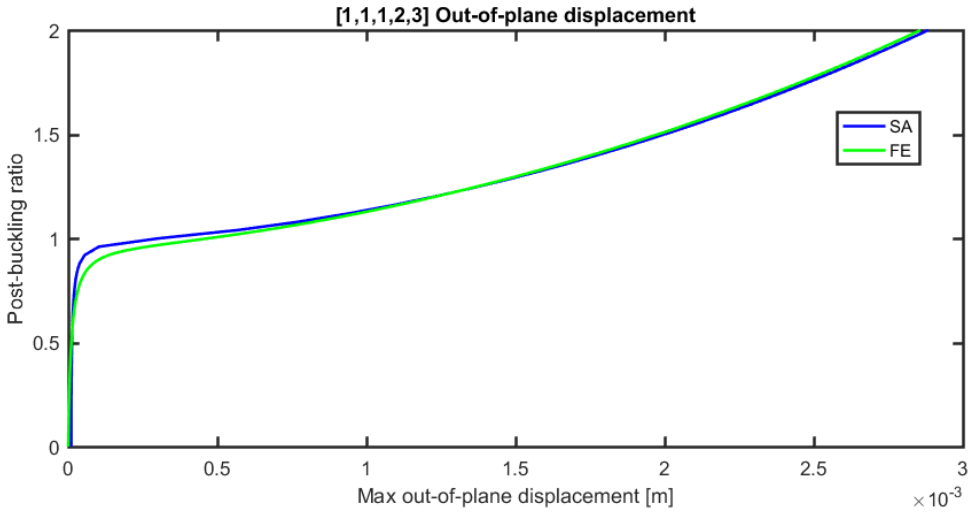

Figure 45: Out-of-plane displacement square simply supported plate under shear (Quasi isotropic)

There is a very a good agreement for this case. The solution is almost identical to the ones obtained for the predominant 0s. It seems that the semi-analytical solution behaves like if it has a smaller initial imperfection, but immediately the out-of-plane solutions match. This behaviour is probably produced by the different way to introduce the initial imperfection in both models. To simplify the formulation, the semi-analytical model only accounts for the most critical combination of half-waves while the FE model uses the exact buckling shape as imperfection. Since in shear, the buckling solution requires multiple combinations, making the introduced imperfection not as critical.

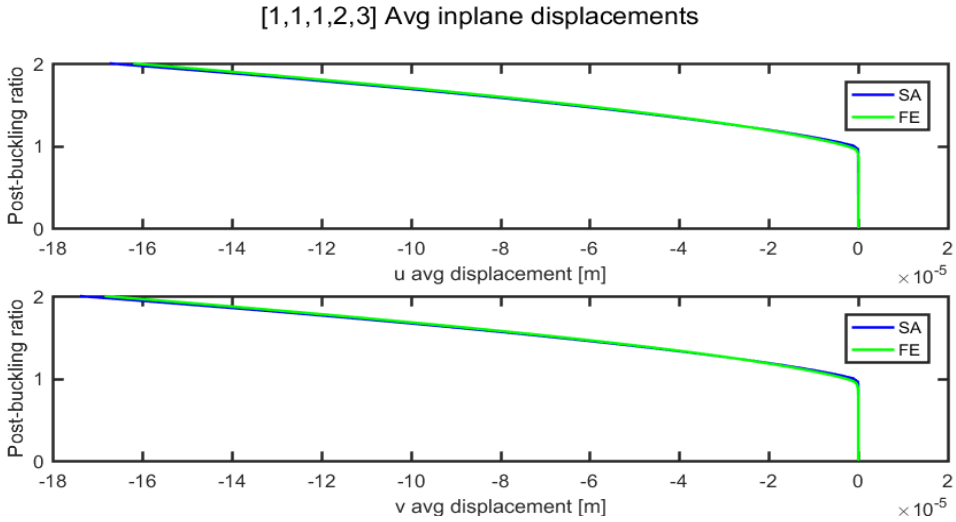

Figure 46: In-plane displacements square simply supported plate under shear (Quasi isotropic)

The in-plane displacements under shear are in excellent agreement. It should be noticed that the post-buckling behaviour is not as linear as in compression cases and also the fact that there is no shrinking or Poisson effects before the buckling load is reached.

4.4.3.3.3. Combined loading

The next results are for a clamped rectangular plate (aspect ratio three) under combined loading.

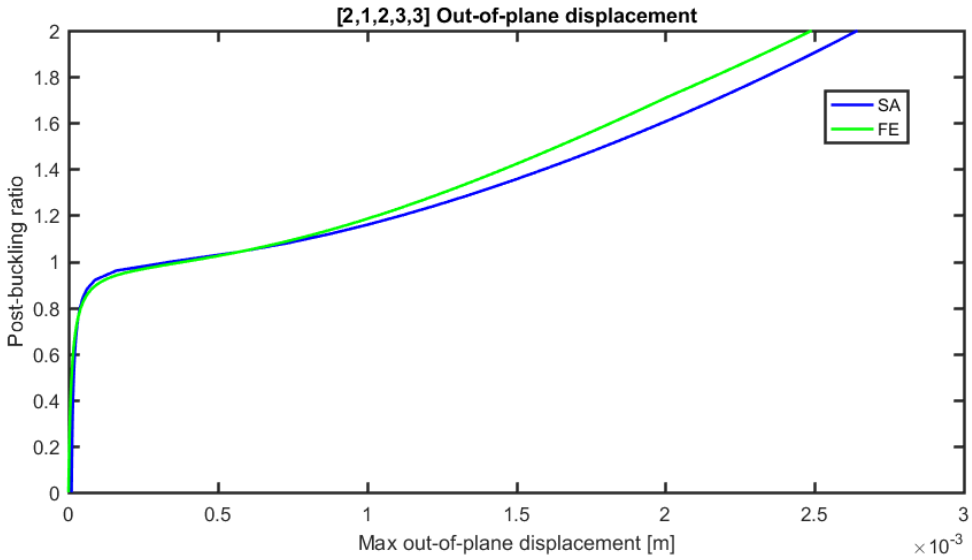

Figure 47: Out-of-plane displacement rectangular clamped plate under combined loading (Quasi isotropic)

The different boundary conditions and aspect ratios seems to not affect the results under combined loading. Once again the agreement is excellent at the beginning of the post-buckling behaviour, but the out-of-plane displacement is over estimated for the higher PB coefficient.

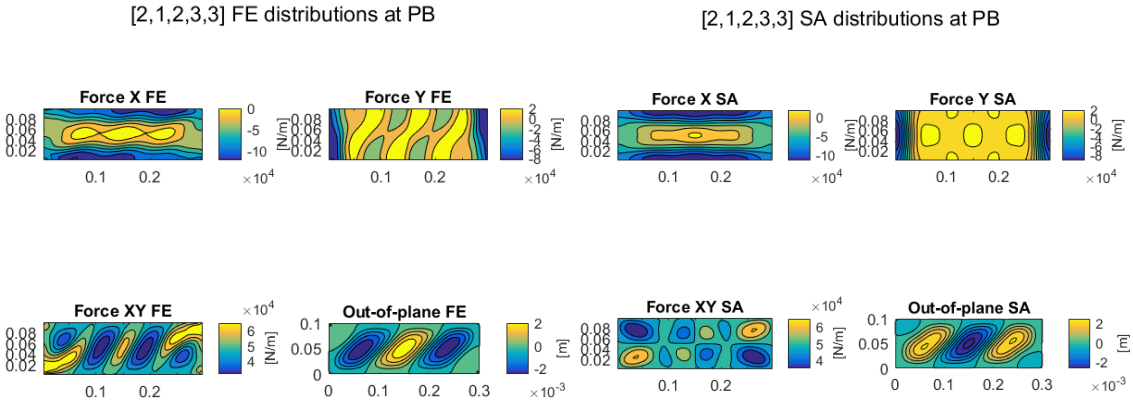

Figure 48: In-plane force and out-of-plane distributions rectangular clamped plate under combined loading (Quasi isotropic). FEM solution on the left, semi-analytical on the right

The in-plane force distributions show clear discrepancies between FE and semi-analytical solutions. The maximum and minimum values are approximately captured, but the distributions are not due to the aforementioned reasons. Those discrepancies seem especially important for the y direction and shear. However, the results given by the semi-analytical solution can prove to be a useful approximation of the plate strength.

4.4.4. Special Cases

Apart from the already reviewed verifications there are some additional interesting cases. The following ones are presented.

4.4.4.1. Constant loading

It has been mentioned that in typical applications is more common to have constant displacement, rather than constant load distribution. Therefore, the verification has

focused on those cases. However, it is still interesting to show that the alternative case can also be solved in case some applications require to solve such case. Actually, constant loading have some advantages on the capacity to deal with in-plane force distributions under shear forces. Figure 49 presents the out-of-plane displacement under shear for a predominant 45s rectangular plate elastically restrained.

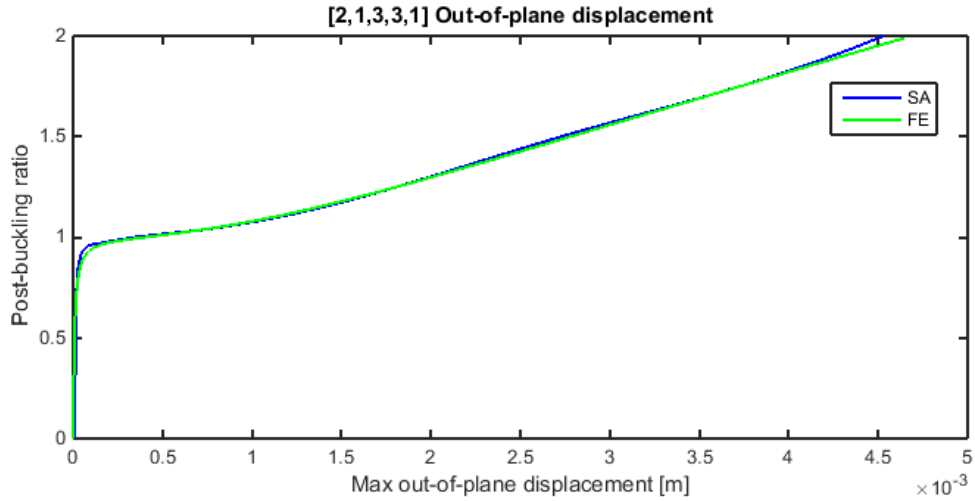

Figure 49: Out-of-plane displacement rectangular elastically restrained plate under constantly distributed combined loading (Predominant 45s)

The out-of-plane displacement shows perfect agreement in this example.

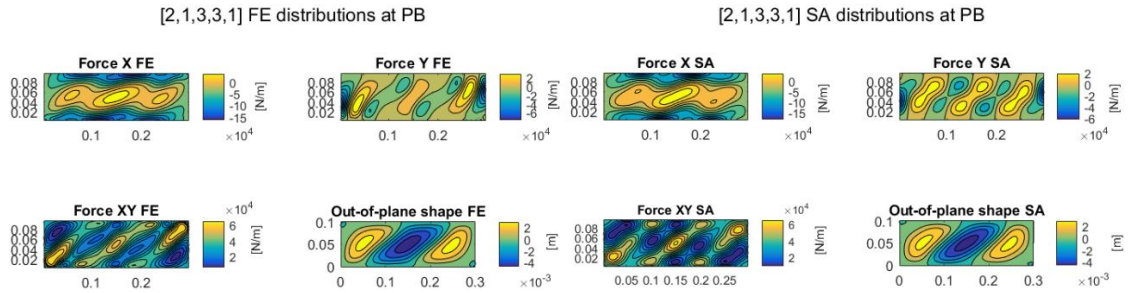

Figure 50: In-plane force and out-of-plane distributions rectangular elastically restrained plate under constantly distributed combined loading (Predominant 45s). FEM solution on the left, semi-analytical on the right

It is also possible to see that the Airy Stress function for constantly applied load is more versatile and is able to adapt better than in constant displacement to the in-plane diagonal force distributions.

4.4.4.2. Mode jumping

Mode jumping was a phenomenon that was not initially accounted for in this project. This explains the use of certain algorithms and approaches which do no facilitate its appearance in the results. However, during the verification of the results, it has been seen that mode jumping was taking place and it limited the capacity of performing reliable verifications.

Next figure shows out-of-plane displacement comparison where semi-analytical solution presents mode jumping from two to three half-waves for a rectangular (aspect ratio three) predominant 0s plate, simply supported under combined loading:

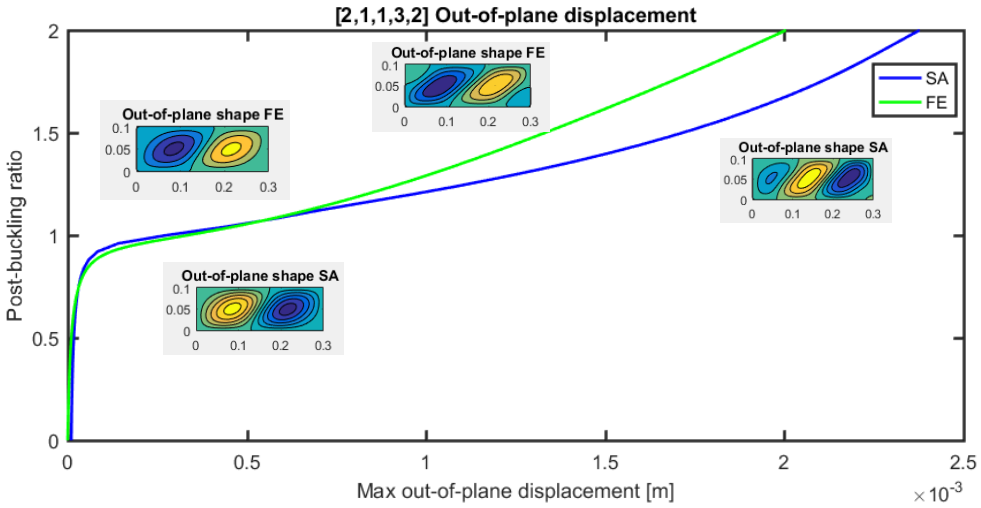

Figure 51: Out-of-plane displacement with mode jumping in the SA solution

The out-of-plane curve has been complemented with the complete shapes for FE and SA models at PB ratios one and two, so it can be seen how the different mode affects the verification.

Additionally, the incapability to reproduce the shape during mode changing might contribute to the overestimation of the maximum out-of-plane displacement.

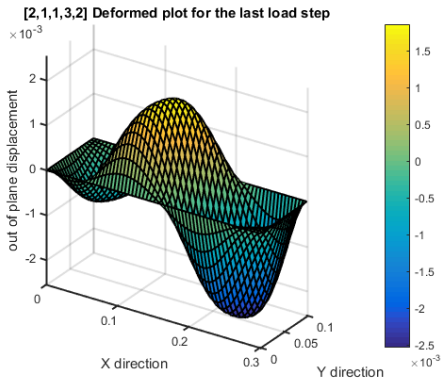

Figure 52: 3D out-of-plane shape

The 3D out-of-plane figure shows how the third wave presents higher amplitude than the rest. It is believed that during the appearance of the new half-way the linear combination of functions that represent the shape struggles to model the additional complexities of a diagonal pattern and the mode change. If mode shape capabilities are added in the future, it would be interesting to investigate how the buckled shape functions can approximate such transitions.

This problem also appears in the reproduction of the force distributions. The symmetries of the derivatives of the Airy Stress function make it impossible to reproduce the additional complexities derived from mode jump transitions. The current approach used, solving both

compatibility and equilibrium equation allows to approximate the solutions but they are still restricted by the combination of functions chosen to represent the results.

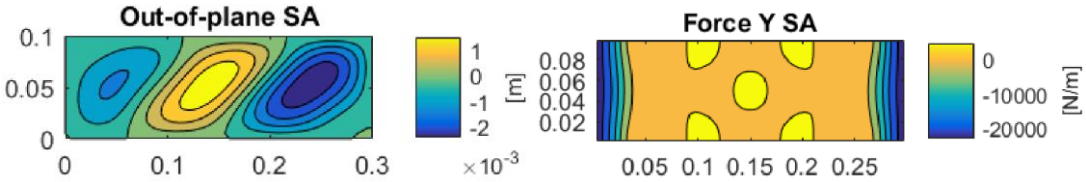

Figure 53: Mode shape transition. Out-of-plane (left) and Force in y distribution (right)

Figure 53 shows the already commented asymmetrical out-of-plane displacement, with greater displacements on the right side. The in-plane force distribution in y direction would be expected to reflect the influence of the irregular shape. However the symmetries of the chosen Airy Stress function limits the results to a too regular distribution. The limitations of the in-plane force distributions, regardless the mode changing, are further developed in the next section.

In conclusion, mode jumping alters the solution, making it difficult to compare SA and FE models. It is necessary to further understand the phenomenon in order to know how it takes place in real structures and how it can be properly incorporated to both FE and SA models. The results studied show that bigger initial imperfections delay or neglect mode jumping in the SA model. Moreover, the number of steps used in Newton-Raphson can also affect mode jumping.

4.4.4.3. In-plane force distribution under shear

It has already been commented the limitations of the current Airy Stress function for constant displacement to capture the in-plane force redistributions during shear loading. This limitations are based on the symmetry of the function $\cos(2mx)$ which makes impossible the appearance of diagonal shape distributions for the in-plane force distributions in the x and y directions.

It is clear that the solutions might be improved by the use of a more advanced linear combination of terms in the Airy Stress function. Preliminary studies on the conditions that such functions should follow suggested the use of the terms with the form $\sin(2mx)$ as they are able to introduce asymmetry in the distribution without modifying the equilibrium of the plate. The following figure shows some promising results of how the reimplementation of the Airy Stress function can improve the current solutions:

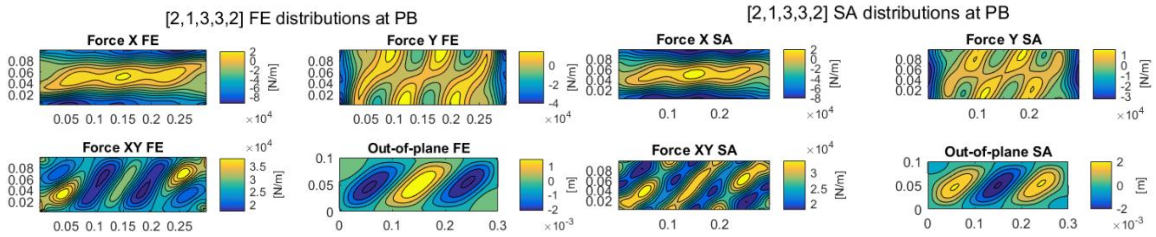

Figure 54: In-plane force and out-of-plane distributions square clamped plate under shear (Predominant 45s). FEM solution on the left, modified semi-analytical on the right

With the modified Airy Stress function the in-plane force distribution pattern improves significantly. If both figures are compared plot by plot, the results are quite similar. Shear seems like the only case where the improvement is more limited.

The next figure is the solution using the regular Airy Stress function. There it is possible to appreciate how the patterns are less accurate.

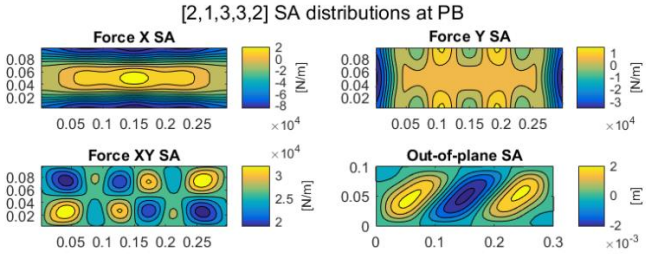

Figure 55: In-plane force and out-of-plane distributions square clamped plate under shear (Predominant 45s).

The new in-plane force distributions are more accurately estimated, capturing the twist produced by the diagonal buckling wave. However, the general solution does not really improve (max out-of-plane displacement or max in-plane forces) and the extra terms required reduce significantly the performance. Due to the previous reasons, it has been decided to neglect this approach in most verifications, but further study on alternative Airy functions can result on an improved solution.

4.5. Conclusions post-buckling

The verifications show excellent to reasonable agreement between semi-analytical and FE solutions for a wide range of aspect ratios, laminate layups, loads and boundary conditions. Results are focused on the prediction of the out-of-plane displacement, but in-plane displacements and in-plane force distributions are also considered, which multiplies the possibilities of the obtained solution. The amount of variables treated and the necessity to present their evolution for the different PB ratios has forced the rationalization of the number of cases presented in the verification. However, the skipped cases and others are included in the annex at (Annex\PBuckling).

Different formulations are presented depending on how the load is applied. Initial work was based on constant load application, but further study encouraged the development of a constant displacement solution. This last case is more representative of the solution of the individual plates in stiffened panels, where the reinforcing members limit the in-plane deflection of the plate. Therefore, taking into account the final objectives of this project, the verification has focused on the final case.

It has been observed that the accuracy of the solution depends mainly on the complexity introduced by the material. The introduction of many 45s and the resulting coupling terms limit the accuracy, especially for high PB ratios. On the other hand, isotropic materials show excellent agreement as shown in section 4.4.1.1 where the different types of figures are presented. Besides, load cases with shear loading (especially when combined with

axial ones) introduce further complexity and affect the accuracy. Whereas, the accuracy does not seem affected by the different boundary conditions presented in the verification[11].

Mode jumping seems to be an important topic that was not considered in the initial stages of the project. The limitations of the approaches used for both SA and FE to deal with mode jumping introduce uncertainty during the verification because they are capable of accounting for it in very few cases, making it very difficult to compare identical cases when one of the models predicts mode jumping while the other doesn't. Moreover, the appearance of this phenomenon modifies the in-plane force distribution, changes the post-buckling stiffness of the plate and obviously alters the out-of-plane response. Therefore, it is considered that in future developments it would be interesting to further study it and use strategies in order to be able to deal with it (for example, using more powerful non-linear solvers such as the ones based on the arc length method).

The solution for the force distribution under shear is limited by the current election of the Airy Stress function. This had been developed initially for specially orthotropic plates under axial loading, and the symmetry that presents makes it unable to capture the effects that diagonal waves have on the force distribution. Anyway, the force predictions (especially maximum values) give a reasonable approximation for preliminary design or optimization purposes. More detailed solutions can be obtained (as partially shown in section 4.4.3.3) by developing a more capable form for the Airy Stress function.

In conclusion, the resolution of the post-buckling behaviour for composite plates presents important challenges. However, the developed formulation is able to return good results under a wide range of conditions which makes the approach suitable for more advanced applications such as stiffened panel solvers.

[11] Additional verifications presented in the digital annex do show negative effects on the accuracy for asymmetrically elastic restrained plates.

5. Stiffened panel integration

5.1. Introduction

The main objectives of this Thesis are the development of solutions for both buckling and post-buckling of composite plates with boundary conditions able to reproduce the restrain of real stiffeners. Therefore, several algorithms have been developed and their capacity to solve an important range of cases has been demonstrated. However, the final purpose of Fokker Aerostructures is to develop a procedure able to cope with stiffened panels. Therefore, creating a link between the individual elements and the realistic stiffened structure providing a complete analysis procedure.

The stiffened panel[12] geometry is presented in the following figure. The different elements are presented in different colors: yellow for the stiffeners, green for the frames and red for the skin.

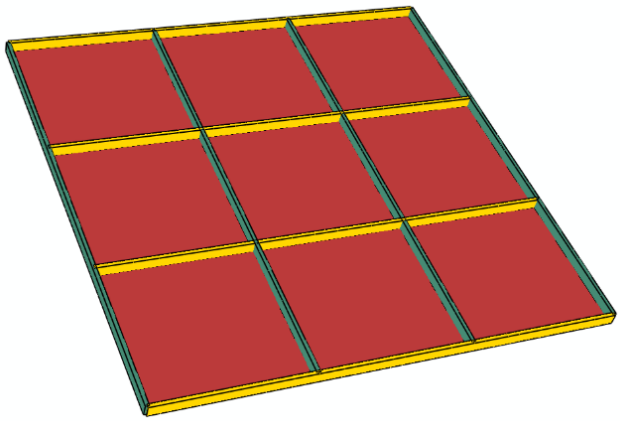

Figure 56: Stiffened panel sketch

This chapter introduces the developed formulations implemented for the stiffened panel solver. First of all, the main individual modules and their formulations are introduced. These are the 1D beam model, the *GJ-k* relation and the load redistribution. Once the different modules have been explained, the stiffened panel formulation is presented. The chapter finishes with a preliminary verification of the implemented program in Matlab (with a graphical user interface GUI) against FEM results, in order to show the possibilities of the solver developed for stiffened panels.

[12] Notice the difference between plate and panel. The first is used to describe each of the individual portion of skin surrounded by stiffeners and frames, while the second is a reference to the whole structure including skin, stiffeners and frames.

5.2. 1D beam model

The first step to develop a stiffened panel solution is being able to determine the behaviour of the stiffeners and frames. The model has to be able to solve mainly the axial stiffness of a beam (to solve the redistribution of loads between plates and beams) and its torsional stiffness (in order to estimate the torsion elastic restrain). Therefore, a 1D beam model is sufficient to cope with the requirements, as long as instability phenomena are not taken into account.

The 1D theory is required to solve beams with different open and closed sections and different composite lay-ups while keeping a good accuracy and a straightforward formulation. Due to time limitations, it was decided to make a quick research of the available theories and developed procedures, as exposed during the Literature review (in section 2.5). After studying some different options it was decided to implement Kollar and Pluzsik 1D beam theory [38] due to its capacity to work with arbitrary lay-up while keeping a closed form solution (for further details see the reference). Moreover, the use of an already developed theory which has undergone verification was very attractive as it permitted to focus the time on the development of the stiffened panel formulation.

Kollar's and Pluzsik's theory models the beam behaviour with the following 4 by 4 stiffness matrix:

$$\begin{Bmatrix} N_x \\ M_y \\ M_z \\ T_{SV} \end{Bmatrix} = \begin{bmatrix} P_{11} & P_{12} & P_{13} & P_{14} \\ P_{21} & P_{22} & P_{23} & P_{24} \\ P_{31} & P_{32} & P_{33} & P_{34} \\ P_{41} & P_{42} & P_{43} & P_{44} \end{bmatrix} \begin{Bmatrix} \varepsilon_x^0 \\ \frac{1}{\rho_y} \\ \frac{1}{\rho_x} \\ \theta \end{Bmatrix} \tag{124}$$

The main terms for the stiffened panel resolution are the axial stiffness of the beam P_{11} (usually named EA) and the torsional stiffness P_{44}, which is typically referred as *GJ*. The bending stiffness P_{22} (commonly known as EI) is also of interest as their value determines if the assumption of straight edges is accurate. Additionally, the other bending stiffness P_{33} restrains the out-of-plane displacement when the panel buckles. It has already been commented that Mittelstedt [41] determined the minimum bending stiffness for several cases.

5.3. Determination of the *GJ-k* relation

5.3.1. Introduction

The torsional stiffness of beams is typically modelled using one-dimensional Saint-Venant torsion theory. According to this model, the torsion moment is proportional to the first derivative of the beam's twist angle with respect to the longitudinal direction.

$$T = GJ\frac{d\theta}{dz} \tag{125}$$

This approach has been used in some plate formulations to more accurately introduce the elastic restrain of stiffeners [17]. However, working with the derivative of the angle implies a rather complex distribution of the applied moment in the edge, and therefore a complex approach to apply the boundary conditions. In this Thesis, a simpler approach is used based on torsional springs like many other authors in the literature [28, 29, 31, 34].

$$T = k\theta \tag{126}$$

This approach is very convenient because the elastic restrain along the edge is constant, making easier to solve the corresponding boundary conditions. However, when modeling a stiffener, the equivalent *k* caused by the beam torsional rigidity *GJ* must be calculated.

5.3.2. Effective *GJ*

The restrain provided by stiffeners or frames has to be distributed to the adjacent plates. When it is an internal member, two plates are restrained by the same beam element. The approach used in literature [17, 21] assumes that the distribution is evenly distributed to each plate so the effective *GJ* seen by each plate is one half of the original. The same approach is used in this Thesis.

This means that in a stiffened panel, the different plates can have different boundary conditions depending on their position with respect to the panel. In regularly stiffened panels (constant spacing and equal stiffeners or frames) four different sets of boundary conditions are possible.

5.3.3. New *GJ* method

During the Literature study (section 2.5) it was already mentioned that the different methods found in the literature to cope with this problem were not found satisfactory due to different reasons (lack of accuracy, not applicable to all required cases, excessive complexity), therefore it was decided to develop a new approach suitable for the case at hand.

The new proposed solution is based on directly finding the relation between *GJ* and *k* such as the energy stored by either elastic restrain in every edge is the same, therefore giving the same buckling load. To find this relation, the following formulation is developed.

The restrain energy with torsional springs is:

$$\begin{aligned} U_k = \frac{1}{2}\int \left\{ k_1 \left(\frac{\partial w}{\partial x}\right)^2 \Big|_{x=0} + k_2 \left(\frac{\partial w}{\partial x}\right)^2 \Big|_{x=a} \right\} dy \\ + \frac{1}{2}\int \left\{ k_3 \left(\frac{\partial w}{\partial y}\right)^2 \Big|_{y=0} + k_4 \left(\frac{\partial w}{\partial y}\right)^2 \Big|_{y=b} \right\} dx \end{aligned} \tag{127}$$

The restrain energy with De Saint Venant torsion bars is:

$$U_{SV} = \frac{1}{2}\int\left\{GJ_1\left(\frac{\partial^2 w}{\partial x \partial y}\right)^2\Big|_{x=0} + GJ_2\left(\frac{\partial^2 w}{\partial x \partial y}\right)^2\Big|_{x=a}\right\}dy + \frac{1}{2}\int\left\{GJ_3\left(\frac{\partial^2 w}{\partial x \partial y}\right)^2\Big|_{y=0} + GJ_4\left(\frac{\partial^2 w}{\partial x \partial y}\right)^2\Big|_{y=b}\right\}dx \tag{128}$$

Then the energy is compared edge by edge:

$$U_{k_1} = U_{SV_1} \rightarrow \frac{1}{2}\int\left\{k_1\left(\frac{\partial w}{\partial x}\right)^2\Big|_{x=0}\right\}dy = \frac{1}{2}\int\left\{GJ_1\left(\frac{\partial^2 w}{\partial x \partial y}\right)^2\Big|_{x=0}\right\}dy \tag{129}$$

The variables *k* and *GJ* are constants so they can be taken outside the integrals. To simplify the next calculations, the equation is transformed to dimensionless variables using the following relations:

$$\begin{gathered} W = \frac{w}{h}, \quad \xi = \frac{x}{a}, \quad \eta = \frac{y}{b}, \quad \lambda = \frac{a}{b}, \\ k^*_{1,2} = \frac{k_{1,2}a}{D^*_{11}A_{22}h^2}, \quad k^*_{3,4} = \frac{k_{3,4}b}{D^*_{22}A_{22}h^2}, \\ GJ^*_{1,2} = \frac{GJ_{1,2}}{D^*_{11}A_{22}h^2a}, \quad GJ^*_{3,4} = \frac{GJ_{3,4}}{GJ^*_{22}A_{22}h^2b} \end{gathered} \tag{130}$$

Substituting them in equation 129 and using the out-of-plane shape presented in eq. 82:

$$\begin{aligned} &\frac{1}{2}k_1^*\frac{D^*_{11}A_{22}h^2}{a}\int\left\{\left(\frac{h}{a}\right)^2\sum_{m,n=1}^{MN}\left(W_{mn}\frac{\partial X_m}{\partial \xi}Y_n\right)^2\Big|_{\xi=0}\right\}bd\eta \\ &= \frac{1}{2}GJ_1^*D^*_{11}A_{22}h^2a\int\left\{\left(\frac{h}{ab}\right)^2\sum_{m,n=1}^{MN}\left(W_{mn}\frac{\partial X_m}{\partial \xi}\frac{\partial Y_n}{\partial \eta}\right)^2\Big|_{\xi=0}\right\}bd\eta \end{aligned} \tag{131}$$

After the proper simplifications:

$$k_1^* = GJ_1^*\lambda^2\frac{\int\left\{\sum_{m,n=1}^{MN}\left(W_{mn}\frac{\partial X_m}{\partial \xi}\frac{\partial Y_n}{\partial \eta}\right)^2\Big|_{\xi=0}\right\}d\eta}{\int\left\{\sum_{m,n=1}^{MN}\left(W_{mn}\frac{\partial X_m}{\partial \xi}Y_n\right)^2\Big|_{\xi=0}\right\}d\eta} \tag{132}$$

The previous expressions have been converted from dimensionless variables and extended to all four edges:

$$k_{1,2} = \frac{GJ_{1,2}\lambda^2}{a^2} \frac{\int \left\{ \sum_{m,n=1}^{MN} \left(W_{mn} \frac{\partial X_m}{\partial \xi} \frac{\partial Y_n}{\partial \eta} \right)^2 \Big|_{\xi=0} \right\} d\eta}{\int \left\{ \sum_{m,n=1}^{MN} \left(W_{mn} \frac{\partial X_m}{\partial \xi} Y_n \right)^2 \Big|_{\xi=0} \right\} d\eta}$$

$$k_{3,4} = \frac{GJ_{3,4}}{\lambda^2 b^2} \frac{\int \left\{ \sum_{m,n=1}^{MN} \left(W_{mn} \frac{\partial X_m}{\partial \xi} \frac{\partial Y_n}{\partial \eta} \right)^2 \Big|_{\xi=0} \right\} d\eta}{\int \left\{ \sum_{m,n=1}^{MN} \left(W_{mn} \frac{\partial X_m}{\partial \xi} Y_n \right)^2 \Big|_{\xi=0} \right\} d\eta} \quad (133)$$

Equation 133 presents an obvious problem. The relation requires to know beforehand the buckled shape solution[13], but this solution depends on the torsional restrain *k*. To cope with this problem, an iterative algorithm is implemented. The initial guess is obtained assuming the plate has buckled in square sinusoidal half-waves (number proportional to the aspect ratio). The following flow chart should clarify the behaviour of the algorithm:

[13] The amplitudes of the buckling solution cannot be solved during the linear buckling analysis. However, those can be non-dimensionalized and use the eigenvector solution as the dimensionless amplitudes.

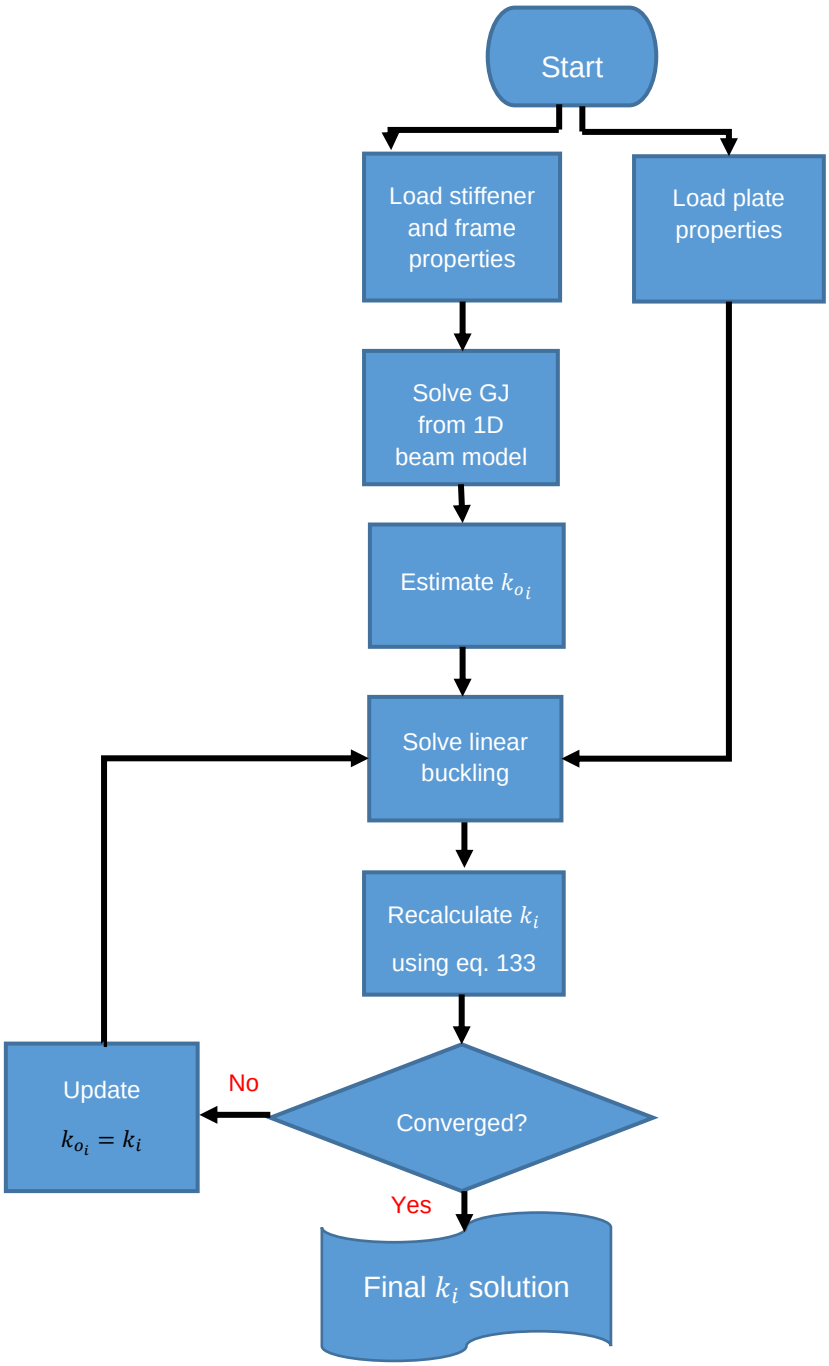

Figure 57: Flowchart GJ-k algorithm

5.3.4. Verification of obtained *GJ-k relations*

This new method has shown to give accurate results plus a stable and fast convergence. The accuracy of the new method has been evaluated in two steps. The first consisted in comparing the closed form solution for buckling given by Bisagni in [17] with the one provided with the developed semi-analytical model for buckling. Bisagni's solution is based on a simpler formulation for De Saint Venant torsion bars, so it is possible to directly compare the method with a closed form solution depending on *GJ*.

The verification is limited to the cases covered by Bisagni's closed form solution: uniaxial compression with the loading edges simply-supported and the others elastically restrained by the same value. Therefore, in order to execute the verification, several lay-ups are tested for different *GJ* values ranging from virtually simply-supported to clamped conditions. Then the difference between the buckling loads predicted by both methods are plotted in semilogarithmic scale.

The first thing to consider, is that when *GJ* is either very small or very big, the boundary conditions are virtually simply supported or clamped, and the accuracy of the *GJ-k* relation is no longer important (both *GJ* and *k* will be close to zero or infinite). Those regions give constant solutions and therefore the error there is constant.

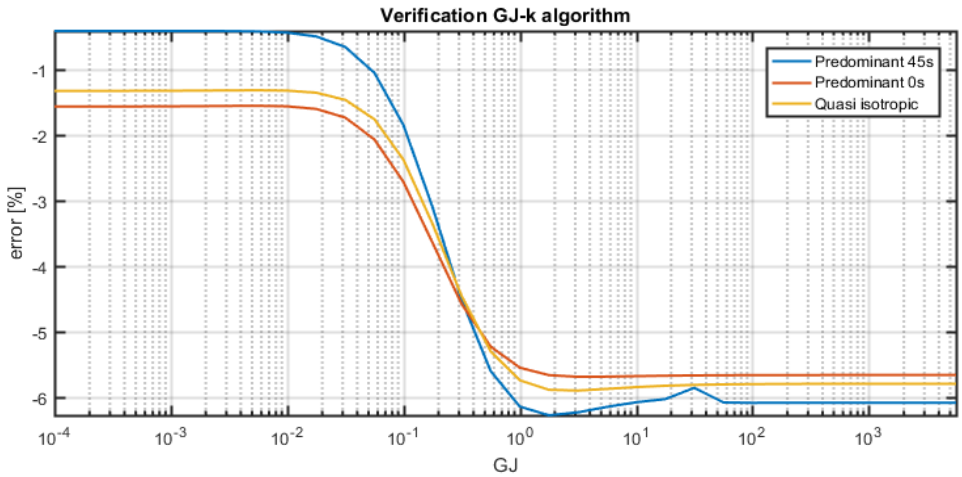

Figure 58: Verification GJ-k algorithm for square plates

The 6% maximum difference between solutions for virtually clamped conditions seems quite significant, but it does not indicate an error on the *GJ-k* relation proposed. For sufficiently big *GJ* (not matter the inaccuracies of the GJ-k relation) the correspondent *k* will represent a fully clamped case (that is the reason for the big range of GJ values tested).

The clamped solutions for plates (see section 3.3) were accurately solved by the proposed formulation which indicates that the error source is the closed form solution used [17]. A 6% error in the closed form solution can seem too big, but it must be reminded the complexity of the involved equations and the amount of approximations required to have a manageable closed form expression. For example, Bisagni's expression is limited to specially orthotropic laminates, while the tests involves mid-plane symmetric laminates.

Therefore, the accuracy of the closed form solution limits somehow the conclusions that can be obtained from the comparison. However, the fact that the intermediate solutions are in smooth transition between the fixed errors for simply supported and clamped conditions gives confidence that *GJ-k* relation is a good approach.

The next verification deals with the same case but with rectangular plates (aspect ratio 3):

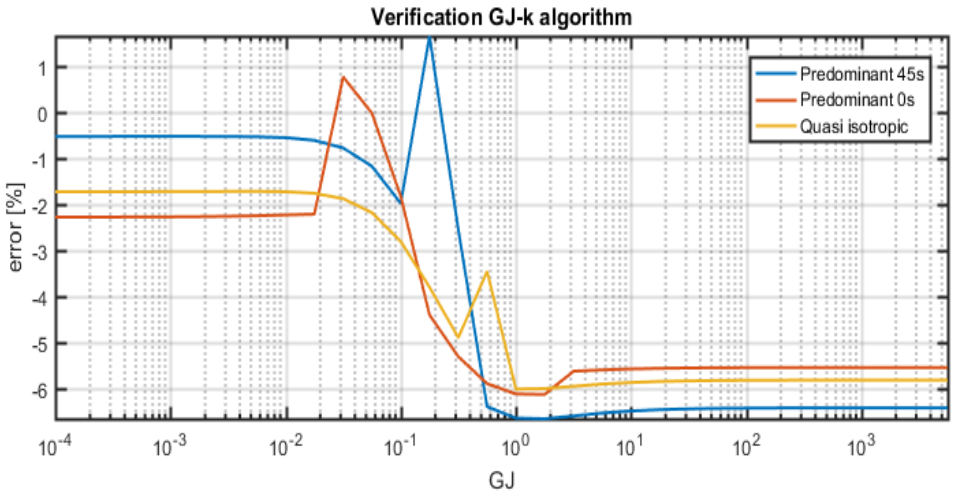

Figure 59: Verification GJ-k algorithm for rectangular plates

The difference for the ideally clamped case is again quite important. However, the verifications performed in chapter 3 should guarantee that the error source is again due to the limitations of the closed from solution.

On the other hand, the transition between both values is not as smooth as in square plates. The origin of the spikes have been found to be differences in the mode jumping between both solutions. Anyway, the jump in the predictions are around 3% maximum, which seems a reasonable error for the *GJ-k* algorithm when dealing with mode changing.

The current results show that the algorithm results might be okay, but the limitations in the closed form solution limits the conclusions that can be drawn. Final verifications of the developed algorithm with FE are required. The verifications have been performed using the whole stiffened panel in section 5.7.

5.4. Load redistribution

All the analytical and semi-analytical solutions for post-buckled stiffened panels found in the literature were limited to panels with stiffener members only in the longitudinal direction. This is a special case in stiffened panels, as they are usually stiffened in both direction by stiffeners (longitudinal) and frames (transversal) as shown by figure 54. The developed solution intends to solve this more general configuration, which obviously increases the complexity of the problem.

Panels stiffened only by longitudinal members have the following advantages:

- There is no load coupling (a panel under uniaxial compression have its individual plates or bays under the same load type as the stiffened panel).
- Post-buckling stiffness can be reduced to one term only and be easily calculated from the in-plane displacements.
- The load redistribution can be solved once for pre-buckling and once for post-buckling, since the ratio of load shared by skin and stiffeners is almost constant for each.

The introduction of transverse members no longer allows for the previous simplifications. The complexity of the case has been dealt with the following strategies:

5.4.1. Step by step strain compatibility

When the load is increased in a bi-stiffened panel, the strain compatibility might force a new redistribution of loads which at the same time might affect the stiffness of the plates and hence the load redistribution itself. Therefore, it is clear that some iterative or step by step strategy might be required to solve the problem.

The proposed solution uses a step by step strategy, taking advantage of how the post-buckling solution is obtained. For every new load, the new redistribution is solved using the previous results of the plates' stiffness.

The load redistribution is recalculated for every load step through the strain compatibility of the different members, which means that both the plate and the stiffeners must have the same strain in the x direction, and the frames in the y direction.

The main assumption to be able to use this approach is that the load is applied as a constant displacement along all the edges (including stiffeners and frames). This way, it can be considered that the different members are loaded in their neutral axis, even if the global neutral axis moves due to the post-buckling of the skin. With this approach, the problem is reduced to two dimensions and global bending can be neglected.

To apply this approach it is necessary to calculate the stiffness of the panel as the combination of the stiffness of the different elements:

$$\boldsymbol{K}_{panel} = \boldsymbol{K}_{plates} + \boldsymbol{K}_{stiffeners} + \boldsymbol{K}_{frames} \tag{134}$$

The stiffness of the beam members (stiffeners and frames) is reduced to a 1D axial term. The axial stiffness takes a constant value (no instabilities allowed) calculated through the 1D beam model. It is necessary to account for the number of members in each direction for the global stiffness.

$$\begin{gathered}\boldsymbol{K}_{stiffeners} = \begin{pmatrix} EA_{stiffeners} \cdot n_{stiffeners} & 0 & 0 \\ 0 & 0 & 0 \\ 0 & 0 & 0 \end{pmatrix} \\ \boldsymbol{K}_{frames} = \begin{pmatrix} 0 & 0 & 0 \\ 0 & EA_{frames} \cdot n_{frames} & 0 \\ 0 & 0 & 0 \end{pmatrix}\end{gathered} \tag{135}$$

The stiffness of the plates requires a more complex approach, as its value might change due to post-buckling behaviour. The details of how it is solved are developed in the next section.

From the stiffness of the panel it is possible to calculate the global strains caused by every load increment.

$$\Delta\boldsymbol{\varepsilon}_{panel} = \boldsymbol{K}_{panel}^{-1}\Delta\boldsymbol{N} \tag{136}$$

Where ΔN is the load increment at panel level. Then the load redistribution for every member is solved.

$$\begin{cases} \Delta \boldsymbol{N}_{plates} = \boldsymbol{K}_{plates} \Delta \boldsymbol{\varepsilon}_{panel} \\ \Delta \boldsymbol{N}_{stiffeners} = \boldsymbol{K}_{stiffeners} \Delta \boldsymbol{\varepsilon}_{panel} \\ \Delta \boldsymbol{N}_{frames} = \boldsymbol{K}_{frames} \Delta \boldsymbol{\varepsilon}_{panel} \end{cases} \quad (137)$$

Finally, the post-buckling behaviour of the plate for the new load step can be solved, and its post-buckling stiffness calculated to solve the next step. By using a sufficient number of steps, the solution obtained is able to reproduce the real behaviour of the stiffened plate.

5.4.2. Plate stiffness

The main difficulty to solve the load redistribution is obtaining an accurate solution for the plate stiffness, especially during post-buckling. Different methods are used depending on the load level in an attempt to overcome their limitations.

5.4.2.1. Pre-buckling stiffness

Before buckling, the stiffness of the plate can be considered to be constant as long as the effect of the imperfection is neglected, which is a reasonable assumption for the cases tested. The stiffness is given by the *A* term from the ABD matrix. This 3 by 3 matrix allows to account for the coupling of all the forces and strains, hence permitting a good resolution of the Poisson effects introduced in the panel.

5.4.2.2. Post-buckling stiffness

Once the panel is on the post-buckling range, the stiffness of the plate drops significantly, driven by the out-of-plane deformation. Typical methods to find the new stiffness are based on the in-plane displacement of the plate. However, this method does not allow a proper resolution of the 3 by 3 stiffness matrix, as the three different force components can be related to the three displacement components (including twisting) to create a system of three equations and therefore being able to solve a maximum of three independent terms from the stiffness matrix.

This limitation has been dealt by diagonalizing the stiffness matrix, so only three stiffness terms are required. This of course, limits the possibility of capturing the coupling between directions. This effect is especially important before buckling because Poisson effects can modify importantly the buckling load of a plate. However, once the plate has buckled, it is not critical to account which load term is responsible for each strain as long as the load redistribution towards the beams is properly captured.

To solve the post-buckled stiffness matrix, the strain increments in the plate are calculated from the increment in in-plane displacements and rotation per load step.

$$\begin{cases} \Delta \varepsilon_x = \dfrac{\Delta u}{a} \\ \Delta \varepsilon_y = \dfrac{\Delta u}{b} \\ \Delta \varepsilon_{xy} = \Delta \gamma \end{cases} \quad (138)$$

Then, the stiffness components are solved from the in-plane load increments in the plate related to the strains:

$$\boldsymbol{K}_{plates} = \begin{pmatrix} \frac{\Delta N_x}{\Delta \varepsilon_x} & 0 & 0 \\ 0 & \frac{\Delta N_y}{\Delta \varepsilon_y} & 0 \\ 0 & 0 & \frac{\Delta N_{xy}}{\Delta \gamma} \end{pmatrix} \tag{139}$$

What might cause problems using this approach, is that when some of the loads in the plate are missing, the strains in that direction are no longer accounted for. For example, a plate under shear would suffer in-plane displacement u and v. However, using a diagonalized stiffness matrix, the load redistribution in the plate will show 0 axial strains. This problem has been approximately solved by moving those neglected stiffness terms from the diagonal and accounting them as coupling stiffness terms, ensuring they are taken into account. The following equation shows the example for the post-buckling stiffness to be used in pure shear:

$$\boldsymbol{K}_{plates} = \begin{pmatrix} 0 & 0 & \frac{\Delta N_{xy}}{\Delta \varepsilon_x} \\ 0 & 0 & \frac{\Delta N_{xy}}{\Delta \varepsilon_y} \\ \frac{\Delta N_{xy}}{\Delta \varepsilon_x} & \frac{\Delta N_{xy}}{\Delta \varepsilon_y} & \frac{\Delta N_{xy}}{\Delta \gamma} \end{pmatrix} \tag{140}$$

5.5. Stiffened panel solution

The main parts of the solution of the stiffened panel have been discussed. This section exposes the global solution process, the different assumptions made and presents an overview of the limitations derived by the formulation.

5.5.1. The included configurations

The configurations included in the solution have been limited. It must be taken into account that the program developed is still a preliminary version of the tool that Fokker Aerostructures has in mind for stiffened panels. The main guidelines are:

- The load redistribution accounts for stiffened panels where the stiffeners and their spacing are constant. The same is stated for the frames.
- The load is applied as a contant displacement in both the skin and stiffening members. That means that load is always applied in the neutral axis of the panel regardless of wheter it is working in post-buckling range (in such case the neutral axis change its position).
- It has been seen that the boundary conditions of each plate depend on its position and there can be up to 4 different boundary sets (due to the effective *GJ* as explained in section 5.3.2). This differences are taken into account to estimate the

buckling load of the panel, however the panel is solved using the post-buckling response of the most critical plate (due to the effective *GJ* this is the one not sharing any outer border, if possible). This reduces by 4 the required time to solve post-buckling while being a good approximation in most of the cases and conservative for the rest.

- The post-buckling solution of the plates is based on constant displacement. It is assumed that stiffeners and frames are stiff enough so they keep roughly straight in post-buckling (they also are not allowed to undergo any instability).
- While the axial loading is distributed among plates and beams (according to their stiffness) the shear load is assumed to be resisted only by the plates. This is a typical conservative approach that simplifies the resolution of such cases. However, the redistribution of load to the beams of post-buckled plates under shear is included using the stiffness presented in eq. 140.

5.5.2. Solution procedure

The solution of stiffened panels is first presented with the help of a flowchart. Afterwards, the main steps are further explained.

5.5.2.1. Flowchart:

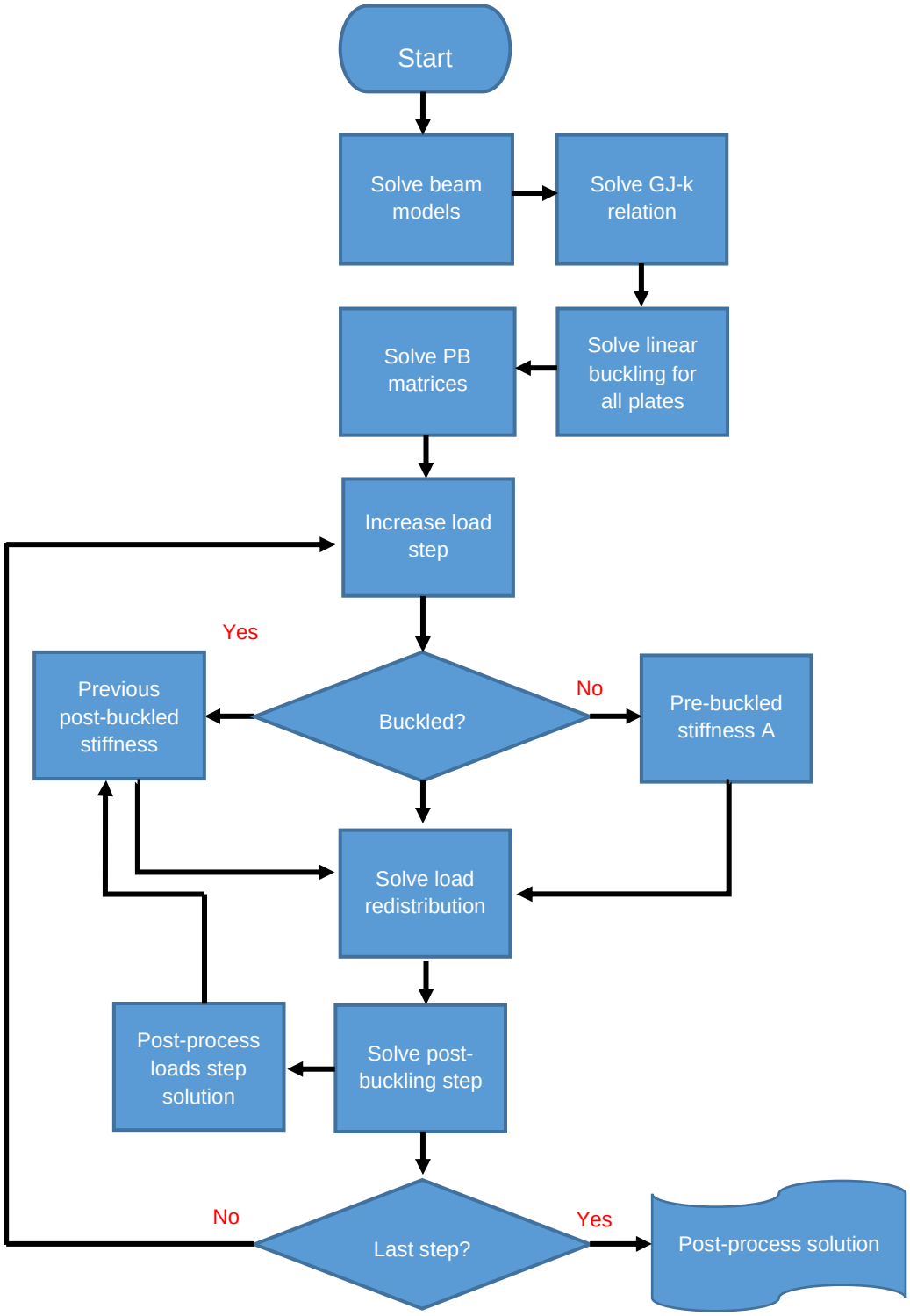

Figure 60: Flowchart stiffened panel solution

5.5.2.2. Algorithm explanation

The details of the stiffened panel are introduced by the means of a graphical user interface GUI (See figure 59). The data is divided into geometry, material properties, load case, analysis and solver. The semi-analytical solution is solved then following the steps outlined in the flowchart.

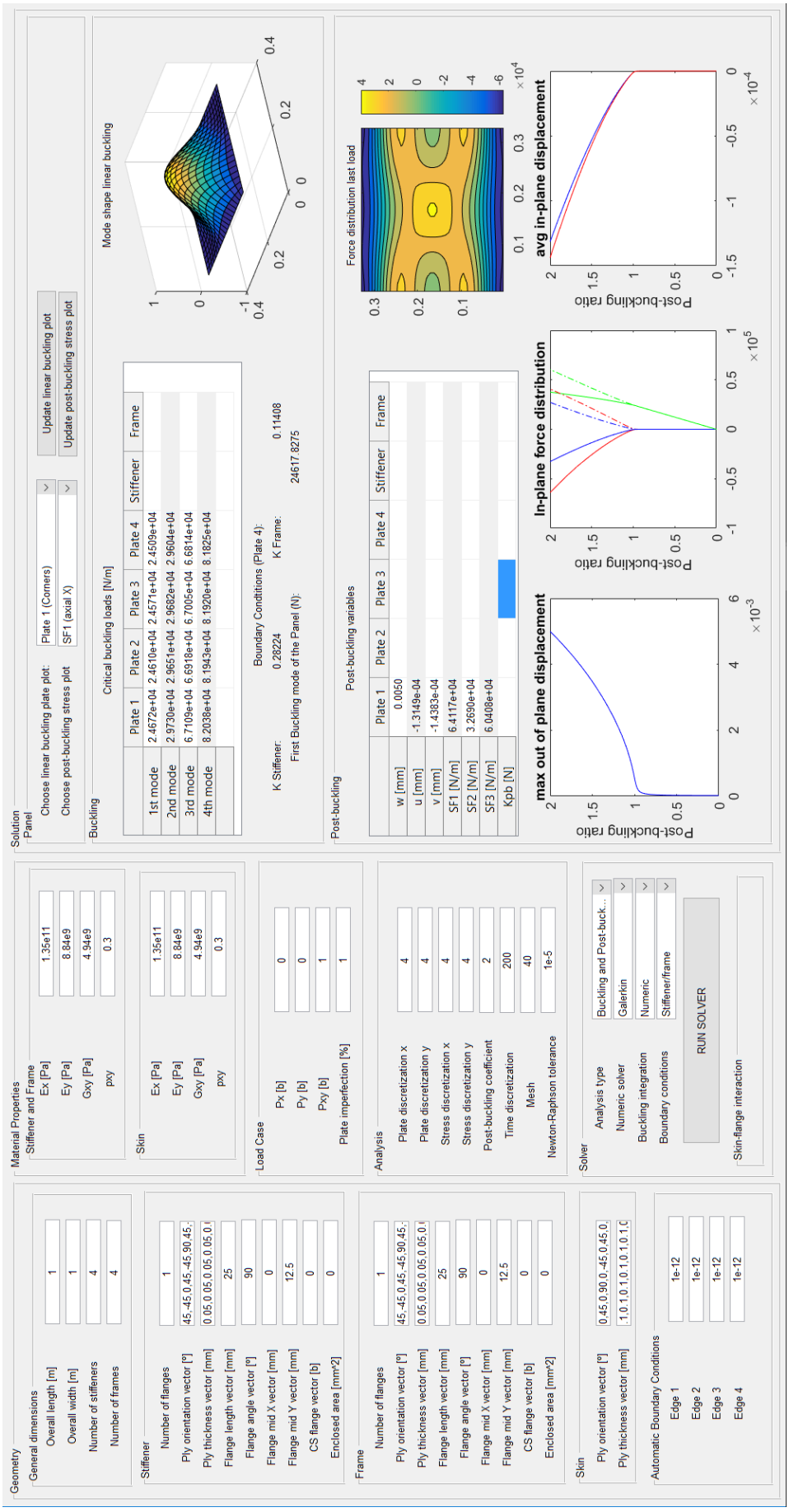

Figure 61: GUI stiffened panel

First of all, the 1D beam theory is used to model the axial and torsional stiffness of stiffeners and frames. From the last, the relation *GJ-k* is solved using the iterative algorithm introduced in section 5.3. Once the boundary conditions have been properly solved, the buckling load of the skin is solved taking into account the load redistribution during pre-buckling. However, remembering the concept of the effective GJ, there are up to 4 plate configurations (with different buckling loads) so two strategies are possible:

- Using the most critical value as initial buckling of the panel.
- Average the initial buckling load proportionally to the different plate solutions

The difference between buckling loads in the same panel are typically very small when the boundary condition is closer to simply supported or clamped conditions. However, in the case of intermediate values, the differences can be significant. The first FE verifications have shown better agreement using the second solution, however the first approach should not be discarded completely as it can be useful for further approaches and has the advantage of being more conservative.

The post-buckling solution is obtained for the most critical plate (inner one) loading step by step with the constant displacement algorithm. However, between load steps, it is necessary to recalculate the load that goes into the skin using strain compatibility as explained in section 5.4.1. Finally the main results for the complete solution are automatically plotted in the GUI for an easy assessment.

5.6. FE Model

The FE model follows the same guidelines as in post-buckling of plates. The main differences are obviously the inclusion of stiffeners and frames, modelled with shell elements, and the fact that the FE model is not automatically generated with a Python script. This makes more difficult to perform more systematic verifications as in chapters 3 and 4.

The load is applied keeping the edges straight, including stiffeners and frames. This way, the load is automatically redistributed as if applied in the neutral axis, and there is no additional bending in the panel. The initial imperfection for post-buckling is again obtained from the previously calculated local buckling, through the use of the keyword editor.

The post-processing of the results has been done manually with the post-processing module provided in Abaqus software.

5.7. Solution and verification

The verification has been done comparing the semi-analytical and FE solutions for several relevant cases. The development of the stiffened panel solution is still somehow preliminary, with several typical features not yet included in the solution algorithm. Therefore, the verification will be limited to cases satisfying the following conditions:

- **Edge stiffeners**: The current solutions verifications are limited to edge stiffeners (rectangular section). This stiffener can be placed either over the skin (named unsymmetric) or crossing the skin with half flange at each side (named symmetric). More complex stiffener are contemplated (including closed section) but is still necessary to develop strategies to account for the interaction of the stiffener

flanges attached to the skin and redefinining the effective length of the plate (with hat stiffeners the distance between the centerline of the stiffeners is obviously not the best approach, further studies are required to decide the best option).

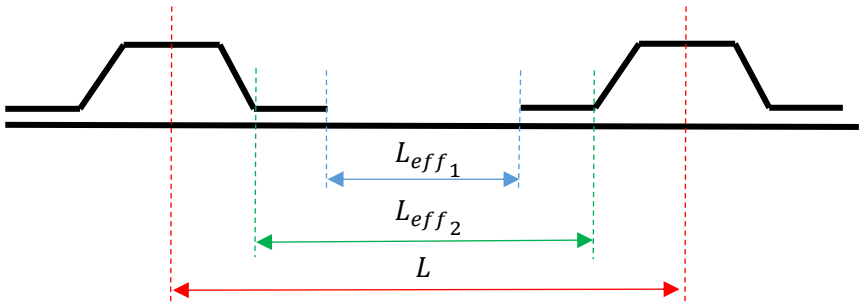

Figure 62: Possible plate lengths for hat stiffeners

Moreover, it has been found that T stiffeners, despite not having a relevant interaction with the skin, they do present interaction with the frames, resulting in a stiffer solution than expected. Such, cases might be solved with the current solution due to the conservativeness of the case, but it is recommended to further develop the formulation to account for such interactions, probably implementing them in the *GJ-k* relation.

- **Compression and shear**: It is always a good practice to start with the simpler cases and validate them before jumping to more complex ones. Therefore, verifications start with uniaxial and biaxial compression. Finally, shear is studied for buckling, but the verification is not extended to post-buckling.
- **Local buckling**: Some of the proposed configurations might present global buckling, where skin and stiffeners buckle together before local. However, such possibility was not a phenomenon to be developed in this Thesis, therefore global buckling will be ignored and taken the most critical local buckling solution instead.
- **Mode jumping**: It has been found that some panel configurations present mode jumping or different buckling modes for different plates. Such cases, will have to be discarded as the current solution was not developed to cope properly with more jumping. This result further encourages the further development of the formulation to become fully compatible with mode jumping.

To verify both the load redistribution and the capability of *GJ-k* algorithm, the verification covers a unique panel configuration where the stiffener and frame flange thickness are changed in order to model different boundary conditions, ranging from almost simply supported to clamped, and also different skin to stiffeners/frames load ratios.

Finally, the verification is divided into two different parts. The first one tests the agreement between both models regarding the initial local buckling load and mode. The second part, involves the post-buckling solution variables: out-of-plane displacement, in-plane displacement and in-plane forces.

5.7.1. Buckling verification

The results of the verification are summarized in tables. The tables contain information on the case number, the buckling load given by the semi-analytical model, FE model using symmetric stiffeners/frames and FE model with unsymmetric stiffeners/frames (in the SA model both configuration give identical results). Besides the buckling loads, the error between the semi analytical and the two FEM solution is given as a percentage. The mode column verifies if the predicted mode shapes from the SA and FE solutions are the same. The last column gives the values for the dimensionless torsional spring stiffness *k* for the stiffener and frame of the center plate (taking into account the effective *GJ*).

The semi-analytical solution does not distinguish between symmetrically or unsymmetrically stiffened plates because the load is always applied keeping the displacement of skin and stiffeners/frames constant, and also because the *GJ* in 1D beam theory does not depend on any offset. However, it has been observed that the FE solution for edge stiffeners does depend on the symmetry. Therefore, both solutions are given to compare the accuracy between the semi-analytical solution and both cases.

The different cases are obtained by modifying the thickness of the stiffener and frame flanges, while keeping the height constant to 25 mm. The following table gathers the different cases tested:

Table 4: Case number description

Case number	Skin thickness [mm]	Stiffener thickness [mm]	Frame thickness [mm]
1	2	1	1
2	2	1	2
3	2	1	4
4	2	1	8
5	2	1	16
6	2	2	16
7	2	4	16
8	2	8	16
9	2	16	16
10	2	32	32

The panel configurations studied have 4 stiffeners and 4 frames, allowing then for all the possible configuration of boundary conditions (accounting for the effective *GJ*) while limiting the complexity of the case. The selected edge stiffeners have always the same height, 25 mm.

5.7.1.1. Uniaxial compression

The uniaxial compression configuration has been analyzed for a rectangular panel (1.5 x 1 m) with QI layup for the skin, stiffeners and frames (see table 1 for the layup details). The following figure shows the buckled stiffened panel in the FE module.

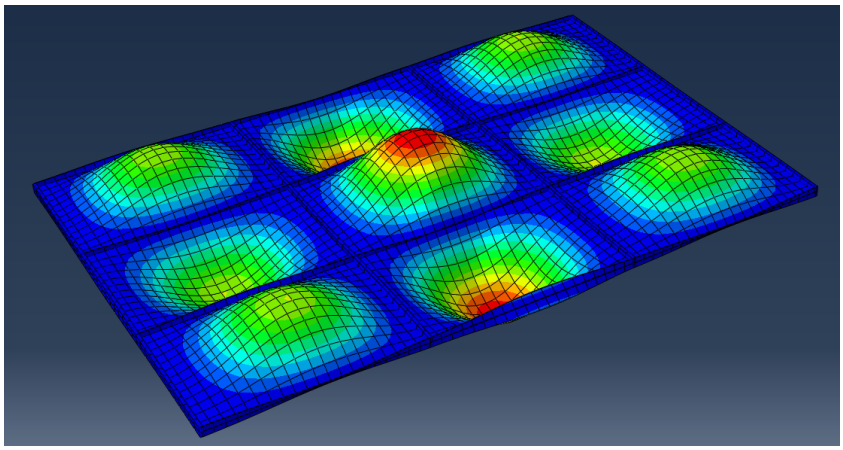

Figure 63: Stiffened panel under uniaxial compression. Buckled solution symmetric FE model.

The results obtained are:

Table 5: Results buckling stiffened panel under uniaxial compression

Case	Buckling SA [N]	Buck. FE sym. [N]	Buck. FE unsym. [N]	Error sym.	Error unsym.	Mode	k^*
1	14286.1	14583	14564	-2.0%	-1.9%	yes	0.034 / 0.065
2	14403	14781	14751	-2.6%	-2.4%	yes	0.034 / 0.523
3	15689	15972	15672	-1.8%	0.1%	yes	0.035 / 4.211
4	17016.7	17066	16547	-0.3%	2.8%	yes	0.04 / 34.15
5	16630.7	16730	16390	-0.6%	1.5%	yes	0.042 / 274.6
6	17887.2	17988	17747	-0.6%	0.8%	yes	0.341 / 274.8
7	22820.2	23108	22164	-1.2%	3.0%	yes	2.81 / 278.8
8	37687.9	34614 / 37658	31805 / 36291	8.9 / 0.1%	18.5 / 3.8%	no	81.3 / 328.9
9	49429.8	49138	46770 / 48104	0.6%	5.7 / 2.8%	yes / no	653 / 341.1
10	69720.9	70277	68665 / 69788	-0.8%	1.5 / -0.1%	yes / no	5261 / 2745

The proposed semi-analytical solution shows excellent agreement in most of the cases, with some exceptions when the mode shape is not properly predicted. In such cases, it is found that the FE solution with the same shape as predicted by the SA model does present good to excellent agreement (see the second solution separated by a slash). The discrepancies suggest the *GJ-k* relation is properly predicted, but near the mode shape change there might be some effect (interaction between plates) that affects the result. It might be necessary to further study such phenomenon.

It is also interesting the differences between symmetric and un-symmetric (conventional blade stiffeners) FE models, which are significant in some cases. A possible cause of the differences might be the limitations of the 1D beam theory for thin edge stiffeners (proposed model does not account for warping). More conventional stiffening members should not suffer as much for this problem, however, skin-stiffener interactions are still to be developed (current results would be conservative).

Finally, notice that the last column verifies that the different stiffeners and frames allow for different elastic restrains ranging from nearly simply-supported to nearly clamped solutions. The dimensionless k value depends on multiple factors (like the buckling shape), which explains that the same stiffener geometry can have different values in different cases.

5.7.1.2. Bi-axial compression

The bi-axially compressed configuration ($P_x = P_y$), has been performed for a square stiffened panel (1 x 1 m) with predominant 45s layup for the skin, stiffener and frames (see table 1 for the layup details). The results obtained are the following.

Table 6: Results buckling stiffened panel under bi-axial compression

Case	Buckling SA [N]	Buck. FE sym. [N]	Buck. FE unsym. [N]	Error sym.	Error unsym.	Mode	k^*
1	8021.3	8101.2	8130.2	-1.0%	-1.3%	yes	0.121 / 0.09
2	8522	8713.7	8676.8	-2.2%	-1.8%	yes	0.121 / 0.732
3	10845.7	10947	10396	-0.9%	4.3%	yes	0.125 / 5.869
4	14209.5	13843	12743	2.6%	11.5%	yes	0.142 / 47.17
5	15621.2	15450	14613	1.1%	6.9%	yes	0.15 / 377.9
6	16388	16301	15414	0.5%	6.3%	yes	1.2 / 379.2
7	18931.4	18612	17548	1.7%	7.9%	yes	9.67 / 403.1
8	21879.4	21305	20307	2.7%	7.7%	yes	78.45 / 459
9	24129.4	23717	22998	1.7%	4.9%	yes	629.4 / 477.4
10	30727.7	30817	30555	-0.3%	0.6%	yes	5073 / 3842

The results show important differences between the symmetrical and unsymmetrical FE models. The correlation of the semi-analytical results with the first is very good, while the correlation with the second shows some poor (unconservative) results for the central cases (nearly simply supported and clamped conditions work well).

In this configuration, with square plates and bi-axial loading, there has not been any problem with the mode shape as all the models predicted 1 half-wave in all the cases. This has resulted in more reliable results in comparison with the first configuration.

Once again, it can be concluded that the *GJ-k* relation seems to work with symmetric stiffened models, but some unaccounted effects will need to be studied in the case of un-symmetric stiffeners.

5.7.1.3. Shear

The last studied configuration is rectangular (3 x 1 m) stiffened panel with different layups (the skin with predominant 0s, and the stiffeners and frames with predominant 45s). The results obtained are the following.

Table 7: Results buckling stiffened panel under shear

Case	Buckling SA [N]	Buck. FE sym. [N]	Buck. FE unsym. [N]	Error sym.	Error unsym.	Mode	k^*
1	754.4	755.65	777.3	-0.2%	-2.9%	yes/par[14]	7.265 / 21.6
2	759.52	766	783.6	-0.8%	-3.1%	yes/par	7.421 / 180.9
3	761.1	776.1	785.6	-1.9%	-3.1%	par	7.498 / 1461
4	761.36	781.4	786.6	-2.6%	-3.2%	par	7.51 / 1.2e4
5	761.39	782.9	787.2	-2.7%	-3.3%	par	7.511 / 9.4e4
6	902.23	941	937.3	-4.1%	-3.7%	par	73.18 / 1e5
7	933.35	979.3	977.4	-4.7%	-4.5%	par	612.5 / 1e6
8	936.8	986.2	985.1	-5.0%	-4.9%	yes	5819 / 1.1e6
9	937.2	990.6	989.6	-5.4%	-5.3%	yes	4.7e5 / 1.1e6
10	937.2	994.95	993.6	-5.8%	-5.7%	yes	3.7e6 / 8.6e6

This case presents the highest complexity due to the highest aspect ratio, the higher complexity of shear loading and the laminate mismatch between stiffeners/frames and

[14] Par means that the agreement is partial because the different plates show different buckling shapes.

skin. Shear has been seen to be more sensitive to global buckling, so in order to compare local buckling results, the skin thickness has been reduced to 0.5mm in all the cases. The result is higher dimensionless spring stiffnesses (see last column of table 6).

The results show that there is a growing error from 0 to 6% between analytical predictions and FE solutions. This result was expected as the SA model does not account for the extra shear stiffness that the stiffener/frame grid contributes to the panel, which is obviously bigger for the more massive stiffeners/frames. Despite the differences, the results are still interesting because correlation is very good for intermediate stiffeners/frames, the maximum errors are not excessive and in all the cases the error are conservative.

The differences between symmetric and un-symmetric stiffeners are not as important as in axial loading configurations. Moreover, the SA model is able to properly predict the mode shape in most of the cases. The first cases show two half-waves and the last three, showing again the aforementioned tendency of nearly clamped plates to buckle in more half-waves. However, the transition in FE is not direct and some cases show different buckling shapes combining 2 and 3 half-waves in the different plates of the stiffened panel. Those cases have been marked with ‘par’ to indicate that the agreement is partial.

The use of stiffeners/frames with higher transversal inertia should result in somehow poorer results due to the bigger influence of the stiffener/frame grid in the global stiffness. However, results should still be conservative. If a higher accuracy is required, additional consideration would be required to account for the extra stiffness. On the other hand, the use of stiffeners/frames with higher transversal inertia might also result in better predictions of the mode shape, since there would be less interaction between the different plates and the assumptions of straight edges would be more accurately satisfied.

5.7.2. Post-buckling verification

The post-buckling verification involves comparing more variables, as it has been seen in chapter 4. Therefore, due to the great amount of information to analyse, only some of the cases used for buckling are extended to the post-buckling verification. Those cases are randomly chosen to try to cover as many different conditions as possible.

The first step to properly solve post-buckling is having a good buckling estimation. Otherwise, all post-buckling curves would be shifted. Therefore, the cases chosen are verified against the symmetrically stiffened FE models (the ones showing better agreement with SA in buckling).

5.7.2.1. Uniaxial compression

Two different cases are verified for post-buckling behaviour under uniaxial compression. The cases conditions are taken from the buckling verification (see table 4 for the case description and table 5 for the buckling results).

5.7.2.1.1. Case 4

Case 4 consists in very weak stiffeners (1mm) and intermediate size frames (8mm). Such weak stiffeners encourage that the critical buckling solution of the panel is not the local plate buckling but a general buckling mode with 3 half-waves across the panel. Anyway, the current analysis focuses on the local buckling only.

The FE solution shows divergence at a post-buckling ratio of 1.71, therefore, this is the studied range of solutions. Notice that the post-buckling ratio refers to the panel buckling load and due to the loss of stiffness during post-buckling, this ratio is different in the individual plates.

The following figure shows the results predicted by the semi-analytical model for each individual plate. The out-of-plane displacement is given in m, the in-plane force in N/m and the in-plane displacement in m. The colour convention is the same as shown in section 4.4.1.1 for post-buckling.

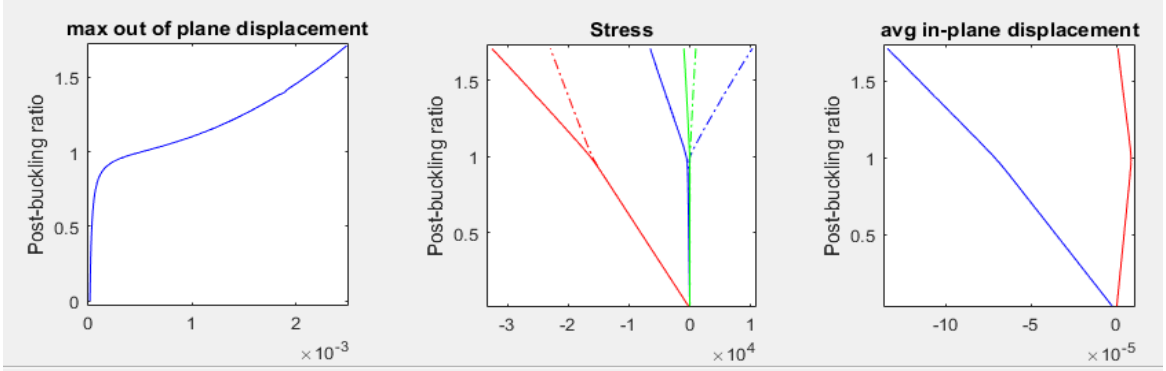

Figure 64: Summary semi-analytical post-buckling solution 1

The FE solution predicts also a regular post-buckled solution with similar buckle amplitudes for each independent plate. The following table shows the maximum values obtained at the highest post-buckling ratio (in-plane forces are characterized by the maximum and the minimum, separated by a slash). See that units have been changed to N/mm for convenience.

Table 8: Summary stiffened panel verification 1

	Out-of-plane displacement [mm]	In-plane force X [N/mm]	In-plane force Y [N/mm]	In-plane force XY [N/mm]	In-plane displacement X [mm]
SA model	2.48	-22.9/-32.56	10.27/-6.51	0.98 / -0.98	-0.134
FE model	2.37	-22.7/-31.72	9.04/-6.15	1.32 / -1.06	-0.148
Error [%]	4.6%	0.6/2.6%	13.6/5.9%	-25.8/-7.5 %	-9.5%

The results show good agreement between solutions despite the high PB ratio (typical aerospace application use lower values). It is especially interesting the accuracy to predict the in-plane forces in the x direction, since these are the ones taking higher values under uniaxial compression. The in-plane displacement in y has been neglected as it takes very small values under uniaxial compression.

It could have been expected to obtain somehow better prediction of the out-of-plane displacement taking into account the good correlation of the buckling load (-0.3%) and the stresses. Despite the 4.6% error in the maximum value, the trend is properly captured. The following figure shows the FE solution curve.

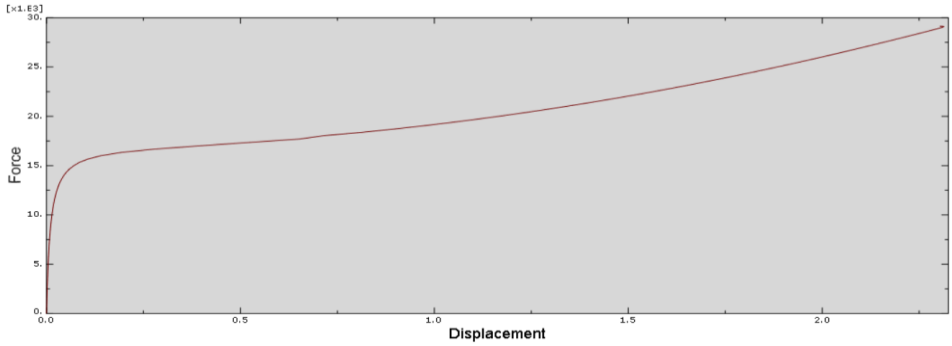

Figure 65: FE out-of-plane displacement curve

5.7.2.1.2. Case 10

Case 10 is a heavily reinforced panel, so the boundary conditions of individual plates are close to clamped and most of the load goes through the stiffeners. The boundary conditions force the plates to buckle with two half-waves.

The FE solution has not had any convergence problem until the target PB ratio 2, so all this range is studied. The following figure presents the SA solution for each individual plate:

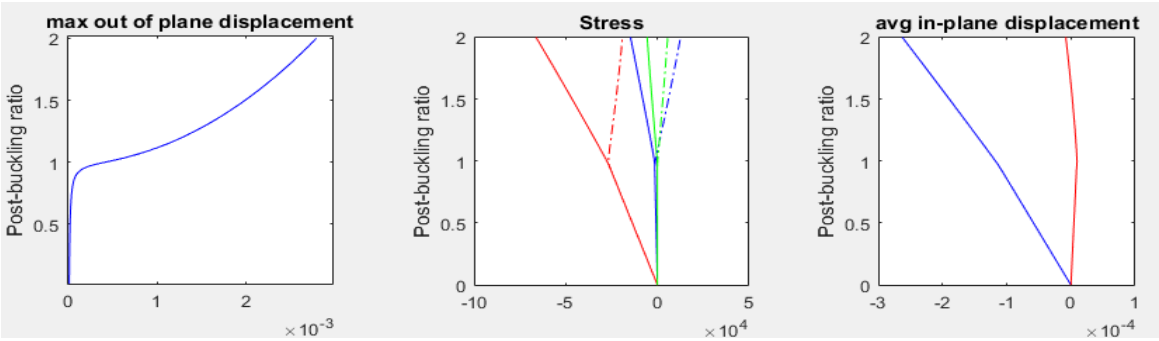

Figure 66: Summary SA post-buckling solution 2

Again, the comparison with FE is presented in a table:

Table 9: Summary stiffened panel verification 2

	Out-of-plane displacement [mm]	In-plane force X [N/mm]	In-plane force Y [N/mm]	In-plane force XY [N/mm]	In-plane displacement X [mm]
SA model	2.79	-19.04/-66.23	12.65/-14.71	5.61/-5.61	-0.263
FE model	2.84	-21.29/-62.11	11.28/-11.02	5.72/-4.75	-0.261
Error [%]	-1.8%	-10.6/6.6%	12.1/33.5%	-1.9/18.1%	0.8%

The results show excellent agreement regarding the displacements but being less accurate with the force predictions. Such results are coherent with the forces obtained from the second derivatives of the Airy Stress function.

There has been an attempt to increase the number of Airy Stress terms (from 16 to 36) but no significant improvement was achieved predicting the in-plane forces.

Despite such inaccuracies on the maximum values, the SA solution is able to capture the force redistributions. The following figures present the solutions obtained by SA and FE models at PB ratio two.

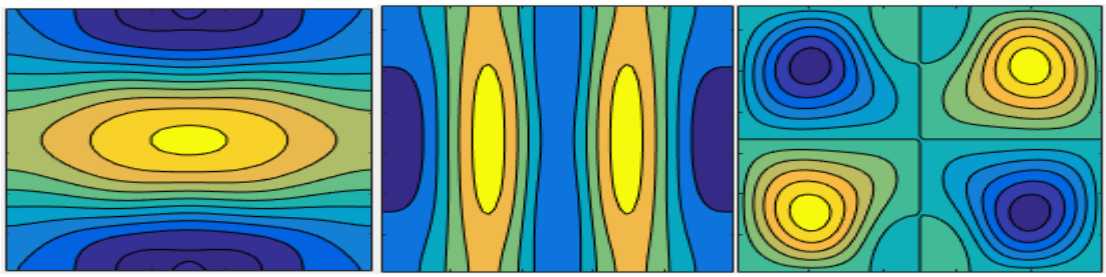

Figure 67: Force redistribution SA solution

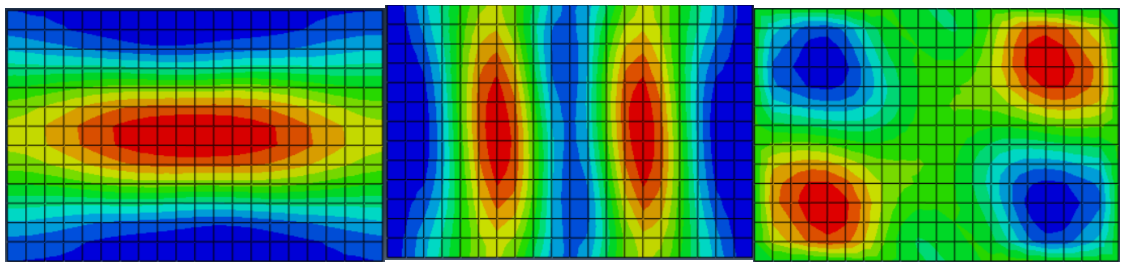

Figure 68: Force redistribution FE solution

The redistribution patterns predicted by both methods are almost identical for all three different forces. This result gives confidence in the ability of the SA solution to predict the force redistributions in stiffened panels.

5.7.2.2. Bi-axial compression

Two different cases are tested under bi-axial compression. Again the case description can be consulted from table 4 while the buckling loads were presented in table 6.

5.7.2.2.1. Case 2

Case 2 consists in a stiffened panel with slim stiffeners and frames. Therefore, the boundary conditions are close to simply supported and most of the load is carried by the skin.

The verification has been performed until a PB ratio 2. The prediction of the local buckling for this case was not as good as previous cases (-2.2%). The following figure presents the SA solution.

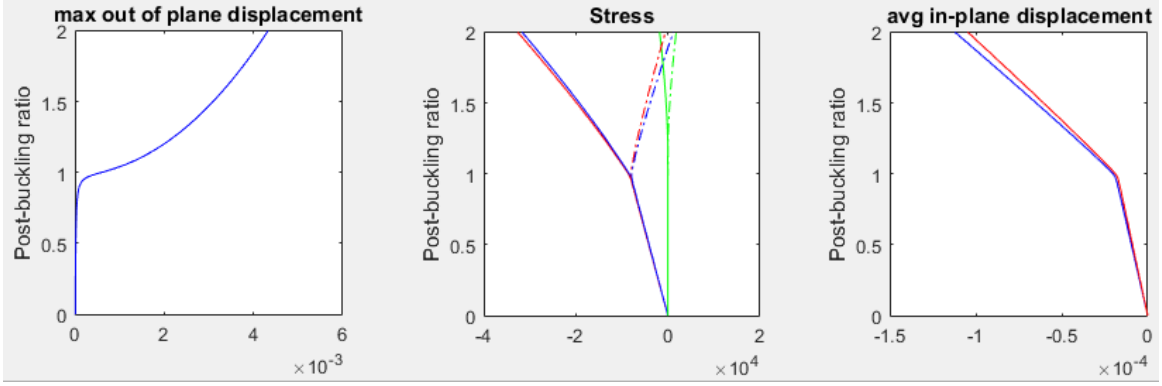

Figure 69: Summary SA post-buckling solution 3

The stiffened panel is loaded in both axial directions, and stiffeners and frames are similar, therefore the solutions in x and y directions are similar. The comparison with FE is presented in the following table:

Table 10: Summary stiffened panel verification 3

	Out-of-plane displacement [mm]	In-plane force X [N/mm]	In-plane force Y [N/mm]	In-plane force XY [N/mm]	In-plane displacement X and Y [mm]
SA model	4.33	-0.538/-32.6	-1.14/-31.7	1.8/-1.8	-0.121/-0.105
FE model	4.49	-1.44/-35.75	0.278/-36	1.38/-2.52	-0.109/-0.101
Error [%]	-3.6%	-62.6/-8.8%	-510.1/-11.9%	30.4/-28.6%	11/3.6%

The results show good agreement with the out-of-plane displacement, but in-plane displacements and forces present regular to very bad results. However, there is an explanation for the biggest errors. The maximum values for both forces in X and Y are close to zero, so when calculating the relative errors between both results, small discrepancies can give important errors. If the errors is calculated in relation to the maximum absolute stress then more coherent results are obtained (-2.52/-3.94% instead of -62.6/-510.1%).

Moreover, it is interesting that the shear force distribution is overestimated by a 30% for the maximum and underestimated by another 30% for the minimum. The reason for this offset in the solution is the aforementioned symmetry of shear redistribution, which results in a symmetric distribution of the shear around 0. However, in cases where D_{16} and D_{26} are important (note that the laminate is predominant 45s), this distribution is not symmetric.

The FE out-of-plane solution of the inner plate shows the effect of the 45s to make the buckled shape more diagonal.

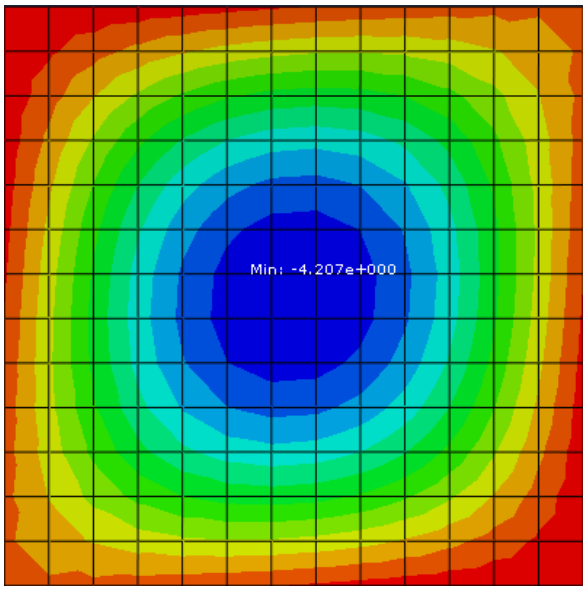

Figure 70: FE out-of-plane solution verification 3

Besides, the figure shows the maximum out-of-plane displacement for the central plate. Note that this value is closer (+2.8% error) to the SA solution and different from the one presented in the FE in the summary table. The reason is that SA solution assumes that the global behaviour of the panel can be solved from the solution of one plate, using the most critical. However, plates are not identical, and some variations are normal (note that the boundary conditions are not identical for every plate). The results given in the summary table are the maximums found in the whole panel, therefore, providing a conservative approach.

5.7.2.2.2. Case 7

Case 7 consists in high stiffness frames while stiffeners take medium values. The case then resembles plates clamped on the longitudinal direction while elastically restrained in the transversal one.

The verification has been performed again until a PB ratio 2. The prediction of the local buckling for this case was better than in the previous one (1.7%). The following figure presents the SA solution.

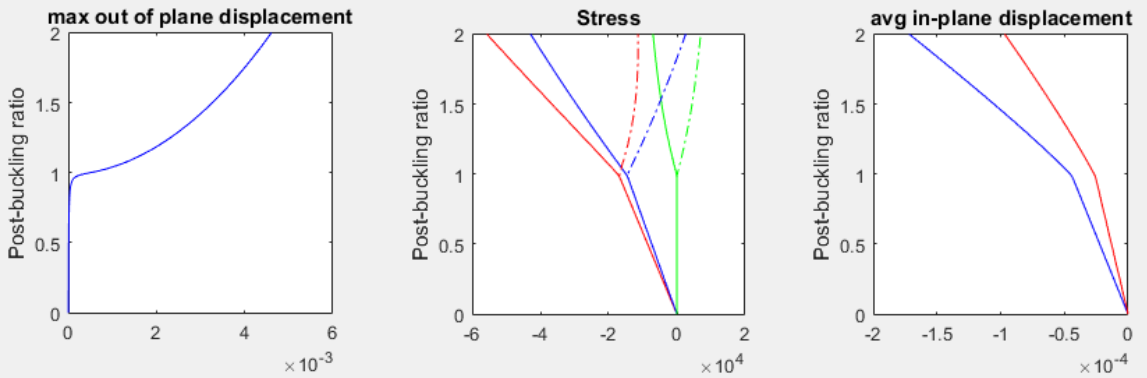

Figure 71: Summary SA post-buckling solution 4

The new solution presents more differences between x and y directions because of the differences between stiffeners and frames. The comparison with FE is presented in the following table:

Table 11: Summary stiffened panel verification 4

	Out-of-plane displacement [mm]	In-plane force X [N/mm]	In-plane force Y [N/mm]	In-plane force XY [N/mm]	In-plane displacement X and Y[mm]
SA model	4.61	-11.39/-55.69	2.59/-42.87	6.99/-6.99	-0.172/-0.097
FE model	4.58	-10.83/-50.12	0.014/39.28	8.85/-8.71	-0.168/-0.093
Error [%]	0.7%	5.2/11.1%	1.8e4/9.1%	-21.0/-19.7%	2.4/4%

The results show excellent agreement regarding all displacements. Forces present worse results, in line with what has been seen and is expected for such cases (around 10%). The relative error for the maximum forces in y direction is very big again due to the proximity of the results to zero. This situation is similar to the previous case, and has already been mentioned how to cope with that. It is interesting to notice that the results for the force distributions are conservative, except for shear.

5.8. Conclusions stiffened panels

The solution presented for stiffened panels shows how the developed formulations for buckling and post-buckling can be used to create powerful tools to solve complex structures in real aerospace applications. The solution proposed is still somehow preliminary and should be considered as a proof of the new approaches used and the future possibilities of the analytical framework for composites design that Fokker Aerostructures is developing.

The implemented formulation can give good to excellent agreement predicting initial local buckling of stiffened panels. It has been seen that the solution is still limited to some simplistic structural approaches like using edge stiffeners or regularly stiffened panels. Besides, it has shown some issues with non-symmetric stiffened panels or predicting the buckling load when there is a change in the number of half-waves.

Regarding the solution for the post-buckling behaviour, it has been shown that the cases where the buckling load is properly predicted, it can handle post-buckling with good agreement with all displacement variables and good approximate results of the force distributions.

The verification approach is not as systematic as in buckling and post-buckling of plates due to the lower degree of maturity of the solution. The limitations of the PB solution have been outlined during the chapter, but they are summarized now in the following points:

- The interaction between skin and stiffeners/frames for typical sections, such as hat stiffeners, have not been developed yet. Therefore, effective plate lengths are not considered and overconservative solutions might be obtained when using the current formulation. Therefore, to have a more meaningful verification, this has been limited to edge stiffeners.
- The buckling load needs to be properly calculated in order to solve post-buckling, therefore the limitations found for the buckling verification can be automatically extended to post-buckling. The inaccuracies seen in shear buckling and the lack of extra time are the main reasons the verification has not been extended to post-buckling for that case.
- The semi-analyitcal approach to solve post-buckling of plates does not work well with mode jumping. After the experiences gained, this phenomenon seems to be more important than it was foreseen. Post-buckling solution of stiffened panels is obiously limited by the capabilities of the plate solution. For example, in the first post-buckled case it was not possible to get results over PB ratio 1.7 due to convergence problems in the FE solution.
- The buckling solution is able to account for having different buckling loads for the different plates. However, to simplify the procedure, the post-buckling solution is based on the most critical plate. This approach seems to have worked well for the current cases, but it should be taken into account in future developments.

Despite the limitations, the encouraging results obtained prove the validity of the developed approaches for both stiffeners elastic restrains and load redistribution, and encourage the further development of the semi-analytical solution presented in this Thesis. Current cases studied show very accurate buckling predictions, especially for symmetric cases with errors around 1-2% for axial loading. Moreover, out-of-plane displacement in post-buckling is predicted with an error below 5% for all the cases and the in-plane forces show good agreement in general. Therefore, the results are quite satisfactory for the first solutions of the new developed formulation. Further improvements should increase their accuracy and applicability to more complex cases.

Further conclusions and recommendations can be found in the last chapter.

6. Final conclusions and recommendations

This chapter reviews the work done during this thesis and the general conclusions reached. Furthermore, the final recommendations are presented, taking into account that this Thesis is part of a larger project.

6.1. Thesis review

The main objectives of this thesis included the development of a formulation able to solve buckling and post-buckling of plates in order to predict the behaviour of stiffened panels after local buckling. The main interest was that the formulation should be able to account for the elastic restrain provided by the stiffeners/frames in order to obtain good predictions of the stiffened panel behaviour. An additional interesting feature was the possibility to solve any mid-plane symmetric laminate as specially orthotropic models were not able to reproduce the behaviour of the typical laminates used by Fokker Aerostructures in common applications.

The main authors in the field were studied in order to gain insight of the current state of the art. Then, it was determined that the researched formulations for buckling were not sufficient to deal with all the configurations required and an alternative solution was proposed following the work developed by different authors. The special conditions made necessary to adopt a semi-analytical formulation to solve buckling when most of the authors opt for more straight forward closed form solutions.

A post-buckling formulation was developed based on the work of Qiao in [34] using the expressions for the out-of-plane displacements implemented during the buckling solution. Further modifications were required in order to model the behaviour of the plate with constant edge displacement, assumption that better approaches the behaviour of plates in stiffened panel configurations.

The agreement of the proposed formulations were validated through an extensive verification against FEM. The accuracy of the presented SA solution was determined for the different cases under interest and the encountered limitations were resolved when possible and detailed when not.

During the last part of the project, the developed solutions were incorporated into a more extensive formulation to cope with stiffened plates. The studied literature on the field did not give satisfying solutions on how the torsional stiffness provided by the stiffeners could be converted into equivalent boundary conditions. A new procedure was developed in order to solve the relation between *GJ* and the constant elastic restrain k_i. The formulation also features a method to solve the load redistribution based on strain compatibility for panels stiffened in both directions, a common situation which is not examined extensively in literature.

The developed solution for stiffened panel works well but it is not able to cope with some special conditions. However, encouraging results were obtained proving the capabilities of modelling the elastic restrain provided by stiffeners and obtaining accurate buckling and post-buckling results using an analytical approach.

6.2. Conclusions

The formulation developed for linear buckling has given the most accurate results when compared to FE. Solutions can be obtained for all the cases suggested as long as the number of terms is sufficient (and the computational capacity is available). Some problems regarding the numerical approach have been addressed, such as catastrophic cancellation when using analytical integration, or imposing the natural boundary conditions in the Galerkin method. The only limitation left was the high influence of transverse shear in moderately thin laminates. However, this limitation is intrinsic of the thin plate theory used and authors have already discussed why typical fibre reinforced materials are especially sensitive.

The post-buckling solution requires a more complex approach due to the non-linearity of the post-buckling phenomenon, the more complex out-of-plane shape and the fact that in-plane forces are not constant and the redistribution needs to be solved as well. Therefore, the accuracy and robustness of the results is below what was achieved in buckling. The main limitations found are:

- The Airy Stress function for applied displacement is originally developed for specially orthotropic plates under axial loads. It is possible to solve also shear and non specially orthotropic plates by using a series expansion of the original terms. However, it has been detected that some effects such as diagonal redistribution (due to diagonal buckling shape) cannot be taken into account by the current method no matter how many terms are used.
- The current formulation was not developed taking mode jumping into consideration, which complicates the verification of results when it does take place. Mode jumping is a complex and challenging phenomenon depending on many variables such as plate imperfection, boundary conditions, etc. Its proper prediction is out of the scope of this Thesis.

Despite the limitations, the verifications showed that the current solution is able to approximately solve post-buckling for many cases, providing excellent agreement with FE when the limiting conditions are not present.

The solution presented for stiffened panels in based on the developed formulations for plates, therefore the conclusions reached for the plates are also applicable. Despite the necessity to include additional assumptions, the formulation developed has been able to successfully cope with the main difficulties in a stiffened panel: the resolution of the elastic restrain imposed in the plate by the stiffeners/frames and the load redistribution between all the elements.

In conclusion, the various formulations developed have proven their capacity to solve buckling and post-buckling of plates and stiffened panels through semi-analytical procedures, delivering accurate solutions when compared to FEM and with a reduced

computational cost, though further optimization of the methods is still possible. The limitations of the current solutions have been detailed in order to understand the real possibilities.

6.3. Recommendations

A series of recommendations are made either to improve the current formulation or to further extend it. Moreover, some recommendations focus in the development of the complete project of creating an analytical framework for stiffened panels of which this Thesis is only a part.

6.3.1. Buckling

The conclusions already outlined that the objectives for buckling were satisfied. Some additional recommendations are issued for the sake of the performance optimization of the solution. The current formulation implementation has focused in its easy incorporation to a verification procedure, however it is expected that the formulation will be transferred to another program language to incorporate it to the final analytical framework tool.

For high performance algorithms, it has been seen that using analytical integration of the different matrix terms results in very good performance. Due to catastrophic cancellation of the hyperbolic terms, this has been seen to cause problems when using more than 5 terms per side. Possible solutions to improve the performance are:

- Restrict the analysis to 5 or less terms so analytical integration works fine with the current solution. This option is valid for plates with small aspect ratios.
- It might be possible to get rid of the catastrophic cancellation by using a different mode shape form. Trigonometric functions have been traditionally used especially because sines were able to exactly solve ideal cases, but several authors have successfully used orthogonalized polynomials, which are easier to either integrate analytically or numerically using exact gauss integration. This possibility could be studied to check if it can increase performance.
- The mode shape solution relies on the resolution of the eigenbeam value functions for the given boundary conditions. During this process, it is necessary to solve a non-linear equation in order to obtain the mode values for each term. Other authors like Bisagni and Qiao [31, 34] prefer to use linear interpolations of the simply supported and clamped solutions to simplify the solution (though limiting the formulation to symmetric two by two boundary conditions). This approach might be less sensitive to catastrophic cancellation.

During the Thesis it has also been discussed the possibility to develop a formulation for infinite plate. This would dramatically increase the performance for the more computationally demanding cases where plates have large aspect ratios.

Another additional possibility would be extending the formulation to shallow shells (including curvature in the plates).

6.3.2. Post-buckling

Post-buckling involved a more complex formulation which also allows for further improvements. Some of the recommendations remarked for buckling are also applicable

to post-buckling. Different mode shapes might be used to increase the performance or to capture more localized effects on the post-buckled solutions. The development of an infinite plate formulation for post-buckling is also really interesting as it would boost the performance for high aspect ratios. In the case of including shells, it would be necessary to adapt the formulation and check that the assumptions and approximations used are still valid for this more complex case.

During the conclusions, two main limitations have been outlined for post-buckling of plates, in order to cope with them, the following possibilities could be studied:

- The current Airy Stress function for constant displacement was developed for specially orthotropic plates under axial loading. The use of series, allows for reasonable approximations when those conditions are not meet, but it usually requires a certain number of terms and the results are not perfect. Further improvement might be obtained by developing a new Airy Stress function formulation able to cope with those cases. A preliminary new solution was given to prove the idea, and the results showed that it is able to better reproduce the in-plane force distributions though at a significant computational cost.
- Mode change has proven to be an important phenomenon in post-buckling of plates. The current method struggles to approximate the behaviour mainly due to the use of Newton-Raphson algorithm. Several works have shown that Arc-length methods are more suited to reproduce the behaviour during mode change due to their ability to work with near zero or negative stiffness. The incorporation of mode change capabilities would also require a study of how this phenomenon takes place, which are the most important variables and how the numerical analysis correlates with experimental tests.

6.3.3. Stiffened panel

The stiffened panel solution is still to be further developed to be able to cope with all the cases treated in buckling and post-buckling of plates. Moreover, more complex stiffened panel configurations are still to be included. Therefore, the recommendations presented for stiffened panels are of special importance.

The improvement of both buckling and post-buckling solutions for plates would obviously affect the solution for stiffened panels, so the previous recommendations are also applicable.

As seen during the verification, the stiffened panel solution has not been fully developed for all the cases, so there are several important recommendations that can be presented.

- The load redistribution between the different elements has been achieved by applying a strain compatibility between all of them. This method has proved to work well, but there have been difficulties to evaluate the post-buckling stiffness of the plates. The plate stiffness is ideally given as a 3 by 3 matrix that relates the different displacements with the different loads. During post-buckling, the stiffness is typically calculated from the in-plane displacement derived from the out-of-plane displacement and in-plane forces, however this relation does not allow to calculate a 3 by 3 matrix due to the lack of independent equations. The proposed

diagonalized method allows for a straightforward calculation, but the simplification might result in additional errors when working with more complex cases. Steen in [45] introduces a formulation able to solve the post-buckling stiffness matrix by using plate shortening instead of load control. A similar method could be developed if the previous finally does not meet the requirements.

- The current stiffened plate formulation has focused on the simplified case of blade stiffeners and does not account for the interference between stiffener and skin for the most typical composite sections such as hat stiffeners. It is recommended to include those by establishing effective plate widths taking into account the transverse size of the section. Different approaches exist on the literature so verification would be required to test them and adopt the most accurate or conservative.
- Once the stiffened plate formulation has reached the required maturity is would be useful to develop a more systematic approach to verify different cases and configurations, such as done for buckling and post-buckling of plates.
- The current buckling solution accounts for the different boundary conditions of the different plates and the resulting different buckling loads. However, the post-buckling formulation does not account for those differences and obtains the panel solution assuming the most critical plate behaviour. It might be interesting to adapt the formulation to account for independent plate solutions which should represent an improvement for situations when different buckling wave patterns are present or when mode change might appear at buckling onset in some plates.
- If the previous point is adopted, then the formulation could be extended to arbitrarily stiffened plates (different spacing and sections for stiffeners/frames) instead of the current approach limited to regularly stiffened panels(same spacing and sections for stiffeners/frames). However, it should be decided if it is an interesting feature for common applications.

6.3.4. Analytical framework for stiffened panels

As it has been explained, this Thesis is part of a bigger project supported by Fokker Aerostructures to develop an Analytical framework able to predict the behaviour of stiffened panels made of composite laminates. Such tool should be able to give fast approximations of the panel strength in order to improve the preliminary design and optimization of such structures.

The solutions obtained from this thesis can be used to calculate important failure modes in stiffened panels.

- **Post-buckling plate strength**: The current solution does not include plate strength analysis for post-buckling, however, the resolution of the in-plane forces and out-of-plane displacement give all the required variables to solve the mid-plane strain and curvatures of the laminate. Then, different failure analysis methods might be used to assess material failure.
- **Skin-stiffener separation**: The post-buckling solution is the first step in order to solve the skin-stiffener separation in stiffened panels, as it is necessary to know the out-of-plane displacement and force distributions in order to solve the different stresses involved in skin-stiffener separation.

Additionally, some of the remaining modules of the analytical framework can be directly derived from the formulations implemented during this Thesis.

- **Global buckling**: The solution given for local buckling of plates can be adapted to cope with global buckling by smearing the properties of stiffeners and frames in the skin.
- **Crippling**: It has been mentioned the possibility to implement an infinite plate formulation to optimize the solution for high aspect ratios. Infinite plate formulations are also used to solve local buckling of the beam flanges which is an important failure mode in stiffened panels. A crippling solution would also require to implement free edge boundary conditions and to adapt the elastic restrains for beam flanges.

Appendix A

Design code for post-buckling figures

As it has been mentioned, the different verification figures contain a 5 digits code in order to easily distinguish the different cases. All the introduced figures in this Thesis have been previously detailed in addition to the mentioned code.

- **Aspect ratio (i)**: The first digit makes reference to the aspect ratio of the plate. One means square plate while the rest of aspect ratios follow the rule $AR = 2i - 1$. The short side is always constant and has a value of 0.1 m.
- **Thickness ratio (j)**: The thickness is given as the thickness to width (short side) ratio following the expression $\frac{t}{b} = \frac{j}{100}$. This means that for $j = 1$ the thickness is 1 mm. Then thickness is not mentioned it is always assumed the thinnest configuration (to avoid thin plate theory limitations).
- **Boundary condition (k)**: The boundary conditions are independently defined at every edge by the torsional spring stiffness (in N). The following rule is followed:

Table 12: Boundary condition code values

k value	Spring stiffness per edge [N]
1	[0,0,0,0] -> Simply supported
2	[inf,inf,inf,inf] -> Clamped
3	[200,200,200,200] -> Elastically restrained

- **Load combination (i)**: The loads are defined as Nx, Ny and Nxy respectively (in normalized form). The following table contains the different cases:

Table 13: Load code values

i value	In-plane loads [N/m]
1	[1,0,0] -> Uniaxial compression
2	[0,0,1] -> Shear
3	[1,0,1] -> Combined loading

- **Laminate (m)**: The laminate layups have been detailed in table 1. $m = 1$ corresponds to the predominant 45s, $m = 2$ to the predominant 0s and $m = 3$ to the QI laminate.

Bibliography

[1] E. F. Bruhn, *Analysis and design of airplane structures rev. ed*. Cincinnati :: Tri-State Offset Company, 1949.

[2] C. Niu. (1999). *Airframe structural design practical design information and data on aircraft structures (2nd ed. ed.)*.

[3] A. E. H. Love, "The Small Free Vibrations and Deformation of a Thin Elastic Shell," *Proceedings of the Royal Society of London,* vol. 43, pp. 352-353, 1887.

[4] F. Y. M. Wan and H. J. Weinitschke, "On shells of revolution with the Love-Kirchhoff hypotheses," *Journal of Engineering Mathematics,* vol. 22, pp. 285-334, 1988.

[5] T. Von Kármán, *Festigkeitsprobleme im maschinenbau*. Leipzig: [publisher not identified], 1910.

[6] G. R. Kirchhoff, "Uber das Gleichgewicht und die Bewegung einer elastischen Scheibe," 1850.

[7] S. G. Lekhnitskii, *Anisotropic plates*, 2nd ed. / ed. New York :: Gordon and Breach, 1968.

[8] S. A. Ambartsumyan, *Theory of anisotropic shells*. Washington :: NASA, 1964.

[9] K. Marguerre, "Zur theorie der gekrümmten platte grosser formänderung," in *Proceedings of the 5th international congress for applied mechanics*, 1938, pp. 93-101.

[10] C.-Y. Chia, *Nonlinear analysis of plates*. New York ;: McGraw-Hill International Book Co., 1980.

[11] C. Kassapoglou. (2013). *Design and analysis of composite structures : with applications to aerospace structures (Second edition. ed.)*.

[12] R. M. Jones, *Mechanics Of Composite Materials*: Taylor & Francis, 1998.

[13] J. E. Ashton and J. M. j. a. Whitney, *Theory of laminated plates*. Stamford, Conn :: Technomic, 1970.

[14] S. P. Timoshenko and J. M. Gere, "Theory of Elastic Stability (2nd Edition)," ed: Dover Publications, 1989.

[15] J. M. Whitney, *Structural analysis of laminated anisotropic plates*. Lancaster :: Technomic, 1987.

[16] L. P. Kollar and I. A. Veres, "Buckling of Rectangular Orthotropic Plates Subjected to Biaxial Normal Forces," *Journal of Composite Materials,* vol. 35, pp. 625-635, April 1, 2001 2001.

[17] C. Bisagni and R. Vescovini, "Analytical formulation for local buckling and post-buckling analysis of stiffened laminated panels," *Thin-Walled Structures,* vol. 47, pp. 318-334, 3// 2009.

[18] R. Vescovini and C. Bisagni, "Single-mode solution for post-buckling analysis of composite panels with elastic restraints loaded in compression," *Composites Part B,* vol. 43, pp. 1258-1274, 2012.

[19] E. F. Bruhn and R. J. H. Bollard, *Analysis and design of flight vehicle structures*. Cincinnati :: Tri-State Offset Company, 1973.

[20] C. Niu. (2011). *Airframe stress analysis and sizing (3rd ed. ed.)*.

[21] J. K. Paik and A. K. Thayamballi, "Buckling strength of steel plating with elastically restrained edges," *Thin-Walled Structures,* vol. 37, pp. 27-55, 5// 2000.

[22] L. C. Bank and J. Yin, "Buckling of orthotropic plates with free and rotationally restrained unloaded edges," *Thin-Walled Structures,* vol. 24, pp. 83-96, // 1996.

[23] J. M. Ortega, "The Newton-Kantorovich Theorem," *The American Mathematical Monthly,* vol. 75, pp. 658-660, 1968.

[24] P. Qiao and L. Shan, "Explicit local buckling analysis and design of fiber–reinforced plastic composite structural shapes," *Composite Structures,* vol. 70, pp. 468-483, 10// 2005.

[25] Q. Chen and P. Qiao, "Shear buckling of rotationally-restrained composite laminated plates," *Thin-Walled Structures,* vol. 94, pp. 147-154, 9// 2015.

[26] C. Mittelstedt, H. Erdmann, and K.-U. Schröder, "Postbuckling of imperfect rectangular composite plates under inplane shear closed-form approximate solutions," *Archive of Applied Mechanics,* vol. 81, pp. 1409-1426, 2010.

[27] E. Byklum and J. Amdahl, "A simplified method for elastic large deflection analysis of plates and stiffened panels due to local buckling," *Thin-Walled Structures,* vol. 40, pp. 925-953, 11// 2002.

[28] G. Romeo and G. Frulla, "Nonlinear analysis of anisotropic plates with initial imperfections and various boundary conditions subjected to combined biaxial compression and shear loads," *International Journal of Solids and Structures,* vol. 31, pp. 763-783, 1994/03/01 1994.

[29] G. Romeo and G. Frulla, "Post-buckling behaviour of graphite/epoxy stiffened panels with initial imperfections subjected to eccentric biaxial compression loading," *International Journal of Non-Linear Mechanics,* vol. 32, pp. 1017-1033, 11// 1997.

[30] D. K. Shin, O. H. Griffin Jr, and Z. Gürdal, "Postbuckling response of laminated plates under uniaxial compression," *International Journal of Non-Linear Mechanics,* vol. 28, pp. 95-115, 1// 1993.

[31] R. Vescovini and C. Bisagni, "Two-step procedure for fast post-buckling analysis of composite stiffened panels," *Computers & Structures,* vol. 128, pp. 38-47, 2013.

[32] M. Beerhorst, M. Seibel, and C. Mittelstedt, "Fast analytical method describing the postbuckling behavior of long, symmetric, balanced laminated composite plates under biaxial compression and shear," *Composite Structures,* vol. 94, pp. 2001-2009, 5// 2012.

[33] D. G. Stamatelos, G. N. Labeas, and K. I. Tserpes, "Analytical calculation of local buckling and post-buckling behavior of isotropic and orthotropic stiffened panels," *Thin-Walled Structures,* vol. 49, pp. 422-430, 3// 2011.

[34] Q. Chen and P. Qiao, "Post-buckling behavior of imperfect laminated composite plates with rotationally-restrained edges," *Composite Structures,* vol. 125, pp. 117-126, 2015.

[35] Q. J. Yang and B. Hayman, "Prediction of post-buckling and ultimate compressive strength of composite plates by semi-analytical methods," *Engineering Structures,* vol. 84, pp. 42-53, 2/1/ 2015.

[36] V. Z. Vlasov and Y. Schechtman, *THIN-WALLED ELASTIC BEAMS*. Jerusalem :: Israel Program for Scientific Translations, 1961.

[37] J. B. Ever, L.-A. Roberto, and F. D. Julio, "On the Mechanics of Thin-Walled Laminated Composite Beams," *Journal of Composite Materials,* vol. 27, pp. 806-829, 1993.

[38] L. P. Kollar and A. Pluzsik, "Analysis of Thin-Walled Composite Beams with Arbitrary Layup," *Journal of Reinforced Plastics and Composites,* vol. 21, pp. 1423-1465, 2002.

[39] A. Pluzsik and L. P. Kollar, "Effects of Shear Deformation and Restrained Warping on the Displacements of Composite Beams," *Journal of Reinforced Plastics and Composites,* vol. 21, pp. 1517-1541, 2002.

[40] H. Salim and J. Davalos, "Torsion of Open and Closed Thin-Walled Laminated Composite Sections," *Journal of Composite Materials,* vol. 39, pp. 497-524, 2005.

[41] C. Mittelstedt, "Closed-form buckling analysis of stiffened composite plates and identification of minimum stiffener requirements," *International journal of engineering science.,* vol. 46, p. 1011, 2008.

[42] G. Tarján and L. s. Kollár, "Buckling of axially loaded composite plates with restrained edges," *Journal of Reinforced Plastics and Composites,* vol. 29, pp. 3521-3529, 2010.

[43] C. Mittelstedt and M. Beerhorst, "Closed-form buckling analysis of compressively loaded composite plates braced by omega-stringers," *Composite Structures,* vol. 88, pp. 424-435, 2009.

[44] A. Baucke and C. Mittelstedt, "Closed-form analysis of the buckling loads of composite laminates under uniaxial compressive load explicitly accounting for bending–twisting-coupling," *Composite Structures,* vol. 128, pp. 437-454, 9/15/ 2015.

[45] E. Steen, E. Byklum, and J. Hellesland, "Elastic postbuckling stiffness of biaxially compressed rectangular plates," *Engineering Structures,* vol. 30, pp. 2631-2643, 2008.

Glossary

Acronyms

FE/FEM	Finite element/Finite element method
CLPT	Classical laminate plate theory
BC	Boundary condition
QI	Quasi isotropic
SF	Section forces
PB	Post-buckling
SA	Semi-analytical
AR	Aspect ratio

Main symbols

$\boldsymbol{A,B,D}$	Terms of the ABD matrix
$\boldsymbol{a}$	Compliance of $\boldsymbol{A}$
u,v,w	Plate displacements. u and v are the in-plane and w the out-of-plane
N_x, N_y, N_{xy}	In-plane forces per unit length
a,b	Plate length and width distances
P_x, P_y, P_{xy}	In-plane forces
ϕ	Airy stress function
$\boldsymbol{X, Y}$	Shape functions to reproduce out-of-plane displacement and force distribution
$\boldsymbol{k}$	Torsion spring stiffness imposed as a boundary condition
$\boldsymbol{GJ}$	Stiffener torsional stiffness
Π	Total potential energy

ϵ	Infinitessimal increment
δ	First variation of a functional
φ	Characteristis displacement function
M_x, M_y, M_{xy}	In-plane moments
$\bar{M}_x, \bar{M}_y, \bar{M}_{xy}$	Applied edge in-plane moments
$\boldsymbol{E}$	Natural boundary error term
M, N	Number of terms displacement shape function
P, Q	Number of terms Airy stress function
$\boldsymbol{C}$	Amplitude coefficient of the shape function
$\boldsymbol{\alpha}$	Mode coefficient of the shape function
$\boldsymbol{\varepsilon^0}$	Mid-plane plate strains
$\boldsymbol{\kappa}$	Plate curvatures
AR	Aspect ratio of the plate
$\boldsymbol{K}$	Stiffness matrix